

# A calibrated optogenetic toolbox of stable zebrafish opsin lines

Antinucci P<sup>1\*</sup>, Dumitrescu AS<sup>2\*</sup>, Deleuze C<sup>2</sup>, Morley HJ<sup>1</sup>, Leung K<sup>1</sup>, Hagley T<sup>1</sup>, Kubo F<sup>3,4</sup>, Baier H<sup>3</sup>  
Bianco IH<sup>1\*#</sup>, Wyart C<sup>2\*#</sup>

\* Equal contribution

# Corresponding authors: C.W., [claire.wyart@icm-institute.org](mailto:claire.wyart@icm-institute.org), I.H.B., [i.bianco@ucl.ac.uk](mailto:i.bianco@ucl.ac.uk)

## Affiliations

<sup>1</sup>Department of Neuroscience, Physiology & Pharmacology, UCL, Gower Street, London, WC1E 6BT, UK.

<sup>2</sup>Institut du Cerveau et de la Moelle épinière (I.C.M.), Sorbonne Universités, UPMC Univ Paris 06, Inserm, CNRS, Hôpital Pitié-Salpêtrière, Paris, France.

<sup>3</sup>Department Genes – Circuits – Behavior, Max Planck Institute of Neurobiology, 82152 Martinsried, Germany.

<sup>4</sup>Center for Frontier Research, National Institute of Genetics, 1111 Yata, Mishima, 411-8540, Japan.

## Keywords

Optogenetics, opsin, transgene, zebrafish, calibration, photocurrent, behaviour, electrophysiology, channel, pump, CoChR, ChR2(H134R), CheRiff, ChrimsonR, Chronos, eArch3.0, eNpHR3.0, GtACR1, GtACR2

## Abstract

Optogenetic actuators with diverse spectral tuning, ion selectivity and kinetics are constantly being engineered providing powerful tools for controlling neural activity with subcellular resolution and millisecond precision. Achieving reliable and interpretable *in vivo* optogenetic manipulations requires reproducible actuator expression and calibration of photocurrents in target neurons. Here, we developed nine transgenic zebrafish lines for stable opsin expression and calibrated their efficacy *in vivo*. We first used high-throughput behavioural assays to compare opsin ability to elicit or silence neural activity. Next, we performed *in vivo* whole-cell electrophysiological recordings to quantify the amplitude and kinetics of photocurrents and test opsin ability to precisely control spiking. We observed substantial variation in efficacy, associated with differences in both opsin expression level and photocurrent characteristics, and identified conditions for optimal use of the most efficient opsins. Overall, our calibrated optogenetic toolkit will facilitate the design of controlled optogenetic circuit manipulations.

## 31 Introduction

32 Optogenetics has greatly advanced our ability to investigate how neural circuits process information  
33 and generate behaviour by allowing manipulation of neural activity with high spatio-temporal  
34 resolution in genetically-defined neurons (Miesenbock, 2009; Boyden, 2011; Miesenbock, 2011;  
35 Adamantidis *et al.*, 2015; Boyden, 2015; Deisseroth, 2015; Deisseroth and Hegemann, 2017). The  
36 efficacy with which optogenetic actuators – such as microbial opsins – can control neuronal spiking  
37 *in vivo* depends on biophysical properties, expression level and membrane trafficking of the opsin,  
38 physiological properties of the target cell and the intensity profile of light delivered within scattering  
39 tissue.

40 Accordingly, two primary experimental requirements should be met to enable controlled and  
41 reproducible *in vivo* optogenetic circuit manipulations: (i) reproducible opsin expression levels  
42 (across cells and animals), with stable expression systems offering higher reliability and homogeneity  
43 than transient ones (Kikuta and Kawakami, 2009; Yizhar *et al.*, 2011; Sjulson *et al.*, 2016), and  
44 (ii) calibrated photocurrents recorded in target neurons (Huber *et al.*, 2008; Li *et al.*, 2019). While  
45 previous studies have compared the physiological effects of opsin activation in single cells using  
46 standardised conditions [e.g. (Berndt *et al.*, 2011; Mattis *et al.*, 2011; Prigge *et al.*, 2012; Klapoetke *et al.*,  
47 2014; Berndt *et al.*, 2016; Mardinly *et al.*, 2018)], these comparisons were primarily performed *in vitro*  
48 or *ex vivo* using transient expression strategies.

49 In this study, we took advantage of the genetic accessibility and transparency of zebrafish (Arrenberg  
50 *et al.*, 2009; Del Bene and Wyart, 2012; Arrenberg and Driever, 2013; Portugues *et al.*, 2013; Forster *et al.*,  
51 2017) to generate nine stable transgenic lines for targeted opsin expression using the GAL4/UAS  
52 binary expression system (Scheer and Campos-Ortega, 1999; Asakawa and Kawakami, 2008) and  
53 quantitatively compare their efficacy for inducing or silencing neuronal spiking. We selected opsins  
54 that were reported to induce photocurrents with large amplitude [CoChR (Klapoetke *et al.*, 2014),  
55 CheRiff (Hochbaum *et al.*, 2014), ChR2<sub>(H134R)</sub> (Gradinaru *et al.*, 2007), eArch3.0 (Mattis *et al.*, 2011),  
56 GtACR1–2 (Govorunova *et al.*, 2015)] and/or fast kinetics [Chronos, ChrimsonR (Klapoetke *et al.*,  
57 2014), eNpHR3.0 (Gradinaru *et al.*, 2010)]. We first assessed the efficacy of these stable lines to control  
58 activity in intact neural populations via high-throughput behavioural assays at both embryonic and  
59 larval stages. Next, we made *in vivo* electrophysiological recordings from single low input-resistance  
60 motor neurons to calibrate photocurrents and test the ability of each line to elicit or silence spiking.  
61 We observed broad variation in behavioural response rates, photocurrent amplitudes and spike  
62 induction, likely due to differences in both opsin properties and expression levels. For the best opsin  
63 lines, we identified conditions that allowed control of individual action potentials within high-  
64 frequency spike trains. Overall, our toolkit will enable reliable and robust optogenetic interrogation  
65 of neural circuit function in zebrafish.

## 66 Results

### 67 Generation of stable transgenic lines for targeted opsin expression in zebrafish

68 To maximise the utility of our optogenetic toolkit, we used the GAL4/UAS binary expression system  
69 for targeted opsin expression in specific cell populations (Figure 1). We generated nine stable UAS  
70 lines for opsins having different ion selectivities and spectral tuning, fused to a fluorescent protein  
71 reporter (tdTomato or eYFP; Figure 1A and Supplementary File 1) (Asakawa *et al.*, 2008; Arrenberg *et al.*,  
72 *et al.*, 2009; Horstick *et al.*, 2015). GAL4 lines were used to drive expression in defined neuronal  
73 populations, such as motor neurons (Figure 1B) (Scott *et al.*, 2007; Wyart *et al.*, 2009; Bohm *et al.*, 2016).  
74 High levels of expression were achieved in most cases (Figure 1C), with only few opsins showing  
75 intracellular puncta suggestive of incomplete trafficking to the plasma membrane (CheRiff and  
76 GtACR2) or low expression (Chronos). To quantitatively compare opsin lines, we performed  
77 standardised behavioural tests at embryonic and larval stages (Figure 1D) and calibrated  
78 photocurrents and modulation of spiking in larval primary motor neurons (Figure 1E).

### 79 Escape behaviour triggered by optogenetic activation of embryonic trigeminal neurons

80 As a first test of our opsin lines, we evaluated their ability to activate embryonic neurons (Figure 2A–  
81 C), which are characterised by high input resistance (Drapeau *et al.*, 1999; Saint-Amant and Drapeau,  
82 2000). We used the *Tg(isl2b:GAL4)* transgene (Ben Fredj *et al.*, 2010) to drive expression of opsins in  
83 the trigeminal ganglion (Figure 2B,C). In this class of somatosensory neuron, optogenetic induction  
84 of few spikes has been shown to reliably elicits escape responses (Douglass *et al.*, 2008), characterised  
85 by high-amplitude bends of the trunk and tail (Kimmel *et al.*, 1990; Saint-Amant and Drapeau, 1998;  
86 Sagasti *et al.*, 2005). Brief pulses of light (5 or 40 ms-long) induced escape responses in embryos (28–  
87 30 hours post fertilisation, hpf) expressing all cation- and anion-conducting channelrhodopsins  
88 (Figure 2C–E and Video 1), while no movement was elicited in opsin-negative siblings (Figure 2F,G  
89 and Figure 2–figure supplement 1,2;  $N = 69 \pm 26$  fish per group, mean  $\pm$  SD). The excitatory effect of  
90 GtACRs suggests that increasing chloride conductance depolarises neurons at this developmental  
91 stage. For all opsins, response probability increased monotonically with light power (Figure 2F,G).  
92 Escape behaviour could also be evoked via transient opsin expression, in which animals were tested  
93 one day after injection of DNA constructs into single cell-stage *Tg(isl2b:GAL4)* embryos (Figure 2F).  
94 Some opsins showed higher response probability in transient transgenic animals (CheRiff, CoChR  
95 and GtACRs), likely due to higher expression levels.

96 With blue light, CoChR elicited escapes at the highest response probability (65–100% at 112–  
97 445  $\mu\text{W}/\text{mm}^2$ ; Figure 2F,G) and response latency decreased with increasing irradiance (insets in  
98 Figure 2F,G). As expected from its red-shifted absorption spectrum, ChrimsonR was the only cation  
99 channelrhodopsin to evoke escapes using amber light ( $\sim 70\%$  response probability at 322  $\mu\text{W}/\text{mm}^2$ ;  
100 Figure 2F,G) (Klapoetke *et al.*, 2014). Consistent with their respective red- and blue-shifted absorption  
101 spectra, GtACR1 triggered escapes upon amber and blue light stimulation whereas GtACR2 elicited  
102 responses only with blue light (Figure 2F,G) (Govorunova *et al.*, 2015).

### 103 Tail movements triggered by optogenetic activation of larval spinal motor neurons

104 Next, we compared the efficacy of cation channelrhodopsin lines to induce behaviour by activation  
105 of larval motoneurons, from which we would later record photocurrents. We used the  
106 *Tg(mnx1:GAL4)* transgene (Bohm *et al.*, 2016) to target expression to spinal motor neurons  
107 (Figure 3A,B) and subjected head-restrained zebrafish (6 days post fertilisation, dpf;  $N = 28 \pm 8$  fish

108 per group, mean  $\pm$  SD) to either single light pulses (2 or 10 ms-long) or pulse trains at 20 or 40 Hz  
109 (Figure 3C,D and Video 2,3) while monitoring tail movements.

110 Optogenetically-evoked tail movements were triggered with short latency following light onset  
111 ( $8.3 \pm 6.9$  ms, mean  $\pm$  SD) in opsin-expressing larvae only, whereas visually-evoked swim bouts  
112 occurred at much longer latency ( $316 \pm 141$  ms, mean  $\pm$  SD) in both opsin-expressing larvae and  
113 control siblings (Figure 3E). We restricted our analyses to optogenetically-evoked movements,  
114 initiated within 50 ms of stimulus onset (corresponding to a minimum of the probability density  
115 distribution of latency; dotted line in Figure 3E). Optogenetically-evoked tail movements comprised  
116 a sequence of left-right alternating half beats, thereby resembling natural swim bouts (Figure 3C,D  
117 and Video 2,3). Response probability increased with irradiance (Figure 3F and Figure 3-figure  
118 supplement 1) and CoChR again elicited tail movements with the highest probability and shortest  
119 latency in response to blue light (96–100% at 0.63–2.55 mW/mm<sup>2</sup>; Figure 3F,G). Only the ChrimsonR  
120 line responded to red light (~78% response probability at 1 mW/mm<sup>2</sup>; Figure 3F). Tail movements  
121 evoked by single light pulses typically had shorter duration and fewer cycles than visually-evoked  
122 swims (Figure 3H–K). However, longer movements (> 100 ms, 4–5 cycles) were often observed in  
123 response to single light pulses (see response to 2 ms pulse in Figure 3D and Video 2) indicating  
124 engagement of spinal central pattern generators. This may occur through recruitment of  
125 glutamatergic V2a interneurons connected to motor neurons via gap junctions (Song *et al.*, 2016)  
126 and/or by proprioceptive feedback via cerebrospinal fluid-contacting neurons (Wyart *et al.*, 2009;  
127 Fidelin *et al.*, 2015; Bohm *et al.*, 2016). Pulse train stimuli evoked swim bouts of longer duration, with  
128 swims in CoChR and ChrimsonR lines showing modest frequency-dependent modulation of cycle  
129 number (Figure 3L–Q).

### 130 ***In vivo* whole-cell recording of photocurrents in larval primary motor neurons**

131 To calibrate photocurrents *in vivo*, we performed whole-cell voltage clamp recordings from single  
132 primary motor neurons (pMNs) in 5–6 dpf larvae (Figure 4A). Each opsin was stimulated with a  
133 wavelength close to its absorption peak (1–30 mW/mm<sup>2</sup>; Figure 4-figure supplement 1A). We  
134 recorded over 125 neurons, including control cells from opsin-negative animals, from which 86 cells  
135 were selected following strict criteria for recording quality (see Material and methods; N = 3–19  
136 included cells per group; Figure 4-figure supplement 1B). Opsin-expressing pMNs displayed  
137 physiological properties, such as membrane resistance, resting membrane potential and cell  
138 capacitance, comparable to opsin-negative neurons (Figure 4B,C and Figure 4-figure  
139 supplement 1C,D). All cation channelrhodopsins induced inward currents upon light stimulation,  
140 which were not observed in opsin-negative pMNs (Figure 4D). Notably, CoChR and ChrimsonR  
141 generated the largest photocurrents (CoChR  $475 \pm 186$  pA, mean  $\pm$  SD, N = 8 cells, ChrimsonR  
142  $251 \pm 73$  pA, N = 7; Figure 4E). We did not observe significant irradiance-dependent modulation of  
143 photocurrent amplitude in any opsin line, likely due to the high range of irradiance we tested  
144 (Figure 4-figure supplement 1F). Photocurrent kinetics influence the temporal precision with which  
145 single action potentials can be evoked (Mattis *et al.*, 2011). Therefore, we measured the photocurrent  
146 activation time (i.e. time to peak response from light onset), which results from the balance between  
147 activation and inactivation of the opsin, and deactivation time constant (i.e. the response decay time  
148 constant,  $\tau_{\text{off}}$ ), which is determined by the rate of channel closure at light offset (Mattis *et al.*, 2011;  
149 Schneider *et al.*, 2015). Comparable activation times were observed across opsin lines (4–5 ms;  
150 Figure 4F). Deactivation time constants were more variable between opsins, with Chronos showing

151 the fastest deactivation kinetics ( $4.3 \pm 0.4$  ms,  $N = 3$  cells, mean  $\pm$  SD) and the other opsins displaying  
152 similar time constants (12–20 ms; Figure 4G).

### 153 **Optogenetic induction of spiking in larval pMNs**

154 To investigate whether our cation channelrhodopsin lines can induce action potentials in pMNs, we  
155 performed *in vivo* current clamp recordings while providing single light pulses (1–5 ms duration). In  
156 all opsin lines, light stimulation induced voltage depolarisations, which were never observed in  
157 opsin-negative pMNs, and voltage responses above  $-30$  mV were classified as spikes (Figure 5A).

158 CoChR and ChrimsonR were the only opsin lines capable of triggering spiking in this cell type  
159 (Figure 5A and Figure 5–figure supplement 1A–C), as expected from their peak photocurrents  
160 exceeding pMN rheobase (dotted lines in Figure 4E). Notably, 5 ms-long light pulses induced spikes  
161 in all CoChR-expressing neurons ( $N = 7$  out of 7 cells at  $3\text{--}30$  mW/mm<sup>2</sup>), dropping to 88% of cells  
162 spiking with shorter pulses (Figure 5–figure supplement 1A). ChrimsonR was less effective than  
163 CoChR in inducing action potentials, with 36–38% of neurons spiking when using 2–5 ms-long pulses  
164 (2 ms,  $N = 4$  out of 11; 5 ms,  $N = 3$  out of 8 cells) and only 13% spiking with 1 ms-long pulses ( $N = 1$   
165 out of 8 cells). In both opsin lines, the number of evoked spikes increased with longer pulse duration  
166 (Figure 5B and Figure 5–figure supplement 1D).

167 For experiments aiming to replay physiological firing patterns, optogenetic actuators should be  
168 capable of inducing spike trains with millisecond precision and at biological firing frequencies. We  
169 thus tested the ability of CoChR and ChrimsonR to evoke pMN firing patterns across a range of  
170 frequencies (1–100 Hz; Figure 5C). pMNs can spike at high frequency (up to 300–500 Hz) (Menelaou  
171 and McLean, 2012), hence optogenetic induction of high-frequency firing should not be limited by  
172 cell intrinsic physiological properties, but rather by opsin properties and light stimulation  
173 parameters. To assess the fidelity of firing patterns at each stimulation frequency, we measured spike  
174 number per light pulse as well as spike latency and jitter (i.e. standard deviation of spike latency).  
175 ChrimsonR could induce firing up to the highest frequency tested (100 Hz), with each light pulse  
176 typically evoking a single spike (Figure 5C,D). CoChR generated spike bursts in response to the initial  
177 pulses of the train only and could not evoke spiking at stimulation frequencies higher than 50 Hz  
178 (Figure 5C,D). Overall, spikes were induced with short latency (3–4 ms mean latency) and low jitter  
179 (0.25–1.25 ms jitter) with both opsin lines (Figure 5E,G).

### 180 **Optogenetic suppression of coiling behaviour in embryos**

181 Next, we tested the ability of our opsin lines to suppress spontaneous behaviour of zebrafish embryos  
182 (Saint-Amant and Drapeau, 1998; Warp *et al.*, 2012; Mohamed *et al.*, 2017; Bernal Sierra *et al.*, 2018).  
183 We targeted expression of the anion-conducting channels GtACR1 and GtACR2 (Govorunova *et al.*,  
184 2015), the outward proton pump eArch3.0 (Mattis *et al.*, 2011) and the inward chloride pump  
185 eNpHR3.0 (Gradinaru *et al.*, 2010) to spinal cord neurons using the *Tg(s1020t:GAL4)* transgene (Scott  
186 *et al.*, 2007) and examined changes in spontaneous coiling behaviour in response to light (Figure 6A–  
187 D and Video 4). In opsin-expressing embryos (24–27 hpf), light exposure led to a suppression of  
188 coiling behaviour that was followed by a synchronised restart at light offset (Figure 6D,E and Figure  
189 6–figure supplement 1;  $N = 91 \pm 16$  fish per group, mean  $\pm$  SD), as previously reported (Warp *et al.*,  
190 2012; Mohamed *et al.*, 2017). As expected from behaviour with *Tg(isl2b:GAL4)* embryos (Figure 2F,G),  
191 GtACR activation in spinal neurons occasionally induced movements in the initial 1–2 s following  
192 light onset (black arrows in Figure 6D,E), a phenomenon that was not observed with Cl<sup>-</sup>/H<sup>+</sup> pumps.

193 Given these two effects, changes in coil rate were separately quantified for the initial 2 s (Figure 6–  
194 figure supplement 2) and subsequent 8 s period of light exposure (‘late LED ON’; grey horizontal  
195 bars in Figure 6E).

196 All opsin lines suppressed coiling behaviour during the ‘late LED ON’ period (Figure 6F,G). This was  
197 likely a result of distinct mechanisms: hyperpolarisation with  $\text{Cl}^-/\text{H}^+$  pumps versus depolarisation  
198 block with anion channelrhodopsins (see below and Discussion). As previously observed (Friedmann  
199 *et al.*, 2015), light also decreased coiling in control opsin-negative embryos, yet to a significantly lesser  
200 degree than in opsin-expressing animals (Figure 6F,G). GtACRs achieved the strongest suppression  
201 of coil rate using blue light (90–95% decrease at 8.4–225  $\mu\text{W}/\text{mm}^2$ ; Figure 6F). With amber light,  
202 GtACR1, eArch3.0 and eNpHR3.0 showed comparable suppression (80–90% decrease at 50.5–  
203 227  $\mu\text{W}/\text{mm}^2$ ), with GtACR1 achieving ~83% decrease in coil rate even at low irradiance  
204 (15.9  $\mu\text{W}/\text{mm}^2$ ; Figure 6G).

### 205 **Optogenetic suppression of swimming in larvae**

206 To compare the efficacy of our opsin lines to suppress behaviour in larvae, we targeted opsin  
207 expression to spinal motor neurons and interneurons using *Tg(s1020t:GAL4)*, as above, and examined  
208 changes in spontaneous swimming behaviour of 6 dpf animals in response to 10 s-long light pulses  
209 (Figure 7A–C and Video 5;  $N = 25 \pm 9$  fish per group, mean  $\pm$  SD).

210 GtACR1, GtACR2 and eArch3.0 reduced swim bout rate relative to control larvae in response to blue  
211 light, with GtACRs achieving the greatest suppression (20–45% decrease; Figure 7D,E). Consistent  
212 with a previous report (Andalman *et al.*, 2019), opsin-negative larvae showed a 20–30% increase in  
213 bout rate during illumination with blue light (Figure 7E and Figure 7–supplement 1), while no  
214 increase was observed with red light (Figure 7F). Using red light, only eNpHR3.0 could reduce bout  
215 rate and suppression increased with higher irradiance (45% decrease at 1  $\text{mW}/\text{mm}^2$ ; Figure 7F). No  
216 increase in bout rate was found in larvae expressing anion channelrhodopsins even when analysis  
217 was restricted to the initial 2 s of the light period (Figure 7–figure supplement 2A), suggesting  
218 GtACRs do not induce excitatory effects at larval stages. Opsin activation did not affect bout speed  
219 (Figure 7–figure supplement 2B). By contrast, using the *Tg(mnx1:GAL4)* transgene to drive opsin  
220 expression in motor neurons resulted in a decrease in bout speed (~20% reduction), but not bout rate  
221 (Figure 7–figure supplement 3,4).

### 222 **Photocurrents induced by anion channelrhodopsins and chloride/proton pumps**

223 To analyse the physiological effects induced by anion channelrhodopsins and  $\text{Cl}^-/\text{H}^+$  pumps, we  
224 measured their photocurrents through *in vivo* voltage clamp recordings from larval pMNs (5–6 dpf).  
225 Since anion channelrhodopsin function depends on chloride homeostasis (Figure 8A) (Govorunova  
226 *et al.*, 2015) and chloride reversal potential ( $E_{\text{Cl}}$ ) is known to change over development (Ben-Ari, 2002;  
227 Reynolds *et al.*, 2008; Zhang *et al.*, 2010), we recorded GtACR1 photocurrents using two intracellular  
228 solutions: one mimicking  $E_{\text{Cl}}$  in embryonic neurons (–50 mV) (Saint-Amant and Drapeau, 2003) and  
229 the second approximating intracellular chloride concentration in more mature, larval neurons  
230 ( $E_{\text{Cl}} = -70$  mV, see Materials and methods). Inspection of I-V curves for GtACR1 photocurrents  
231 showed that, in both solutions, currents reversed with a positive 5–10 mV shift relative to  $E_{\text{Cl}}$   
232 (Figure 8–supplement 1A,B), as previously observed (Govorunova *et al.*, 2015) and within the  
233 expected error margin given our access resistance (Figure 4–figure supplement 1C; estimated voltage  
234 error for  $E_{\text{Cl}-50\text{ mV}}$  solution,  $4.6 \pm 6.4$  mV, mean  $\pm$  SD,  $N = 5$  cells;  $E_{\text{Cl}-70\text{ mV}}$  solution,  $1.2 \pm 1.3$  mV,

235 N = 3). This suggests that GtACR1 photocurrents were primarily driven by chloride ions, as expected  
236 (Govorunova *et al.*, 2015). The other opsin lines were tested using the ECl<sub>-50 mV</sub> solution only. Neurons  
237 were stimulated with light (1 s-long pulse) at a holding potential matching their measured resting  
238 membrane potential (Figure 4C).

239 Anion channelrhodopsins induced inward, `depolarising` photocurrents (as expected from the  
240 combination of ECl and holding potential), while Cl<sup>-</sup>/H<sup>+</sup> pumps generated outward,  
241 `hyperpolarising` currents (Figure 8B). All opsins except eNpHR3.0 showed bi-phasic photocurrent  
242 responses composed of a fast activation followed by a slow inactivation (Figure 8B), likely due to a  
243 fraction of the opsin population transitioning to an inactive state (Chow *et al.*, 2010; Mattis *et al.*, 2011;  
244 Schneider *et al.*, 2015). We measured both the peak photocurrent (Figure 8C) as well as the steady-  
245 state current during the last 5 ms of the light period (Figure 8D). GtACRs induced photocurrents with  
246 peak amplitude 3–10 times larger than those generated by Cl<sup>-</sup>/H<sup>+</sup> pumps (Figure 8C), while steady-  
247 state currents were similar across opsins (Figure 8D). Some degree of irradiance-dependent  
248 modulation of photocurrents was observed, primarily in peak amplitude (Figure 8–supplement 2C–  
249 E). To characterise photocurrent kinetics, we computed activation, inactivation (or  $\tau_{des}$ ) and  
250 deactivation time constants (Mattis *et al.*, 2011). GtACR photocurrents had the fastest activation  
251 kinetics (~1 ms at 30 mW/mm<sup>2</sup>; Figure 8E and Figure 8–figure supplement 2F). However,  
252 deactivation kinetics of Cl<sup>-</sup>/H<sup>+</sup> pumps were 2–10 times faster than those induced by GtACRs (14–  
253 22 ms eNpHR3.0, 27–37 ms eArch3.0; Figure 8G and Figure 8–figure supplement 2H) and showed  
254 little inactivation (600–1000 ms eArch3.0; Figure 8F and Figure 8–figure supplement 2G).

### 255 **Optogenetic inhibition of pMN spiking**

256 To investigate the ability of anion channelrhodopsins and Cl<sup>-</sup>/H<sup>+</sup> pumps to suppress neural activity,  
257 we recorded pMNs in current clamp mode. In control opsin-negative neurons, light delivery (1 s)  
258 induced negligible voltage deflections (Figure 9A). By contrast, anion channelrhodopsins generated  
259 membrane depolarisation towards ECl while the Cl<sup>-</sup>/H<sup>+</sup> pumps hyperpolarised the cell (Figure 9A),  
260 in accordance with recorded photocurrents. The absolute peak amplitude of voltage deflections was  
261 comparable between opsin lines (10–25 mV), with 10–40% decrease between peak and steady-state  
262 responses in all cases except eNpHR3.0, which generated stable hyperpolarisation (Figure 9B,C and  
263 Figure 9–figure supplement 1A,B). In a subset of GtACR1- (N = 4 out of 7) and GtACR2-expressing  
264 neurons (N = 2 out of 6), spiking was induced at light onset when using the ECl<sub>-50 mV</sub> solution  
265 (Figure 9A; GtACR1 6.7 ± 7.1 spikes; GtACR2 1.5 ± 0.7, mean ± SD). This is consistent with the  
266 movements evoked at light onset in young, 1 dpf embryos expressing GtACRs (Figure 2 and 6). The  
267 kinetics of voltage decay to baseline following light offset matched those of recorded photocurrents  
268 (Figure 9D and Figure 9–figure supplement 1C).

269 Next, we compared the utility of our opsin lines to inhibit pMN firing. First, we induced larval pMNs  
270 to fire at 5 Hz by injecting pulses of depolarising current (5 ms, 1.2–1.5× rheobase) and  
271 simultaneously delivered 5 ms light pulses to inhibit selected spikes (Figure 9E). We found that  
272 GtACRs and eNpHR3.0 could effectively inhibit spikes (80–95% suppression), while light pulses did  
273 not alter firing in opsin-negative neurons (Figure 9F). In agreement with our current clamp  
274 recordings, a subset of GtACR1-expressing neurons (N = 4 out of 7) tested in the embryonic ECl<sub>-50 mV</sub>  
275 solution failed to suppress spikes and instead induced extra action potentials in response to light  
276 pulses, resulting in a negative spike inhibition efficacy (Figure 9F). Data from eArch3.0-expressing  
277 neurons could not be collected due to degradation in the quality of recordings or cells becoming

278 highly depolarised (i.e. resting membrane potential  $> -50$  mV) by the later stages of the protocol,  
279 suggesting that repeated eArch3.0 activation may alter electrical properties of neurons (Williams *et*  
280 *al.*, 2019).

281 Lastly, we asked whether we could inhibit firing over periods of tens to hundreds of milliseconds.  
282 We injected long pulses of depolarising current (200–800 ms) to elicit tonic pMN firing, and  
283 simultaneously provided shorter light pulses (50–200 ms; 3–10 mW/mm<sup>2</sup>) in the middle of the spike  
284 train (Figure 9G). Both GtACR1 and eNpHR3.0 successfully inhibited spiking during the light pulse,  
285 with complete suppression in 60–100% of cells at 10 mW/mm<sup>2</sup> irradiance (Figure 9G,H). Notably,  
286 GtACR1 could inhibit tonic spiking even when using the embryonic ECL<sub>-50 mV</sub> solution (Figure 9G,H),  
287 consistent with the suppression of coiling behaviour upon prolonged illumination of GtACR-  
288 expressing embryos (Figure 6).

## 289 Discussion

290 In this study, we generated a set of stable transgenic lines for GAL4/UAS-mediated opsin expression  
291 in zebrafish and evaluated their efficacy in controlling neural activity *in vivo*. High-throughput  
292 behavioural assays and whole-cell electrophysiological recordings provided complementary insights  
293 to guide tool selection. Behavioural assays enabled efficient evaluation of opsin lines in various  
294 sensory and motor cell types and revealed developmental stage-specific effects in intact neural  
295 populations. Electrophysiological recordings from single motor neurons afforded quantification of  
296 photocurrents and systematic evaluation of the ability of these optogenetic tools to elicit or silence  
297 activity at single action potential resolution.

### 298 An *in vivo* platform for opsin tool selection

299 The selection of optogenetic actuators should be based on their ability to reliably control neural  
300 activity *in vivo*. While previous efforts compared opsin efficacy using transient expression strategies  
301 [e.g. viral or plasmid injections, see Mattis *et al.* (2011) and Introduction], here we calibrated opsin  
302 effects in stable transgenic lines, which offer more reproducible expression across experiments and  
303 laboratories (Kikuta and Kawakami, 2009; Yizhar *et al.*, 2011). Overall, there was good qualitative  
304 agreement between behavioural and electrophysiological results, with efficacy in behavioural assays  
305 (even with transient expression) largely predicting rank order in photocurrent amplitudes. This  
306 illustrates the utility of high-throughput behavioural assays for rapid evaluation and selection of  
307 expression constructs prior to more time-consuming generation and characterisation of stable lines  
308 and electrophysiological calibration. We observed broad variation in efficacy across lines, likely  
309 attributable to differences in both the intrinsic properties of the opsin as well as variation in  
310 expression and membrane targeting. Membrane trafficking can also be influenced by the fluorescent  
311 protein fused to the actuator (Arrenberg *et al.*, 2009). In our hands, we observed better expression  
312 with the tdTomato fusion reported here than with previous attempts using a tagRFP fusion protein.  
313 In the future, expression might be further improved through codon optimisation (Horstick *et al.*,  
314 2015), trafficking-enhancing sequences (Gradinaru *et al.*, 2010; Mattis *et al.*, 2011), alternative  
315 expression targeting systems (Luo *et al.*, 2008; Sjulson *et al.*, 2016) and optimisation of the fluorescent  
316 reporter protein.

317 Behavioural and electrophysiological readouts complemented one another and enriched the  
318 interpretation of our results. Electrophysiological recordings in a defined cell type allowed direct and  
319 comparative calibration of photocurrents. Although several opsin lines did not evoke action



320 potentials in low-input-resistance pMNs, behavioural assays showed that all lines induced tail  
321 movements in larvae. This is likely due to recruitment of secondary motor neurons labelled by the  
322 *Tg(mnx1:GAL4)* transgene, which have higher input resistance (Menelaou and McLean, 2012).  
323 Behavioural assays at multiple ages revealed that anion channelrhodopsins can excite neurons in  
324 1 dpf embryos which was corroborated by making whole-cell recordings using a patch solution  
325 reproducing the high intracellular chloride concentration observed in embryonic neurons (Reynolds  
326 *et al.*, 2008; Zhang *et al.*, 2010).

327 Overall, our platform enables efficient selection and calibration of optogenetic tools for *in vivo*  
328 neuroscience. It also enables opsin-specific optimisation of light delivery (i.e. wavelength, pulse  
329 duration, frequency and intensity). For example, we found that equivalent stimulation regimes  
330 produced different rates of spiking adaptation that impacted the ability to control high-frequency  
331 firing, depending on the specific line in question.

### 332 **Robust and precise optogenetic induction of spiking**

333 Which opsin lines are best suited for reliable neural activation? Photocurrent amplitude, measured in  
334 pMNs, was predictive of the ability of opsin lines to induce behaviour via activation of distinct cell  
335 types at both larval and embryonic stages (CoChR > ChrimsonR > ChR2<sub>(H134R)</sub> > Chronos ≥ CheRiff).  
336 The CoChR and ChrimsonR lines showed the highest expression levels among cation  
337 channelrhodopsins and were the only lines capable of inducing action potentials in pMNs, consistent  
338 with their photocurrent amplitudes exceeding pMN rheobase. Notably, CoChR evoked spikes in all  
339 pMNs tested and triggered behaviour with maximal response probability in larvae at irradiance  
340 levels as low as 0.63 mW/mm<sup>2</sup>.

341 Where precise control of a cell's firing pattern is desired, electrophysiological calibration is essential  
342 to tune stimulation parameters for a specific opsin/cell-type combination. Our data indicate that long  
343 light pulses (2–5 ms) can lead to spike bursts and substantial firing rate adaptation during high-  
344 frequency stimulation, likely a result of plateau potentials and inactivation of voltage-gated sodium  
345 channels. Thus, although the CoChR line produced large-amplitude photocurrents and was highly  
346 efficient in evoking spikes, it was also prone to burst firing, which compromised spiking entrainment  
347 with high-frequency stimulations. Therefore, short light pulses (< 2 ms) are better suited for inducing  
348 high-frequency firing patterns with millisecond precision when using CoChR.

### 349 **Excitatory effects of anion channelrhodopsins**

350 Anion channelrhodopsins induced movements at light onset in 1 dpf embryos as well as transient  
351 spiking in pMNs when using an intracellular solution that mimicked the high ECl (-50 mV) of  
352 immature neurons. This is consistent with GtACRs functioning as a light-gated chloride conductance  
353 (Govorunova *et al.*, 2015). The transient nature of spiking and motor activity might be due to the initial  
354 large inward photocurrent depolarising neurons above spiking threshold, while the subsequent  
355 smaller inactivating current would lead to depolarisation block by clamping membrane potential  
356 close to ECl. Transient induction of action potentials with GtACRs has also been observed in rat  
357 cortical pyramidal neurons in brain slices (Malyshev *et al.*, 2017) as well as cultured hippocampal  
358 neurons (Mahn *et al.*, 2018) and has been attributed to antidromic spiking resulting from a positively  
359 shifted ECl in the axon (Mahn *et al.*, 2016; Mahn *et al.*, 2018). In light of this, the use of GtACRs in  
360 immature neurons or subcellular structures should be carefully calibrated and use of Cl<sup>-</sup>/H<sup>+</sup> pumps  
361 may be preferable.

362 **Precise optogenetic inhibition of neural activity**

363 To accurately suppress action potentials, opsin tools must be carefully selected with consideration for  
364 developmental stage and ECl<sup>-</sup>-dependent effects as well as photocurrent kinetics. GtACRs generated  
365 large photocurrents with fast activation kinetics, which can explain why GtACR1 was effective in  
366 inhibiting single action potentials with short light pulses in larval pMNs. Cl<sup>-</sup>/H<sup>+</sup> pump photocurrents  
367 instead showed fast deactivation kinetics, which allowed eNpHR3.0-expressing neurons to rapidly  
368 resume spiking at light offset. Differences in photocurrent kinetics between opsin classes – i.e.  
369 channels vs. pumps – may thus differentially affect the temporal resolution of activity inhibition and  
370 recovery, respectively. The combined behavioural and electrophysiological approach can be  
371 extended in the future to optogenetic silencers based on K<sup>+</sup> channel activation, such as the recently  
372 introduced PAC-K (Bernal Sierra *et al.*, 2018).

373 In conclusion, our calibrated optogenetic toolkit and associated methodology provide an *in vivo*  
374 platform for designing controlled optogenetic experiments and benchmarking novel opsins.

## 375 **Acknowledgements**

376 The authors thank members of the Bianco lab and Wyart lab for helpful discussions. We thank staff  
377 from the UCL and ICM PHENOZ fish facilities for fish care and husbandry (UCL: Carole Wilson and  
378 team; ICM: Sophie Nunes-Figueiredo, Bogdan Buzurin, and Monica Dicu), Irene Arnold-Ammer and  
379 Enrico Kühn (MPI of Neurobiology) assisted with generation of transgenic lines. We also  
380 acknowledge support from the ICM electrophysiology core facility (CELIS-ePhys). P.A. was  
381 supported by a Sir Henry Wellcome Postdoctoral Fellowship (204708/Z/16/Z). A.D. was supported  
382 by a Marie Curie Incoming International Fellowship (H2020-MSCA-IF-2016 Project #752199). F.K.  
383 was supported by a HFSP long-term fellowship (LT393/2010). Generation of opsins in H. B.'s  
384 laboratory was supported by the Max Planck Society (H. B. and F. K.) and the DFG (SPP1926 Next-  
385 Generation Optogenetics). A Sir Henry Dale Fellowship from the Royal Society & Wellcome Trust  
386 (101195/Z/13/Z) and a UCL Excellence Fellowship were awarded to I.H.B. The work in C.W.'s lab  
387 was funded by Human Frontier Science Program (HFSP) Research Grant (RGP063-2018) and the New  
388 York Stem Cell Foundation (NYSCF-R-NI39). The work on electrophysiological calibration of opsins  
389 performed in ICM has also received funding from the ICM foundation, the program `Investissements  
390 d'avenir` ANR-10-IAIHU-06 (Big Brain Theory ICM Program), ANR-11-INBS-0011 (NeurATRIS:  
391 Translational Research Infrastructure for Biotherapies in Neurosciences).

## 392 **Author Contributions**

393 Conceptualisation: PA, AD, CD, IB, CW  
394 Methodology: PA, AD, CD  
395 Software: PA, AD, IB, CW  
396 Validation: PA, AD  
397 Formal analysis: PA, AD  
398 Investigation: PA, AD, CD, HM, KL, TH  
399 Resources: PA, AD, CD, FK, HB, IB, CW  
400 Data curation: PA, AD  
401 Writing—original draft: PA, AD, CW, IB  
402 Writing—review and editing: PA, AD, FK, HB, IB, CW  
403 Visualisation: PA, AD  
404 Funding acquisition: PA, AD, FK, HB, IB, CW  
405 Supervision: HB, IB, CW  
406 Project administration: CW, IB

## 407 **Competing Interests**

408 The authors declare no competing interests.

409 **Materials and methods**

<b>Key Resources Table</b>				
<b>Reagent type (species) or resource</b>	<b>Designation</b>	<b>Source or reference</b>	<b>Identifiers</b>	<b>Additional information</b>
Genetic reagent ( <i>Danio rerio</i> )	<i>Tg(UAS:ChrimsonR-tdTomato)u328Tg</i>	This study	ZFIN ID: ZDB-ALT-190226-2	Available from EZRC
Genetic reagent ( <i>Danio rerio</i> )	<i>Tg(UAS:Chronos-tdTomato)u330Tg</i>	This study	ZFIN ID: ZDB-ALT-190226-3	Available from EZRC
Genetic reagent ( <i>Danio rerio</i> )	<i>Tg(UAS:CoChR-tdTomato)u332Tg</i>	This study	ZFIN ID: ZDB-ALT-190226-4	Available from EZRC
Genetic reagent ( <i>Danio rerio</i> )	<i>Tg(UAS:CheRiff-tdTomato)u334Tg</i>	This study	ZFIN ID: ZDB-ALT-190226-5	Available from EZRC
Genetic reagent ( <i>Danio rerio</i> )	<i>Tg(UAS:GtACR1-tdTomato)u336Tg</i>	This study	ZFIN ID: ZDB-ALT-190226-6	Available from EZRC
Genetic reagent ( <i>Danio rerio</i> )	<i>Tg(UAS:GtACR2-tdTomato)u338Tg</i>	This study	ZFIN ID: ZDB-ALT-190226-7	Available from EZRC
Genetic reagent ( <i>Danio rerio</i> )	<i>Tg(UAS:eArch3.0-eYFP)mpn120</i>	This study	transgene	Available from Baier lab
Genetic reagent ( <i>Danio rerio</i> )	<i>Tg(UAS:eNpHR3.0-eYFP)mpn121</i>	This study	transgene	Available from Baier Lab

Genetic reagent ( <i>Danio rerio</i> )	<i>Tg(UAS:Cr.ChR2-YFP)icm11Tg</i>	PMID: 26752076	ZFIN ID: ZDB-ALT-150324-2	Available from EZRC (Fidelin <i>et al.</i> , 2015)
Genetic reagent ( <i>Danio rerio</i> )	<i>Tg(UAS:GFP)zf82</i>	PMID: 19835787	ZFIN ID: ZDB-ALT-080528-1	Asakawa <i>et al.</i> , 2008
Genetic reagent ( <i>Danio rerio</i> )	<i>Tg(isl2b.2:GAL4-VP16, myl7:EGFP)zc60Tg</i>	PMID: 20702722	ZFIN ID: ZDB-ALT-101130-1	Ben Fredj <i>et al.</i> , 2010
Genetic reagent ( <i>Danio rerio</i> )	<i>Tg(isl2b:GAL4-VP16, myl7:TagRFP)zc65</i>	PMID: 21905164	ZFIN ID: ZDB-FISH-150901-13523	Fujimoto <i>et al.</i> , 2011
Genetic reagent ( <i>Danio rerio</i> )	<i>Et(-0.6hsp70l:GAL4-VP16)s1020tEt</i>	PMID: 17369834	ZFIN ID: ZDB-ALT-070420-21	Scott <i>et al.</i> , 2007
Genetic reagent ( <i>Danio rerio</i> )	<i>Tg(mnx1:GAL4)icm23Tg</i>	PMID: 26946992	ZFIN ID: ZDB-ALT-160120-1	Böhm <i>et al.</i> , 2016
Genetic reagent ( <i>Danio rerio</i> )	<i>Et(-109Xla.Eef1a1:GFP)mn2Et</i>	PMID: 15347431	ZFIN ID: ZDB-ALT-080625-1	Balciunas <i>et al.</i> , 2004
Recombinant DNA reagent	<i>pTol1-UAS:ChrimsonR-tdTomato</i>	This study	Addgene ID: 124231	Available from Addgene
Recombinant DNA reagent	<i>pTol1-UAS:Chronos-tdTomato</i>	This study	Addgene ID: 124232	Available from Addgene
Recombinant DNA reagent	<i>pTol1-UAS:CoChR-tdTomato</i>	This study	Addgene ID: 124233	Available from Addgene
Recombinant DNA reagent	<i>pTol1-UAS:CheRiff-tdTomato</i>	This study	Addgene ID: 124234	Available from Addgene

Recombinant DNA reagent	<i>pTol1-UAS:GtACR1-tdTomato</i>	This study	Addgene ID: 124235	Available from Addgene
Recombinant DNA reagent	<i>pTol1-UAS:GtACR2-tdTomato</i>	This study	Addgene ID: 124236	Available from Addgene
Recombinant DNA reagent	<i>pTol1-UAS:ChR2(H134R)-tdTomato</i>	This study	Addgene ID: 124237	Available from Addgene
Recombinant DNA reagent	<i>pTol2-UAS:eArch3.0-eYFP</i>	This study	plasmid	Available from Baier lab
Recombinant DNA reagent	<i>pTol2-UAS:eNpHR3.0-eYFP</i>	This study	plasmid	Available from Baier lab
Sequence-based reagent	ChrimsonR_fw	This study	PCR primer	CTCAGCGTAAA GCCACCATGGG CGGAGCT
Sequence-based reagent	Chronos_fw	This study	PCR primer	CGTAAAGCCAC CATGGAAACAG CC
Sequence-based reagent	tdT_rev_40bp	This study	PCR primer	CTCGAGATCTC CATGTTTACTTA TACAGCTCATCC ATGCC
Sequence-based reagent	CoChR_fw	This study	PCR primer	CTCAGCGTAAA GCCACCATGCT GGGAAACG
Sequence-based reagent	CoChR_rev	This study	PCR primer	TACTACCGGTG CCGCCACTGT
Sequence-based reagent	CoChR_tdT_fw	This study	PCR primer	ACAGTGGCGGC ACCGGTAGTA
Sequence-based reagent	tdT_rev_45bp	This study	PCR primer	CTAGTCTCGAG ATCTCCATGTTT ACTTATACAGCT CATCCATGCC
Sequence-based reagent	CheRiff_fw	This study	PCR primer	CTCAGCGTAAA GCCACCATGGG CGGAGCT

Sequence-based reagent	CheRiff_rev	This study	PCR primer	CTACCGGTGCC GCCACTTTATCT TCCTCTGTCACG
Sequence-based reagent	CheRiff_tdT_fw	This study	PCR primer	TAAAGTGGCGG CACCGGTAGTA GCAGTGAG
Sequence-based reagent	GtACR1_fw	This study	PCR primer	CTCAGCGTAAA GCCACCATGAG CAGCATCACCT GTGATC
Sequence-based reagent	GtACR1_rev	This study	PCR primer	CTACCGGTGCC GCGGTCTCGCC GGCTCTGG
Sequence-based reagent	GtACR1_tdT_fw	This study	PCR primer	CGAGACCGCGG CACCGGTAGTA GCAGTGAG
Sequence-based reagent	GtACR2_fw	This study	PCR primer	CTCAGCGTAAA GCCACCATGGC CTCCCAGGTCT T
Sequence-based reagent	GtACR2_rev	This study	PCR primer	CTACCGGTGCC GCCCTGCCGAA CATTCTG
Sequence-based reagent	GtACR2_tdT_fw	This study	PCR primer	CGGCAGGGCGG CACCGGTAGTA GCAGTGAG
Sequence-based reagent	Chr2(H134R)_fw	This study	PCR primer	CTCAGCGTAAA GCCACCATGGA CTATGGCGGCG
Sequence-based reagent	Chr2(H134R)_rev	This study	PCR primer	TACTCACTGCTA CTACCGGTGCC GCCAC
Sequence-based reagent	Chr2(H134R)_tdT_fw	This study	PCR primer	ACCGGTAGTAG CAGTGAGTAAG G
Sequence-based reagent	eArch3.0_fw	This study	PCR primer	ATGAATTCGCCA CCATGGACCCC ATCGCTCT
Sequence-based reagent	eArch3.0_rev	This study	PCR primer	ATGCATGCTCAT TACACCTCGTTC TCGTAG

Sequence-based reagent	eNpHR3.0_fw	This study	PCR primer	ATGAATTCGCCA CCATGACAGAG ACCCTGC
Sequence-based reagent	eNpHR3.0_rev	This study	PCR primer	TACCATGGTTAC ACCTCGTTCTCG TAGC
Software, algorithm	MATLAB	MathWorks	RRID: SCR_001622	<a href="https://uk.mathworks.com/products/matlab.html">https://uk.mathworks.com/products/matlab.html</a>
Software, algorithm	Python	Anaconda	RRID: SCR_008394	<a href="https://www.anaconda.com">https://www.anaconda.com</a>
Software, algorithm	LabView	National Instruments	RRID: SCR_014325	<a href="http://www.ni.com/en-gb/shop/labview.html">http://www.ni.com/en-gb/shop/labview.html</a>
Software, algorithm	Prism	GraphPad	RRID: SCR_002798	<a href="https://www.graphpad.com/scientific-software/prism/">https://www.graphpad.com/scientific-software/prism/</a>

#### 410 **Experimental model**

411 Animals were reared on a 14/10 h light/dark cycle at 28.5°C. For all experiments, we used zebrafish  
 412 (*Danio rerio*) embryos and larvae homozygous for the *mitfa*<sup>w2</sup> skin-pigmentation mutation (Lister *et al.*,  
 413 1999). All larvae used for behavioural assays were fed *Paramecia* from 4 dpf onward. Animal handling  
 414 and experimental procedures were approved by the UCL Animal Welfare Ethical Review Body and  
 415 the UK Home Office under the Animal (Scientific Procedures) Act 1986.

416 *In vivo* electrophysiological recordings were performed in 5–6 dpf zebrafish larvae from AB and  
 417 Tüpfel long fin (TL) strains in accordance with the European Communities Council Directive  
 418 (2010/63/EU) and French law (87/848) and approved by the Institut du Cerveau et de la Moelle  
 419 épinière, the French ministry of Research and the Darwin Ethics Committee (APAFIS protocol  
 420 #16469-2018071217081175v5).

#### 421 **DNA cloning and transgenesis**

422 To generate the *UAS:opsin-tdTomato* DNA constructs used for transient opsin expression and for  
 423 creating the stable *Tg(UAS:opsin-tdTomato)* transgenic lines, the coding sequences of the opsins listed  
 424 below and the red fluorescent protein tdTomato (from *pAAV-Syn-Chronos-tdTomato*) were cloned in  
 425 frame into a UAS Tol1 backbone (*pT1UciMP*).

426 The source plasmids used for cloning *UAS:opsin-tdTomato* DNA constructs were:

- 427 • ChrimsonR from *pCAG-ChrimsonR-tdT* (Addgene plasmid # 59169)
- 428 • Chronos from *pAAV-Syn-Chronos-tdTomato* (Addgene plasmid # 62726)
- 429 • CoChR from *pAAV-Syn-CoChR-GFP* (Addgene plasmid # 59070)
- 430 • CheRiff from *FCK-CheRiff-eGFP* (Addgene plasmid # 51693)



- 431 • GtACR1 from *pFUGW-hGtACR1-EYFP* (Addgene plasmid # 67795)
- 432 • GtACR2 from *pFUGW-hGtACR2-EYFP* (Addgene plasmid # 67877)
- 433 • ChR2(H134R) from *pAAV-Syn-ChR2(H134R)-GFP* (Addgene plasmid # 58880)

434 The *pCAG-ChrimsonR-tdT*, *pAAV-Syn-Chronos-tdTomato*, *pAAV-Syn-CoChR-GFP* and *pAAV-Syn-*  
435 *ChR2(H134R)-GFP* plasmids were gifts from Edward Boyden (Boyden *et al.*, 2005; Klapoetke *et al.*,  
436 2014). The *FCK-CheRiff-eGFP* plasmid was a gift from Adam Cohen (Hochbaum *et al.*, 2014). The  
437 *pFUGW-hGtACR1-EYFP* and *pFUGW-hGtACR2-EYFP* plasmids were gifts from John Spudich  
438 (Govorunova *et al.*, 2015). The *pT1UciMP* plasmid was a gift from Harold Burgess (Addgene plasmid  
439 # 62215) (Horstick *et al.*, 2015).

440 The cloning was achieved using the In-Fusion HD Cloning Plus CE kit (Clontech) with the following  
441 primers:

- 442 • ChrimsonR\_fw, CTCAGCGTAAAGCCACCATGGGCGGAGCT
- 443 • Chronos\_fw, CGTAAAGCCACCATGGAAACAGCC
- 444 • CoChR\_fw, CTCAGCGTAAAGCCACCATGCTGGGAAACG
- 445 • CoChR\_rev, TACTACCGGTGCCGCCACTGT
- 446 • CoChR\_tdT\_fw, ACAGTGGCGGCACCGGTAGTA
- 447 • CheRiff\_fw, CTCAGCGTAAAGCCACCATGGGCGGAGCT
- 448 • CheRiff\_rev, CTACCGGTGCCGCCACTTTATCTTCCCTCTGTCACG
- 449 • CheRiff\_tdT\_fw, TAAAGTGGCGGCACCGGTAGTAGCAGTGAG
- 450 • GtACR1\_fw, CTCAGCGTAAAGCCACCATGAGCAGCATCACCTGTGATC
- 451 • GtACR1\_rev, CTACCGGTGCCCGGCTCTCGCCGGCTCTGG
- 452 • GtACR1\_tdT\_fw, CGAGACCGCGGCACCGGTAGTAGCAGTGAG
- 453 • GtACR2\_fw, CTCAGCGTAAAGCCACCATGGCCTCCCAGGTCGT
- 454 • GtACR2\_rev, CTACCGGTGCCGCCCTGCCGAACATTCTG
- 455 • GtACR2\_tdT\_fw, CGGCAGGGCGGCACCGGTAGTAGCAGTGAG
- 456 • ChR2(H134R)\_fw, CTCAGCGTAAAGCCACCATGGACTATGGCGGCG
- 457 • ChR2(H134R)\_rev, TACTCACTGCTACTACCGGTGCCGCCAC
- 458 • ChR2(H134R)\_tdT\_fw, ACCGGTAGTAGCAGTGAGTAAGG
- 459 • tdT\_rev\_40bp, CTCGAGATCTCCATGTTTACTTATAACAGCTCATCCATGCC
- 460 • tdT\_rev\_45bp, CTAGTCTCGAGATCTCCATGTTTACTTATAACAGCTCATCCATGCC

461 To generate the stable *Tg(UAS:opsin-tdTomato)* lines, purified *UAS:opsin-tdTomato* DNA constructs  
462 were first sequenced to confirm gene insertion and integrity and, subsequently, co-injected (35 ng/ $\mu$ l)  
463 with Tol1 transposase mRNA (80 ng/ $\mu$ l) into *Tg(KalTA4u508)* zebrafish embryos (Antinucci *et al.*,  
464 2019) at the early one-cell stage. Transient expression, visible as tdTomato fluorescence, was used to  
465 select injected embryos that were then raised to adulthood. Zebrafish codon-optimised *Tol1*  
466 transposase mRNA was prepared by *in vitro* transcription from NotI-linearised *pCS2-Tol1.zf1* plasmid  
467 using the SP6 transcription mMessage mMachine kit (Life Technologies). The *pCS2-Tol1.zf1* was a gift  
468 from Harold Burgess (Addgene plasmid # 61388) (Horstick *et al.*, 2015). RNA was purified using the  
469 RNeasy MinElute Cleanup kit (Qiagen). Germ line transmission was identified by mating sexually  
470 mature adult fish to *mitfa*<sup>w2/w2</sup> fish and subsequently examining their progeny for tdTomato  
471 fluorescence. Positive embryos from a single fish were then raised to adulthood. Once this second  
472 generation of fish reached adulthood, positive embryos from a single `founder` fish were again

473 selected and raised to adulthood to establish stable *Tg(KalTA4u508;UAS:opsin-tdTomato)* double-  
474 transgenic lines.

475 To generate the *UAS:opsin-eYFP* DNA constructs used for creating the stable *Tg(UAS:opsin-eYFP)*  
476 transgenic lines, the coding sequences of the opsins fused with eYFP listed below were cloned into a  
477 UAS Tol2 backbone (*pTol2 14xUAS:MCS*).

- 478 • *eArch3.0-eYFP* from *pAAV-CaMKIIa-eArch\_3.0-EYFP*
- 479 • *eNpHR3.0-eYFP* from *pAAV-Ef1a-DIO-eNpHR 3.0-EYFP*

480 The *pAAV-CaMKIIa-eArch\_3.0-EYFP* and *pAAV-Ef1a-DIO-eNpHR 3.0-EYFP* plasmids were gifts from  
481 Karl Deisseroth (Gradinaru *et al.*, 2010; Mattis *et al.*, 2011).

482 The coding sequences were amplified by PCR using the following primers and cloned into either  
483 EcoRI/NcoI (for eArch3.0) or EcoRI/SphI (for eNpHR3.0) sites of the *pTol2 14xUAS:MCS* plasmid:

- 484 • eArch3.0\_fw, ATGAATTCGCCACCATGGACCCCATCGCTCT
- 485 • eArch3.0\_rev, ATGCATGCTCATTACACCTCGTTCTCGTAG
- 486 • eNpHR3.0\_fw, ATGAATTCGCCACCATGACAGAGACCCTGC
- 487 • eNpHR3.0\_rev, TACCATGGTTACACCTCGTTCTCGTAGC

488 To generate the stable *Tg(UAS:opsin-eYFP)* lines, purified *UAS:opsin-eYFP* DNA constructs were first  
489 sequenced to confirm gene insertion and integrity and, subsequently, co-injected (25 ng/ $\mu$ l) with Tol2  
490 transposase mRNA (25 ng/ $\mu$ l) into *Tg(isl2b:GAL4-VP16, myl7:TagRFP)zc65* (Fujimoto *et al.*, 2011) (for  
491 eArch3.0-eYFP) or *Tg(s1020t:GAL4)* (Scott *et al.*, 2007) (for eNpHR3.0-eYFP) zebrafish embryos at the  
492 early one-cell stage. Transient expression, visible as eYFP fluorescence, was used to select injected  
493 embryos that were then raised to adulthood. Zebrafish codon-optimised Tol2 transposase mRNA was  
494 prepared by *in vitro* transcription from NotI-linearised *pCS2-zT2TP* plasmid using the SP6  
495 transcription mMessage mMachine kit (Life Technologies). The *pCS2-zT2TP* was a gift from Koichi  
496 Kawakami (Suster *et al.*, 2011). RNA was purified using the NucleoSpin Gel and PCR Clean-up kit  
497 (Macherey-Nagel). Germ line transmission was identified by mating sexually mature adult fish to  
498 *mitfa*<sup>w2/w2</sup> fish and, subsequently, examining their progeny for eYFP fluorescence. Positive embryos  
499 from each injected fish were then raised to adulthood. Once this second generation of fish reached  
500 adulthood, positive embryos from a single `founder` fish were again selected and raised to adulthood  
501 to establish stable *Tg(Isl2b:GAL4;UAS:eArch3.0-eYFP)* or *Tg(s1020t:GAL4;UAS:eNpHR3.0-eYFP)*  
502 double-transgenic lines.

### 503 Fluorescence image acquisition

504 Zebrafish embryos or larvae were mounted in 1% low-melting point agarose (Sigma-Aldrich) and  
505 anaesthetised using tricaine (MS-222, Sigma-Aldrich). Imaging was performed using a custom-built 2-  
506 photon microscope [XLUMPLFLN 20 $\times$  1.0 NA objective (Olympus), 580 nm PMT dichroic, band-pass  
507 filters: 510/84 (green), 641/75 (red) (Semrock), R10699 PMT (Hamamatsu Photonics), Chameleon  
508 II ultrafast laser (Coherent Inc)]. Imaging was performed at 1040 nm for opsin-tdTomato lines, while  
509 920 nm excitation was used for opsin-eYFP lines. In both cases, the same laser power at sample  
510 (10.7 mW) and PMT gain were used. For the images displayed in Figure 1C, 3B and 7B and Figure 7-  
511 figure supplement 3B, equivalent imaging field of view and pixel size were used (1200  $\times$  800 px,  
512 0.385  $\mu$ m/px). The imaging field of view and pixel size for images displayed in Figure 2C and 6B  
513 were 960  $\times$  680 px, 0.385  $\mu$ m/px. For all these images, the same acquisition averaging (mean image  
514 from 12 frames) and z-spacing of imaging planes (2  $\mu$ m) were used.

515 The image displayed in Figure 4A was acquired from a single plane on a fluorescence microscope  
516 [AxioExaminer D1 (Zeiss), 63× 1.0 NA objective (Zeiss), Xcite (Xcelitas, XT600) 480 nm LED  
517 illumination, 38HE filtercube (Zeiss), Imagem camera (Hamamatsu)], with an imaging field of view  
518 of 512 × 512 px and 0.135 μm/px pixel size.

## 519 **Behavioural assays**

520 The same monitoring system was used for all behavioural assays (see schematic in Figure 2A) with  
521 some differences. Images were acquired under infrared illumination (850 nm) using a high-speed  
522 camera (Mikrotron MC1362, 500 μs shutter-time) equipped with a machine vision lens (Fujinon  
523 HF35SA-1) and an 850 nm bandpass filter to block visible light. The 850 nm bandpass filter was  
524 removed during embryonic activation assays (in which images were acquired at 1,000 fps) to  
525 determine time of light stimulus onset. In all other assays, lower acquisition rates were used (i.e. 50  
526 or 500 fps) and, within each assay, the frames corresponding to stimulus onset/offset were consistent  
527 across trials.

528 Light was delivered across the whole arena from above using the following LEDs:

### 529 *For embryonic assays*

- 530 • 470 nm OSRAM Golden Dragon Plus LED (LB W5AM).
- 531 • 590 nm ProLight LED (PM2B-3LAE-SD).

### 532 *For larval assays*

- 533 • 459 nm OSRAM OSTAR Projection Power LED (LE B P2W).
- 534 • 617 nm OSRAM OSTAR Projection Power LED (LE A P2W).

535 The 459 and 617 nm LEDs were projected onto the arena with an aspheric condenser with diffuser  
536 surface. Irradiance was varied using constant current drive electronics with pulse-width modulation  
537 at 5 kHz. Irradiance was calibrated using a photodiode power sensor (Thorlabs S121C). LED and  
538 camera control were implemented using LabVIEW (National Instruments).

539 Before experiments, animals were screened for opsin expression in the target neural population at  
540 either 22 hpf (embryonic assays) or 3 dpf (larval assays) using a fluorescence stereomicroscope  
541 (Olympus MVX10). For each opsin, animals with similar expression level were selected for  
542 experiments together with control opsin-negative siblings. To reduce variability in opsin expression  
543 level, all animals used for behavioural experiments were heterozygous for both the GAL4 and UAS  
544 transgenes. Animals were placed in the arena in the dark for around 2 min before starting  
545 experiments. For all assays, each light stimulus was repeated at least 3 times. Each trial lasted 1 s in  
546 behavioural activation assays and 30 s in behavioural inhibition assays.

### 547 *Embryonic activation assay*

548 Opsin expression was targeted to trigeminal ganglion neurons using the *Tg(isl2b:GAL4)* transgene  
549 (Ben Fredj *et al.*, 2010). Behaviour was monitored at 1,000 fps across embryos (28–30 hpf) individually  
550 positioned in agarose wells (~2 mm diameter) in fish facility water and free to move within their  
551 chorion. Embryos were subjected to 5 or 40 ms pulses of blue (470 nm) or amber (590 nm) light at  
552 different irradiance levels (4.5–445 μW/mm<sup>2</sup>) and with a 15 s inter-stimulus interval in the dark.

### 553 *Embryonic inhibition assay*

554 Opsin expression was targeted to spinal primary and secondary motor neurons and interneurons  
555 (Kolmer-Agduhr cells and ventral longitudinal descending interneurons) using the *Tg(s1020t:GAL4)*  
556 transgene (Scott *et al.*, 2007). Behaviour was monitored at 50 fps across embryos (24–27 hpf)

557 individually positioned in agarose wells (~2 mm diameter) with fish facility water and free to move  
558 within their chorion. Embryos were subjected to 10 s pulses of blue (470 nm) or amber (590 nm) light  
559 at different irradiance levels (0–227  $\mu\text{W}/\text{mm}^2$ ) with a 50 s inter-stimulus interval in the dark.

#### 560 **Larval activation assay**

561 Opsin expression was targeted to primary and secondary spinal motor neurons using the  
562 *Tg(mnx1:GAL4)* transgene (Bohm *et al.*, 2016). Behaviour was monitored at 500 fps in 6 dpf larvae with  
563 their head restrained in 2% low-melting point agarose (Sigma-Aldrich) and their tail free to move.  
564 Larvae were subjected to 2 or 10 ms pulses of blue (459 nm) or red (617 nm) light at different  
565 irradiance levels (0.04–2.55  $\text{mW}/\text{mm}^2$ ) with a 20 s inter-stimulus interval in the dark. We also  
566 provided 250 ms trains of light pulses (1 ms pulse duration for blue light at 2.55  $\text{mW}/\text{mm}^2$  or 10 ms  
567 for red light at 1  $\text{mW}/\text{mm}^2$ ) at two pulse frequencies (20 or 40 Hz).

#### 568 **Larval inhibition assays**

569 Opsin expression was targeted to spinal cord neurons using either the *Tg(s1020t:GAL4)* or  
570 *Tg(mnx1:GAL4)* transgene, as above. Behaviour was monitored at 50 fps across larvae individually  
571 positioned in agarose wells (~1.4 cm diameter) with fish facility water in which they were free to  
572 swim. Larvae were subjected to 10 s pulses of blue (459 nm) or red (617 nm) light at different  
573 irradiance levels (0.24–2.55  $\text{mW}/\text{mm}^2$ ) with a 50 s inter-stimulus interval in the dark. Control trials  
574 during which no light pulse was provided were interleaved between light stimulation trials.

#### 575 **Behavioural data analysis**

576 Movie data was analysed using MATLAB (MathWorks). Region of interests (ROIs) containing  
577 individual fish were manually specified. For each ROI, the frame-by-frame change in pixel intensity  
578 –  $\Delta\text{Pixel}$  – was computed in the following way. For each trial, pixel intensity values were low-pass  
579 filtered across time frames and the absolute frame-by-frame difference in intensity ( $dI$ ) was obtained  
580 for each pixel. Pixels showing the highest variance in  $dI$  (top 5<sup>th</sup> percentile) were selected to compute  
581 their mean  $dI$ , corresponding to the ROI  $\Delta\text{Pixel}$  trace for the trial.

582 With the exception of the larval inhibition assay (see below), onset and offset of animal movements  
583 were detected from  $\Delta\text{Pixel}$  traces in the following way. For each ROI,  $\Delta\text{Pixel}$  traces were concatenated  
584 across all trials to estimate the probability density function ( $pdf$ ) of  $\Delta\text{Pixel}$  values. The portion of the  
585 distribution with values below the  $pdf$  peak was mirror-reflected about the  $x$ -axis and a Gaussian was  
586 fitted to the obtained symmetric distribution. The mean ( $\mu$ ) and standard deviation ( $\sigma$ ) of the fitted  
587 Gaussian were then used to compute ROI-specific  $\Delta\text{Pixel}$  thresholds for detecting onset ( $\mu + 6\sigma$ ) and  
588 offset ( $\mu + 3\sigma$ ) of animal movements.

589 For embryonic and larval activation assays, behavioural response latency corresponds to the time  
590 from light stimulus onset to the start of the first detected movement. Movements were classified as  
591 optogenetically-evoked if their response latency was shorter than 200 ms for the embryonic assay or  
592 50 ms for the larval assay, which corresponds to the minimum in the  $pdf$  of response latency from all  
593 opsin-expressing larvae (Figure 3E). For each animal, response probability to each light stimulus type  
594 corresponds to the fraction of trials in which at least one optogenetically-evoked movement was  
595 detected.

596 In the larval activation assay, the tail was tracked by performing consecutive annular line-scans,  
597 starting from a manually-selected body centroid and progressing towards the tip of the tail so as to  
598 define nine equidistant  $x$ - $y$  coordinates along the tail. Inter-segment angles were computed between

599 the eight resulting segments. Reported tail curvature was computed as the sum of these inter-segment  
600 angles. Rightward bending of the tail is represented by positive angles and leftward bending by  
601 negative angles. Number of tail beats corresponds to the number of full tail oscillation cycles. Tail  
602 theta-1 angle is the amplitude of the first half beat. Tail beat frequency was computed as the reciprocal  
603 of the mean full-cycle period during the first four tail oscillation cycles of a swim bout. Bout duration  
604 was determined from  $\Delta$ Pixel traces using the movement onset/offset thresholds described above.

605 For larval inhibition assays, images were background-subtracted using a background model  
606 generated over each trial (30 s duration). Images were then thresholded and the fish body centroid  
607 was found by running a particle detection routine for binary objects within suitable area limits.  
608 Tracking of body centroid position was used to compute fish speed, and periods in which speed was  
609 higher than 1 mm/s were classified as swim bouts. Bout speed was computed as the mean speed over  
610 the duration of each bout.

611 To account for group differences in baseline coil/bout rate and bout speed in inhibition assays, data  
612 was normalised at a given irradiance level by divided by the mean rate/speed across fish in control  
613 (no light) trials.

## 614 **Electrophysiological recordings**

### 615 *Transgenic lines*

616 Opsin expression was targeted to primary motor neurons using the *Tg(mnx1:GAL4)* transgene (Bohm  
617 *et al.*, 2016) with one exception: 11 out of 19 eNpHR3.0-expressing cells were recorded in  
618 *Tg(s1020t:GAL4)* larvae (Scott *et al.*, 2007). As in behavioural assays, all animals used for  
619 electrophysiological experiments were heterozygous for both the GAL4 and UAS transgenes. For  
620 control recordings, we targeted opsin-negative GFP-expressing primary motor neurons in  
621 *Tg(mnx1:GAL4;UAS:EGFP)* (Asakawa *et al.*, 2008) or *Tg(parga-GFP)* (Balciunas *et al.*, 2004) larvae. In  
622 all transgenic lines used, primary motor neurons could be unambiguously identified as the 3–4 largest  
623 cell somas, located in the dorsal-most portion of the motor column (Beattie *et al.*, 1997; Bello-Rojas  
624 *et al.*, 2019). We verified primary motor neuron identity in a small subset of recordings from eYFP-  
625 expressing cells in *Tg(mnx1:GAL4;UAS:Chr2(H134R)-eYFP)* larvae by adding 0.025%  
626 sulforhodamine-B acid chloride dye in the intracellular solution (Sigma-Aldrich) and filling the  
627 neuron to reveal its morphology. To maximise data acquisition in an in vivo preparation, when the  
628 first attempts of primary motor neuron recordings were not successful, we recorded neighbouring,  
629 dorsal located presumed secondary motor neurons (11 out of 86 included cells).

### 630 *Data acquisition*

631 Zebrafish larvae (5–6 dpf) were first paralysed in 1 mM  $\alpha$ -Bungarotoxin solution (Tocris) for 3–6 min  
632 after which they were pinned in a lateral position to a Sylgard-coated recording dish (Sylgard 184,  
633 Dow Corning) with tungsten pins inserted through the notochord. The skin was removed between  
634 the trunk and midbody regions using sharp forceps, after which the dorsal muscle from 2–3 somites  
635 was suctioned with glass pipettes (~50  $\mu$ m opening made from capillaries of 1.5 mm outer diameter,  
636 1.1 mm inner diameter; Sutter). Patch pipettes were made from capillary glass (1 mm outer diameter,  
637 0.58 mm inner diameter; WPI) with a horizontal puller (Sutter Instrument P1000) and had resistances  
638 between 8–16 M $\Omega$ . To first pass the dura, we applied a higher positive pressure (30–40 mm Hg) to the  
639 recording electrode via a pneumatic transducer (Fluke Biomedical, DPM1B), which was then lowered  
640 (20–25 mm Hg) once the electrode was near the cells. We generally recorded data from a single cell  
641 per larva. In a few instances, two cells from separate adjacent somites were recorded in the same fish.

642 External bath recording solution contained the following: 134 mM NaCl, 2.9 mM KCl, 2.1 mM CaCl<sub>2</sub>-  
643 H<sub>2</sub>O, 1.2 mM MgCl<sub>2</sub>, 10 mM glucose, and 10 mM HEPES, with pH adjusted to 7.8 with 9 mM NaOH  
644 and an osmolarity of 295 mOsm. We blocked glutamatergic and GABAergic synaptic transmission  
645 with a cocktail of: 20 μM CNQX or DNQX, 50 μM D-AP5, 10 μM Gabazine (Tocris) added to the  
646 external recording solution. The -50 mV ECl solution contained: 115 mM K-gluconate, 15 mM KCl, 2  
647 mM MgCl<sub>2</sub>, 4 mM Mg-ATP, 0.5 mM EGTA, 10 mM HEPES, with pH adjusted to 7.2 with 11mM KOH  
648 solution, and a 285 mOsm. In these conditions, we calculated the liquid junction potential (LJP;  
649 Clampfit calculator) to be 12.4 mV. The -70 mV ECl solution contained: 126 mM K-gluconate, 4 mM  
650 KCl, 2 mM MgCl<sub>2</sub>, 4 mM Mg-ATP, 0.5 mM EGTA, 10 mM HEPES, pH adjusted to 7.2 with 11mM  
651 KOH solution, 285 mOsm and a 13.3 mV LJP. All reagents were obtained from Sigma-Aldrich unless  
652 otherwise stated.

653 Recordings were made with an Axopatch 700B amplifier and digitised with Digidata 1440A or 1550B  
654 (Molecular Devices). pClamp software was used to acquire electrophysiological data at a sampling  
655 rate of 20 kHz and low-pass filtered at 2 kHz (voltage clamp) or 10 kHz (current clamp). Voltage  
656 clamp recordings were acquired with full whole-cell compensation and ~60% series resistance  
657 compensation, while corrections for bridge balance and electrode capacitance were applied in current  
658 clamp mode. Cells were visualised with a 63×/1.0 NA or a 60×/1.0 NA water-immersion objective  
659 (Zeiss or Nikon, respectively) on a fluorescence microscope equipped with differential interference  
660 contrast optics (AxioExaminer D1, Zeiss or Eclipse FN1, Nikon).

### 661 *Optogenetic stimulation*

662 Light stimulation was performed with either a X-Cite (Xcelitas, XT600) or a broadband white LED  
663 (Prizmatix, UHP-T-HCRI\_DI) light source equipped with a combination of different bandpass and  
664 neutral density filters to modulate irradiance at specific wavelengths (see Figure 4–figure  
665 supplement 1A for wavelengths and irradiance levels used to activate opsins). The onset, duration  
666 and irradiance level of light pulses were triggered and controlled via the Digidata device used for  
667 electrophysiological recordings.

668 For all cells, data was acquired in the following order: (1) series resistance was checked at the  
669 beginning, middle and end of recording; (2) action potential rheobase was determined by injecting  
670 5 ms pulses of current (160–340 pA) in current-clamp gap-free mode; (3) voltage clamp recording of  
671 opsin photocurrents; (4) current clamp recording of voltage responses induced by opsin activation.  
672 Light stimuli were provided from low to high irradiance levels across all protocols. For each protocol,  
673 inter-stimulus intervals were between 10 and 15 s.

674 For cation channelrhodopsins, we used a range of short light pulses. Voltage clamp recordings were  
675 paired with a 5 ms light pulse, while current clamp recordings were performed with 1, 2 or 5 ms-long  
676 pulses. In addition, we tested whether we could optogenetically entrain neurons to spike at  
677 frequencies ranging from 1 to 100 Hz using stimulus trains composed of 2 or 5 ms-long light pulses.

678 For anion channelrhodopsins and Cl<sup>-</sup>/H<sup>+</sup> pumps, voltage and current clamp recordings were paired  
679 with a 1 s light pulse. In addition, we used two different tests of optogenetic inhibition during active  
680 spiking. To assess single spike inhibition efficacy and precision, we evoked spiking by injecting 5 ms  
681 pulses of current at 1.2–1.5× rheobase for 10 trains at 5 Hz (1 s inter-train interval, total of 100 spikes  
682 triggered in 30 s), during which we provided 5 ms-long light pulses paired to the first current  
683 stimulus of the train and a subsequent one with progressively longer latency (Zhang *et al.*, 2007). To  
684 test opsin ability to inhibit tonic firing over longer time periods, we evoked spiking with longer pulses

685 of current (200–800 ms) at 1.2–1.5x rheobase paired with a light pulse (50–200 ms-long) in the middle  
686 of the current stimulation. We first recorded a control current injection-only trial, followed by current  
687 and light pulse trials with a 20 s inter-stimulus interval.

### 688 *Data analysis*

689 Data were analysed using the pyABF module in Spyder (3.3.6 MIT, running Python 3.6, scripts  
690 available here: [https://github.com/wyartlab/Antinucci\\_Dumitrescu\\_et\\_al\\_2020](https://github.com/wyartlab/Antinucci_Dumitrescu_et_al_2020)), MATLAB  
691 (MathWorks) and Clampfit (Molecular Devices). Series resistance ( $R_s$ ) was calculated as a cell  
692 response to a 5 or 10 mV hyperpolarisation step in voltage clamp from a holding potential of  $-60$  mV,  
693 with whole-cell compensation disabled. Membrane resistance ( $R_m$ ) was obtained from the steady  
694 holding current at the new step, and membrane capacitance ( $C_m$ ) corresponds to the area under the  
695 exponentially decaying current from peak to holding. We used the following cell inclusion criteria:  
696 (1) cell spiking upon injection of a 5 ms-long pulse of current; (2) membrane resting potential  $< -$   
697  $50$  mV at all times; (3)  $> 150$  pA current injection necessary to maintain the cell at a holding potential  
698 equal to resting potential in current clamp; (4) series resistance  $< 6\times$  pipette resistance at all times  
699 during the recording. We chose this conservative series resistance range as per previous  
700 electrophysiological procedures in other animal models: i.e. mammalian *in vivo* recordings with  
701 pipette resistance between  $4\text{--}7$  M $\Omega$  and max series resistance between  $10\text{--}100$  M $\Omega$  (Margrie *et al.*,  
702 2002). All reported membrane voltages were liquid junction potential corrected.

703 For voltage clamp recordings, we measured the maximum photocurrent amplitude in a time window  
704 of 100 ms (for cation channelrhodopsins) or 1 s (for anion channelrhodopsins and  $\text{Cl}^-/\text{H}^+$  pumps)  
705 duration starting from light onset. To characterise photocurrent kinetics of cation channelrhodopsins,  
706 we measured the time to peak photocurrent from light onset (i.e. activation time) and computed the  
707 response decay time constant by fitting a monoexponential decay function to the photocurrent from  
708 peak to baseline (i.e. deactivation time constant). To compute photocurrent kinetics of anion  
709 channelrhodopsins and  $\text{Cl}^-/\text{H}^+$  pumps, we fitted monoexponential functions to the following  
710 components of the response: activation time constant was computed from light onset to peak  
711 response, inactivation time constant from peak response to steady state (last 5 ms of light  
712 stimulation), deactivation time constant from steady state to baseline (1 s following light offset)

713 To characterise voltage responses induced by opsins under current clamp, we first classified events  
714 as spikes (when max voltage depolarisation was  $> -30$  mV) or sub-threshold (peak voltage deflection  
715  $< -30$  mV). For each response type, we measured the absolute peak of the response, the time to reach  
716 maximum response from light onset and the time-decay to baseline from peak by fitting a  
717 monoexponential decay function, as above. To assess firing pattern fidelity, we calculated the number  
718 of spikes per light pulse in a train, the latency from light onset to the first spike occurring within a  
719 10 ms time window, and the spike jitter as the standard deviation of spike latency values across a  
720 pulse train with given frequency.

721 Opsin efficacy in inhibiting single spikes was quantified using the following equation:

$$722 \quad I = \frac{S_C - S_{C+L}}{S_C} \times 100$$

723 where  $S_C$  is the mean number of spikes elicited by current pulses when no light was provided,  $S_{C+L}$  is  
724 the mean number of spikes elicited during time periods in which a light pulse was paired with a  
725 current pulse, and  $I$  is the inhibition index (100% being perfect inhibition and negative values  
726 indicating additional spikes were generated during light pulses). Tonic firing inhibition efficacy was

727 quantified by counting the number of spikes occurring during the light delivery period and  
728 normalising this count to provide spikes generated per 50 ms.

### 729 **Statistical analysis**

730 All statistical analyses were performed using Prism (GraphPad). Sample distributions were first  
731 assessed for normality and homoscedasticity. Details regarding the statistical tests used are reported  
732 in Supplementary File 2 for behavioural data and Supplementary File 3 for electrophysiological data.  
733 Significance threshold was set to 0.05 and all reported p-values were corrected for multiple  
734 comparisons. Tests were two-tailed for all experiments. Number of animals/cells are provided for  
735 each graph. No outliers were excluded from the analyses.



## 736 Figure legends

### 737 **Figure 1. Toolkit for targeted opsin expression**

738 **A** List of selected opsins, with spectral absorption and opsin class.

739 **B** Schematics of expression patterns in the GAL4 transgenic driver lines used in this study.

740 **C** Opsin expression in spinal neurons in *Tg(mnx1:GAL4;UAS:opsin-FP)* larvae at 5 dpf (for  
741 eNpHR3.0, the *s1020t:GAL4* transgene was used). Insets show magnified cell bodies to illustrate  
742 opsin membrane expression (for insets, brightness and contrast were adjusted independently for  
743 each opsin to aid visualisation). A, anterior; D, dorsal; P, posterior; V, ventral. Scale bar 20  $\mu\text{m}$  in  
744 large images, 5  $\mu\text{m}$  in insets.

745 **D** Behavioural assays and corresponding figure numbers.

746 **E** *In vivo* electrophysiological recordings and figure numbers.

### 747 **Figure 2. Optogenetic activation of embryonic trigeminal neurons triggers escape responses**

748 **A** Experimental setup for optogenetic stimulation and behavioural monitoring. IR, infrared.

749 **B** Schematic of behavioural assay.

750 **C** Opsin expression in trigeminal neurons in a *Tg(isl2b:GAL4;UAS:CoChR-tdTomato)* embryo at 1 dpf.  
751 Imaging field of view corresponds to black box in (B). A, anterior; D, dorsal; P, posterior; V, ventral.  
752 Scale bar 50  $\mu\text{m}$ .

753 **D** *Tg(isl2b:GAL4;UAS:CoChR-tdTomato)* embryos positioned in individual agarose wells. Behaviour  
754 was monitored at 1,000 frames per second across multiple embryos (28–30 hpf;  $N = 69 \pm 26$  fish per  
755 opsin group, mean  $\pm$  SD) subjected to 5 or 40 ms pulses of full-field illumination (470 or 590 nm,  
756 4.5–445  $\mu\text{W}/\text{mm}^2$ ) with a 15 s inter-stimulus interval.

757 **E** Optogenetically-triggered escape responses detected from  $\Delta\text{Pixel}$  traces in the 3 embryos  
758 indicated in (D). Dotted line indicates maximum latency (200 ms) for a response to be considered  
759 optogenetically-triggered.

760 **F,G** Response probability for transient (E) or stable (F) transgenic embryos expressing different  
761 opsins (mean  $\pm$  SEM, across fish). Insets show response latency for 5 ms blue light pulses in CoChR-  
762 expressing embryos (median  $\pm$  95% CI, across fish).

### 763 **Figure 2–figure supplement 1. Response probability vs. time in transient transgenic embryos 764 expressing opsins in trigeminal neurons**

765 **A–D** Distribution of response probability vs. time for *Tg(isl2b:GAL4)* embryos (28–30 hpf)  
766 expressing different opsins through transient transgenesis (mean + SD, across fish). Embryos were  
767 stimulated with 5 ms (A,B) or 40 ms (C,D) pulses of blue (470 nm; A,C) or amber (590 nm; B,D)  
768 light. Each time bin corresponds to 8 ms.

### 769 **Figure 2–figure supplement 2. Response probability vs. time in stable transgenic embryos 770 expressing opsins in trigeminal neurons**

771 **A–D** Distribution of response probability vs. time for *Tg(isl2b:GAL4)* embryos (28–30 hpf)  
772 expressing different opsins through stable transgenesis (mean + SD, across fish). Embryos were  
773 stimulated with 5 ms (A,B) or 40 ms (C,D) pulses of blue (470 nm; A,C) or amber (590 nm; B,D)  
774 light. Each time bin corresponds to 8 ms.

### 775 **Video 1. Escape responses elicited by optogenetic stimulation of embryonic trigeminal neurons**

776 Escape responses in *Tg(isl2b:GAL4;UAS:CoChR-tdTomato)* embryos (28–30 hpf) triggered by a 5 ms  
777 pulse of blue light (470 nm, 445  $\mu\text{W}/\text{mm}^2$ ). Images were acquired at 1,000 frames per second and  
778 the video plays at 0.1 $\times$  speed. Related to Figure 2.

779 **Figure 2–Source Data 1. Data related to Figure 2.**

780 Data provided as a XLSX file.

781 **Figure 3. Optogenetic activation of larval spinal motor neurons triggers tail movements**

782 **A** Schematics of behavioural assay. Head-restrained, tail-free larvae (6 dpf;  $N = 28 \pm 8$  fish per opsin  
783 group, mean  $\pm$  SD) were exposed to 2 or 10 ms pulses of light (459 or 617 nm, 0.04–2.55 mW/mm<sup>2</sup>)  
784 with a 20 s inter-stimulus interval while their behaviour was monitored at 500 fps. We also  
785 provided 250 ms trains of light pulses at 20 or 40 Hz.

786 **B** Opsin expression in spinal motor neurons in a *Tg(mnx1:GAL4;UAS:CoChR-tdTomato)* larva at  
787 5 dpf. Imaging field of view corresponds to black box in (A). A, anterior; D, dorsal; P, posterior; V,  
788 ventral. Scale bar 50  $\mu$ m.

789 **C** Swim bouts elicited by a pulse train in *Tg(mnx1:GAL4;UAS:CoChR-tdTomato)* larvae (left). The  
790 control, opsin-negative larva (right), does not respond within 148 ms after stimulus onset.

791 **D** Tail tracking, showing optogenetically-evoked swim bouts in a CoChR-expressing larva (bottom  
792 three rows) and a visually-evoked swim in a control opsin-negative larva (top). tbf, tail beat  
793 frequency.

794 **E** Distribution of response latencies for all tail movements in opsin-expressing (red) and control  
795 opsin-negative larvae (grey). Dotted line indicates maximum latency (50 ms) for a response to be  
796 considered optogenetically-triggered. Control larvae exclusively show long latency responses. Each  
797 time bin corresponds to 25 ms.

798 **F,L** Response probability of larvae expressing different opsins for single-pulse (**F**) or pulse-train (**L**)  
799 stimulation (mean  $\pm$  SEM, across fish).

800 **G–Q** Latency (**G,M**), bout duration (**H,N**), tail angle of the first half beat ( $\theta_1$ ; **I,O**), number of cycles  
801 (**J,P**) and tail beat frequency (**K,Q**) for single-pulse (**G–K**) or pulse-train (**M–Q**) stimulation  
802 (mean  $\pm$  SEM, across fish).

803 **Figure 3–figure supplement 1. Response probability vs. time in larvae expressing opsins in**  
804 **spinal motor neurons**

805 **A–D** Distribution of response probability vs. time for *Tg(mnx1:GAL4)* larvae (6 dpf) expressing  
806 different opsins (mean + SD, across fish). Larvae were stimulated with single 2 ms (**A,B**) or 10 ms  
807 (**C,D**) pulses of blue (459 nm; **A,C**) or red (617 nm; **B,D**) light. Each time bin corresponds to 2 ms.

808 **Video 2. Swim bouts elicited by single-pulse optogenetic stimulation of larval spinal motor**  
809 **neurons**

810 Swim responses in 3 head-restrained tail-free *Tg(mnx1:GAL4;UAS:CoChR-tdTomato)* larvae (6 dpf,  
811 left) triggered by a single 2 ms pulse of blue light (459 nm, 0.63 mW/mm<sup>2</sup>). A control opsin-  
812 negative larva is positioned on the right. Images were acquired at 500 frames per second and the  
813 video plays at 0.04 $\times$  speed. Related to Figure 3.

814 **Video 3. Swim bouts elicited by 20 Hz pulse train optogenetic stimulation of larval spinal motor**  
815 **neurons**

816 Swim responses in 3 head-restrained tail-free *Tg(mnx1:GAL4;UAS:CoChR-tdTomato)* larvae (6 dpf,  
817 left) triggered by a train of 1 ms pulses of blue light (459 nm, 20 Hz, 2.55 mW/mm<sup>2</sup>, 250 ms train  
818 duration). A control opsin-negative larva is positioned on the right. Images were acquired at  
819 500 frames per second and the video plays at 0.04 $\times$  speed. Related to Figure 3.

820 **Figure 3–Source Data 1. Data related to Figure 3.**

821 Data provided as a XLSX file.

822 **Figure 4. Electrophysiological recording of photocurrents in primary motor neurons**  
823 **A** Schematics of experimental setup for optogenetic stimulation with *in vivo* whole-cell patch clamp  
824 recordings. Image shows a patched primary motor neuron (pMN) expressing CoChR in a 6 dpf  
825 *Tg(mnx1:GAL4;UAS:CoChR-tdTomato)* larva. Scale bar 5  $\mu\text{m}$ .  
826 **B** Membrane resistance was not affected by opsin expression (mean  $\pm$  SD, across cells).  
827 **C** Resting membrane potential was similar between opsin-expressing and control neurons  
828 (mean  $\pm$  SD).  
829 **D** Examples of inward photocurrents in response to 5 ms light pulses (20 mW/mm<sup>2</sup>).  
830 **E** Peak photocurrent amplitude. CoChR and ChrimsonR induced the largest photocurrents  
831 (mean  $\pm$  SEM, across cells). Dotted lines show range of pMN rheobase. Data is pooled across  
832 stimulus intensity (1–30 mW/mm<sup>2</sup>) but see Figure 4–figure supplement 1 for data at varying  
833 irradiance.  
834 **F** Photocurrent activation time was similar across opsins (mean  $\pm$  SEM).  
835 **G** Chronos photocurrents had the fastest deactivation time constant, while CoChR and ChrimsonR  
836 showed similar deactivation kinetics (mean  $\pm$  SEM).

837 **Figure 4–figure supplement 1. Wavelengths used in electrophysiological recordings and**  
838 **photocurrent properties vs. irradiance**

839 **A** Wavelengths and irradiance levels used for each opsin line and control cells.  
840 **B** Number of cells patched in each group. Numbers and coloured bars indicate included cells while  
841 grey bars indicate excluded cells (see Materials and methods for inclusion criteria).  
842 **C,D** Access resistance (**C**) and cell capacitance (**D**) were comparable between groups (mean  $\pm$  SD,  
843 across cells).  
844 **E** Example photocurrents from a CoChR-expressing cell at different irradiance levels (3–  
845 20 mW/mm<sup>2</sup>).  
846 **F–H** Peak photocurrent amplitude (**F**), activation time (**G**) and deactivation time constant (**H**) vs.  
847 irradiance (mean  $\pm$  SEM, across cells). Dotted lines in (**F**) show range of pMN rheobase. Asterisks  
848 indicate a significant non-zero slope.

849 **Figure 4–Source Data 1. Data related to Figure 4.**

850 Data provided as a XLSX file.

851 **Figure 5. CoChR and ChrimsonR elicited spiking in primary motor neurons**

852 **A** Example membrane depolarisations induced by 5 ms light pulses (20 mW/mm<sup>2</sup>).  
853 **B** Number of optogenetically-evoked spikes vs. pulse duration (across irradiance levels 1–  
854 30 mW/mm<sup>2</sup>). Longer pulse duration induced more spikes in both CoChR- and ChrimsonR-  
855 expressing cells. Left plots show single neurons and right plot shows mean  $\pm$  SEM across cells.  
856 **C** Example voltage responses from CoChR- and ChrimsonR-expressing cells upon pulse train  
857 stimulation (1–100 Hz, 2–5 ms pulse duration).  
858 **D** Number of spikes vs. pulse number within a train (mean  $\pm$  SEM, across cells). In CoChR-  
859 expressing cells, the initial 3–4 pulses of the train induced bursts of 2–4 spikes.  
860 **E** Mean spike latency vs. pulse frequency (mean  $\pm$  SEM).  
861 **F** Spike latency vs. pulse number (mean  $\pm$  SEM). With increasing pulse frequency, CoChR-  
862 expressing cells showed progressively longer spike latency throughout the pulse train.  
863 **G** Spike jitter vs. pulse frequency (mean  $\pm$  SEM). ChrimsonR-expressing cells showed lower spike  
864 jitter than CoChR-expressing cells.

865 **Figure 5–figure supplement 1. Optogenetically-evoked voltage responses**

866 **A** Fraction of cells that generated spikes in response to single light pulses (1–5 ms).

867 **B** Peak depolarisation across irradiance levels (1–30 mW/mm<sup>2</sup>; mean ± SEM, across cells). Orange  
868 line indicates threshold for spike detection (–30 mV).  
869 **C** Time to peak depolarisation (mean ± SEM).  
870 **D** Number of evoked spikes vs. irradiance (1–5 ms pulse duration). In CoChR-expressing cells, 2–  
871 5 ms light pulses induced spike bursts (mean ± SEM).

872 **Figure 5–Source Data 1. Data related to Figure 5.**

873 Data provided as a XLSX file.

874 **Figure 6. Optogenetic suppression of coiling behaviour in embryos**

875 **A** Schematic of the behavioural assay.

876 **B** Opsin expression in spinal motor neurons and interneurons in a *Tg(s1020t:GAL4;UAS:GtACR1-tdTomato)*  
877 embryo at 1 dpf. Imaging field of view corresponds to black box in (A). A, anterior; D,  
878 dorsal; P, posterior; V, ventral. Scale bar 50 μm.

879 **C** Camera field of view showing *Tg(s1020t:GAL4;UAS:GtACR1-tdTomato)* embryos positioned in  
880 individual agarose wells. Behaviour was monitored at 50 frames per second across multiple  
881 embryos (24–27 hpf; N = 91 ± 16 fish per group, mean ± SD) subjected to 10 s light periods  
882 (470 or 590 nm, 0–227 μW/mm<sup>2</sup>) with a 50 s inter-stimulus interval.

883 **D** Tracking of coiling behaviour (mean ΔPixel from 3 trials) for the 3 embryos shown in (C). Black  
884 arrow indicates movements at light onset, whereas grey arrowhead indicates synchronised restart  
885 of coiling behaviour following light offset.

886 **E** Optogenetically-induced changes in coil rate (mean + SD, across fish) in embryos expressing the  
887 anion channelrhodopsin GtACR1 (N = 77 embryos, top) or the Cl<sup>-</sup> pump eNpHR3.0  
888 (N = 111 embryos, bottom). Horizontal dark grey bars indicate the 'late LED On' period. Each time  
889 bin corresponds to 2 s.

890 **F,G** Normalised coil rate during the 'late LED On' period in embryos expressing different opsins  
891 (mean ± SEM, across fish). Control opsin-negative siblings were subjected to the same light stimuli.

892 **Figure 6–figure supplement 1. Coil rate vs. time in embryos expressing different opsins in spinal  
893 neurons**

894 **A,B** Distribution of coil rate vs. time for *Tg(s1020t:GAL4)* embryos (24–27 hpf) expressing different  
895 opsins (mean + SD, across fish). Embryos were subjected to 10 s pulses of blue (470 nm; **A**) or amber  
896 (590 nm; **B**) light. Each time bin corresponds to 2 s.

897 **Figure 6–figure supplement 2. Coil rate vs. irradiance for the initial 2 seconds of light exposure**

898 **A,B** Normalised coil rate during the initial 2 s of the LED On period in embryos (24–27 hpf)  
899 expressing different opsins (mean ± SEM, across fish). Control opsin-negative siblings were  
900 subjected to the same light stimuli.

901 **Video 4. Monitoring of coiling behaviour upon opsin activation in embryonic spinal neurons**

902 Coiling behaviour in *Tg(s1020t:GAL4;UAS:GtACR2-tdTomato)* embryos (24–27 hpf) subjected to a  
903 10 s period of blue light (470 nm, 225 μW/mm<sup>2</sup>). Images were acquired at 50 frames per second and  
904 the video plays at 3× speed. Related to Figure 6.

905 **Figure 6–Source Data 1. Data related to Figure 6.**

906 Data provided as a XLSX file.

907 **Figure 7. Optogenetic suppression of swimming in larvae**

908 **A** Schematic of behavioural assay.

909 **B** Opsin expression in spinal motor neurons and interneurons in a *Tg(s1020t:GAL4;UAS:GtACR1-*  
910 *tdTomato)* larva at 5 dpf. Imaging field of view corresponds to black box in (A). A, anterior; D,  
911 dorsal; P, posterior; V, ventral. Scale bar 50  $\mu\text{m}$ .  
912 **C** *Tg(s1020t:GAL4;UAS:GtACR1-tdTomato)* larvae were positioned in individual agarose wells (left)  
913 and instantaneous swim speed was monitored by centroid tracking (right) at 50 fps (6 dpf;  
914  $N = 25 \pm 9$  fish per group, mean  $\pm$  SD). 10 s light periods were delivered (459 or 617 nm, 0–  
915 2.55  $\text{mW}/\text{mm}^2$ ) with a 50 s inter-stimulus interval.  
916 **D** Optogenetically-induced changes in bout rate (mean + SEM, across fish) in *Tg(s1020t:GAL4)*  
917 larvae expressing GtACR1 ( $N = 24$  larvae, left) or eNpHR3.0 ( $N = 40$  larvae, right). Horizontal grey  
918 bars indicate the time windows used to quantify behavioural changes. Each time bin corresponds to  
919 2 s.  
920 **E,F** Normalised bout rate during the `LED On` period in larvae expressing different opsins  
921 (mean  $\pm$  SEM, across fish) and in control, opsin-negative, siblings.

922 **Figure 7–figure supplement 1. Bout rate vs. time in larvae expressing different opsins in spinal**  
923 **neurons**

924 **A,B** Distribution of bout rate vs. time for *Tg(s1020t:GAL4)* larvae (6 dpf) expressing different opsins  
925 (mean + SD, across fish). Larvae were subjected to 10 s pulses of blue (459 nm; A) or red (617 nm; B)  
926 light. Each time bin corresponds to 2 s.

927 **Figure 7–figure supplement 2. Bout rate and speed vs. irradiance during different time periods in**  
928 ***Tg(s1020t:GAL4)* larvae**

929 **A,B** Normalised bout rate (A) or bout speed (B) during the whole LED On period, the initial 2 s of  
930 light exposure and the `post LED` 8 s period in *Tg(s1020t:GAL4)* larvae (6 dpf) expressing different  
931 opsins (mean  $\pm$  SEM, across fish). Control opsin-negative siblings were subjected to the same light  
932 stimuli.

933 **Figure 7–figure supplement 3. Optogenetic suppression of swimming in *Tg(mnx1:GAL4)* larvae**

934 **A** Schematics of opsin expression pattern and behavioural assay.

935 **B** Opsin expression in spinal motor neurons and interneurons in a *Tg(mnx1:GAL4;UAS:GtACR1-*  
936 *tdTomato)* larva at 5 dpf. Imaging field of view corresponds to black box in (A). A, anterior; D,  
937 dorsal; P, posterior; V, ventral. Scale bar 50  $\mu\text{m}$ .

938 **C** Background-subtracted camera field of view showing *Tg(mnx1:GAL4;UAS:GtACR1-tdTomato)*  
939 larvae positioned in individual agarose wells (left) and tracking of swimming speed for selected  
940 larvae (right). Behaviour was monitored at 50 fps across multiple freely-swimming larvae (6 dpf;  
941  $N = 24 \pm 6$  fish per group, mean  $\pm$  SD) while they were subjected to 10 s light periods  
942 (459 or 617 nm, 0–2.55  $\text{mW}/\text{mm}^2$ ) with a 50 s inter-stimulus interval.

943 **D** Optogenetically-induced changes in bout rate (mean + SEM, across fish) in *Tg(mnx1:GAL4)* larvae  
944 expressing GtACR1 ( $N = 29$  larvae, left) or eArch3.0 ( $N = 23$  larvae, right). Horizontal grey bars  
945 indicate the time windows used for comparative quantification of behavioural changes. Each time  
946 bin corresponds to 2 s.

947 **E,F** Normalised bout speed during the `LED On` period in larvae expressing different opsins  
948 (mean  $\pm$  SEM, across fish). Control opsin-negative siblings were subjected to the same light stimuli.

949 **Figure 7–figure supplement 4. Bout rate and speed vs. irradiance during different time periods in**  
950 ***Tg(mnx1:GAL4)* larvae**

951 **A–D** Normalised bout rate (A–C) or bout speed (D) during the whole `LED On` period (A), the  
952 initial 2 s of the light period (B), or the `post LED` 8 s period (C,D) in *Tg(mnx1:GAL4)* larvae (6 dpf)  
953 expressing different opsins (mean  $\pm$  SEM, across fish). Control opsin-negative siblings were  
954 subjected to the same light stimuli.

955 **Video 5. Suppression of swimming upon opsin activation in larval spinal neurons**

956 Suppression of swimming in *Tg(s1020t:GAL4;UAS:GtACR1-tdTomato)* larvae (6 dpf) during 10 s of  
957 blue light (459 nm, 0.24 mW/mm<sup>2</sup>). Images were acquired at 50 frames per second and the video  
958 plays at 3× speed. Related to Figure 7.

959 **Figure 7–Source Data 1. Data related to Figure 7.**

960 Data provided as a XLSX file.

961 **Figure 8. Photocurrents induced by anion channelrhodopsins and chloride/proton pumps**

962 **A** Action of anion channelrhodopsins (top) and Cl<sup>-</sup>/H<sup>+</sup> pumps (bottom). For anion  
963 channelrhodopsins, photocurrent magnitude and direction depend on chloride reversal potential  
964 (ECl) and holding potential (V<sub>hold</sub>), while Cl<sup>-</sup>/H<sup>+</sup> pumps always induce outward currents.

965 **B** Example photocurrents in response to a 1 s light exposure (20 mW/mm<sup>2</sup>).

966 **C,D** Photocurrent peak (**C**) and steady-state (**D**) amplitude (mean ± SEM, across cells). GtACRs  
967 induced larger photocurrents than Cl<sup>-</sup>/H<sup>+</sup> pumps.

968 **E–G** Photocurrent activation (**E**), inactivation (**F**) and deactivation (**G**) time constants (mean ± SEM).  
969 Photocurrents induced by Cl<sup>-</sup>/H<sup>+</sup> pumps showed minimal inactivation and faster deactivation  
970 kinetics than GtACRs. eNpHR3.0 photocurrents did not inactivate hence no inactivation time  
971 constant was computed.

972 **Figure 8–figure supplement 1. Photocurrent properties vs. irradiance**

973 **A** Example GtACR1 photocurrents obtained by providing a 1 s light periods at different holding  
974 potentials (V<sub>hold</sub>) using intracellular solutions approximating either embryonic or larval ECl. Orange  
975 traces denote holding potentials closest to ECl.

976 **B** GtACR1 photocurrent I-V curves (mean ± SD). Photocurrents reverse with a positive 5–10 mV  
977 shift relative to ECl (dotted lines) in both solutions.

978 **C** Example photocurrents from an eNpHR3.0-expressing cell at different irradiance levels (3–  
979 20 mW/mm<sup>2</sup>).

980 **D,E** Photocurrent peak (**D**) and steady-state (**E**) amplitude vs. irradiance (mean ± SEM, across cells).  
981 Asterisks indicate a significant non-zero slope.

982 **F–H** Photocurrent activation (**F**), inactivation (**G**) and deactivation (**H**) time constants vs. irradiance  
983 (mean ± SEM). eNpHR3.0 photocurrents did not inactivate hence no inactivation time constant was  
984 computed.

985 **Figure 8–Source Data 1. Data related to Figure 8.**

986 Data provided as a XLSX file.

987 **Figure 9. GtACRs and eNpHR3.0 effectively inhibited spiking**

988 **A** Example voltage deflections induced by anion channelrhodopsins and Cl<sup>-</sup>/H<sup>+</sup> pumps in response  
989 to a 1 s light pulse (20 mW/mm<sup>2</sup>).

990 **B–D** Peak (**B**) and steady-state (**C**) responses and deactivation time constant (**D**) of voltage  
991 deflections. All opsins induced similar absolute voltage changes. Anion channelrhodopsins  
992 generated depolarisation with both intracellular solutions while Cl<sup>-</sup>/H<sup>+</sup> pumps generated  
993 hyperpolarisation.

994 **E** Example recordings demonstrating inhibition of single spikes in GtACR1- and eNpHR3.0-  
995 expressing cells with 5 ms light pulses (3 mW/mm<sup>2</sup>).

996 **F** Fraction of spikes that were optogenetically inhibited (mean ± SEM, across cells). All opsins  
997 achieved high suppression efficacy, but GtACR1 induced additional spikes upon light delivery with  
998 the embryonic intracellular solution.

999 **G** Example recordings demonstrating inhibition of sustained spiking in GtACR1- and eNpHR3.0-  
1000 expressing cells.

1001 **H** Quantification of suppression using protocol illustrated in G. Number of spikes per 50 ms during  
1002 light delivery (0–10 mW/mm<sup>2</sup>) is plotted against irradiance. GtACR1 and eNpHR3.0 inhibited tonic  
1003 spiking with similar efficacy (mean ± SEM).

1004 **Figure 9-figure supplement 1. Optogenetically-evoked voltage responses vs. irradiance**

1005 **A–C** Peak (**A**) and steady-state (**B**) responses and deactivation time constant (**C**) of voltage  
1006 deflections vs. irradiance (mean ± SEM, across cells). eArch3.0 was the only opsin showing  
1007 irradiance-dependent modulation of peak voltage response.

1008 **Figure 9–Source Data 1. Data related to Figure 9.**

1009 Data provided as a XLSX file.

## 1010 References

- 1011 Adamantidis, A., Arber, S., Bains, J.S., Bamberg, E., Bonci, A., Buzsaki, G., Cardin, J.A., Costa, R.M., Dan, Y., Goda,  
1012 Y., *et al.* (2015). Optogenetics: 10 years after ChR2 in neurons--views from the community. *Nat Neurosci* *18*, 1202-  
1013 1212.
- 1014 Andalman, A.S., Burns, V.M., Lovett-Barron, M., Broxton, M., Poole, B., Yang, S.J., Grosenick, L., Lerner, T.N.,  
1015 Chen, R., Benster, T., *et al.* (2019). Neuronal Dynamics Regulating Brain and Behavioral State Transitions. *Cell* *177*,  
1016 970-985.e920.
- 1017 Antinucci, P., Folgueira, M., and Bianco, I.H. (2019). Pretectal neurons control hunting behaviour. *Elife* *8*.
- 1018 Arrenberg, A.B., Del Bene, F., and Baier, H. (2009). Optical control of zebrafish behavior with halorhodopsin. *Proc*  
1019 *Natl Acad Sci U S A* *106*, 17968-17973.
- 1020 Arrenberg, A.B., and Driever, W. (2013). Integrating anatomy and function for zebrafish circuit analysis. *Front Neural*  
1021 *Circuits* *7*, 74.
- 1022 Asakawa, K., and Kawakami, K. (2008). Targeted gene expression by the Gal4-UAS system in zebrafish. *Dev Growth*  
1023 *Differ* *50*, 391-399.
- 1024 Asakawa, K., Suster, M.L., Mizusawa, K., Nagayoshi, S., Kotani, T., Urasaki, A., Kishimoto, Y., Hibi, M., and  
1025 Kawakami, K. (2008). Genetic dissection of neural circuits by Tol2 transposon-mediated Gal4 gene and enhancer  
1026 trapping in zebrafish. *Proc Natl Acad Sci U S A* *105*, 1255-1260.
- 1027 Balciunas, D., Davidson, A.E., Sivasubbu, S., Hermanson, S.B., Welle, Z., and Ekker, S.C. (2004). Enhancer trapping  
1028 in zebrafish using the Sleeping Beauty transposon. *BMC Genomics* *5*, 62.
- 1029 Beattie, C.E., Hatta, K., Halpern, M.E., Liu, H., Eisen, J.S., and Kimmel, C.B. (1997). Temporal separation in the  
1030 specification of primary and secondary motoneurons in zebrafish. *Dev Biol* *187*, 171-182.
- 1031 Bello-Rojas, S., Istrate, A.E., Kishore, S., and McLean, D.L. (2019). Central and peripheral innervation patterns of  
1032 defined axial motor units in larval zebrafish. *J Comp Neurol* *527*, 2557-2572.
- 1033 Ben Fredj, N., Hammond, S., Otsuna, H., Chien, C.B., Burrone, J., and Meyer, M.P. (2010). Synaptic activity and  
1034 activity-dependent competition regulates axon arbor maturation, growth arrest, and territory in the retinotectal  
1035 projection. *J Neurosci* *30*, 10939-10951.
- 1036 Ben-Ari, Y. (2002). Excitatory actions of gaba during development: the nature of the nurture. *Nat Rev Neurosci* *3*, 728-  
1037 739.
- 1038 Bernal Sierra, Y.A., Rost, B.R., Pofahl, M., Fernandes, A.M., Kopton, R.A., Moser, S., Holtkamp, D., Masala, N.,  
1039 Beed, P., Tukker, J.J., *et al.* (2018). Potassium channel-based optogenetic silencing. *Nat Commun* *9*, 4611.
- 1040 Berndt, A., Lee, S.Y., Wietek, J., Ramakrishnan, C., Steinberg, E.E., Rashid, A.J., Kim, H., Park, S., Santoro, A.,  
1041 Frankland, P.W., *et al.* (2016). Structural foundations of optogenetics: Determinants of channelrhodopsin ion selectivity.  
1042 *Proc Natl Acad Sci U S A* *113*, 822-829.
- 1043 Berndt, A., Schoenenberger, P., Mattis, J., Tye, K.M., Deisseroth, K., Hegemann, P., and Oertner, T.G. (2011). High-  
1044 efficiency channelrhodopsins for fast neuronal stimulation at low light levels. *Proc Natl Acad Sci U S A* *108*, 7595-7600.
- 1045 Bohm, U.L., Prendergast, A., Djenuone, L., Nunes Figueiredo, S., Gomez, J., Stokes, C., Kaiser, S., Suster, M.,  
1046 Kawakami, K., Charpentier, M., *et al.* (2016). CSF-contacting neurons regulate locomotion by relaying mechanical  
1047 stimuli to spinal circuits. *Nat Commun* *7*, 10866.
- 1048 Boyden, E.S. (2011). A history of optogenetics: the development of tools for controlling brain circuits with light. *F1000*  
1049 *Biol Rep* *3*, 11.



- 1050 Boyden, E.S. (2015). Optogenetics and the future of neuroscience. *Nat Neurosci* 18, 1200-1201.
- 1051 Boyden, E.S., Zhang, F., Bamberg, E., Nagel, G., and Deisseroth, K. (2005). Millisecond-timescale, genetically targeted  
1052 optical control of neural activity. *Nat Neurosci* 8, 1263-1268.
- 1053 Chow, B.Y., Han, X., Dobry, A.S., Qian, X., Chuong, A.S., Li, M., Henninger, M.A., Belfort, G.M., Lin, Y.,  
1054 Monahan, P.E., *et al.* (2010). High-performance genetically targetable optical neural silencing by light-driven proton  
1055 pumps. *Nature* 463, 98-102.
- 1056 Deisseroth, K. (2015). Optogenetics: 10 years of microbial opsins in neuroscience. *Nat Neurosci* 18, 1213-1225.
- 1057 Deisseroth, K., and Hegemann, P. (2017). The form and function of channelrhodopsin. *Science* 357.
- 1058 Del Bene, F., and Wyart, C. (2012). Optogenetics: a new enlightenment age for zebrafish neurobiology. *Dev Neurobiol*  
1059 72, 404-414.
- 1060 Douglass, A.D., Kraves, S., Deisseroth, K., Schier, A.F., and Engert, F. (2008). Escape behavior elicited by single,  
1061 channelrhodopsin-2-evoked spikes in zebrafish somatosensory neurons. *Curr Biol* 18, 1133-1137.
- 1062 Drapeau, P., Ali, D.W., Buss, R.R., and Saint-Amant, L. (1999). In vivo recording from identifiable neurons of the  
1063 locomotor network in the developing zebrafish. *J Neurosci Methods* 88, 1-13.
- 1064 Fidelin, K., Djenoune, L., Stokes, C., Prendergast, A., Gomez, J., Baradel, A., Del Bene, F., and Wyart, C. (2015).  
1065 State-Dependent Modulation of Locomotion by GABAergic Spinal Sensory Neurons. *Curr Biol* 25, 3035-3047.
- 1066 Forster, D., Dal Maschio, M., Laurell, E., and Baier, H. (2017). An optogenetic toolbox for unbiased discovery of  
1067 functionally connected cells in neural circuits. *Nat Commun* 8, 116.
- 1068 Friedmann, D., Hoagland, A., Berlin, S., and Isacoff, E.Y. (2015). A spinal opsin controls early neural activity and drives  
1069 a behavioral light response. *Curr Biol* 25, 69-74.
- 1070 Fujimoto, E., Gaynes, B., Brimley, C.J., Chien, C.B., and Bonkowsky, J.L. (2011). Gal80 intersectional regulation of  
1071 cell-type specific expression in vertebrates. *Dev Dyn* 240, 2324-2334.
- 1072 Govorunova, E.G., Sineshchekov, O.A., Janz, R., Liu, X., and Spudich, J.L. (2015). Natural light-gated anion channels:  
1073 A family of microbial rhodopsins for advanced optogenetics. *Science* 349, 647-650.
- 1074 Gradinaru, V., Thompson, K.R., Zhang, F., Mogri, M., Kay, K., Schneider, M.B., and Deisseroth, K. (2007). Targeting  
1075 and readout strategies for fast optical neural control in vitro and in vivo. *J Neurosci* 27, 14231-14238.
- 1076 Gradinaru, V., Zhang, F., Ramakrishnan, C., Mattis, J., Prakash, R., Diester, I., Goshen, I., Thompson, K.R., and  
1077 Deisseroth, K. (2010). Molecular and cellular approaches for diversifying and extending optogenetics. *Cell* 141, 154-165.
- 1078 Hochbaum, D.R., Zhao, Y., Farhi, S.L., Klapoetke, N., Werley, C.A., Kapoor, V., Zou, P., Kralj, J.M., Maclaurin, D.,  
1079 Smedemark-Margulies, N., *et al.* (2014). All-optical electrophysiology in mammalian neurons using engineered microbial  
1080 rhodopsins. *Nat Methods* 11, 825-833.
- 1081 Horstick, E.J., Jordan, D.C., Bergeron, S.A., Tabor, K.M., Serpe, M., Feldman, B., and Burgess, H.A. (2015).  
1082 Increased functional protein expression using nucleotide sequence features enriched in highly expressed genes in  
1083 zebrafish. *Nucleic Acids Res* 43, e48.
- 1084 Huber, D., Petreanu, L., Ghitani, N., Ranade, S., Hromadka, T., Mainen, Z., and Svoboda, K. (2008). Sparse optical  
1085 microstimulation in barrel cortex drives learned behaviour in freely moving mice. *Nature* 451, 61-64.
- 1086 Kikuta, H., and Kawakami, K. (2009). Transient and stable transgenesis using tol2 transposon vectors. *Methods Mol*  
1087 *Biol* 546, 69-84.

- 1088 Kimmel, C.B., Hatta, K., and Metcalfe, W.K. (1990). Early axonal contacts during development of an identified  
1089 dendrite in the brain of the zebrafish. *Neuron* 4, 535-545.
- 1090 Klapoetke, N.C., Murata, Y., Kim, S.S., Pulver, S.R., Birdsey-Benson, A., Cho, Y.K., Morimoto, T.K., Chuong, A.S.,  
1091 Carpenter, E.J., Tian, Z., *et al.* (2014). Independent optical excitation of distinct neural populations. *Nat Methods* 11,  
1092 338-346.
- 1093 Li, N., Chen, S., Guo, Z.V., Chen, H., Huo, Y., Inagaki, H.K., Chen, G., Davis, C., Hansel, D., Guo, C., *et al.* (2019).  
1094 Spatiotemporal constraints on optogenetic inactivation in cortical circuits. *Elife* 8.
- 1095 Lister, J.A., Robertson, C.P., Lepage, T., Johnson, S.L., and Raible, D.W. (1999). *nacre* encodes a zebrafish  
1096 microphthalmia-related protein that regulates neural-crest-derived pigment cell fate. *Development* 126, 3757-3767.
- 1097 Luo, L., Callaway, E.M., and Svoboda, K. (2008). Genetic dissection of neural circuits. *Neuron* 57, 634-660.
- 1098 Mahn, M., Gibor, L., Patil, P., Cohen-Kashi Malina, K., Oring, S., Printz, Y., Levy, R., Lampl, I., and Yizhar, O.  
1099 (2018). High-efficiency optogenetic silencing with soma-targeted anion-conducting channelrhodopsins. *Nat Commun* 9,  
1100 4125.
- 1101 Mahn, M., Prigge, M., Ron, S., Levy, R., and Yizhar, O. (2016). Biophysical constraints of optogenetic inhibition at  
1102 presynaptic terminals. *Nat Neurosci* 19, 554-556.
- 1103 Malyshev, A.Y., Roshchin, M.V., Smirnova, G.R., Dolgikh, D.A., Balaban, P.M., and Ostrovsky, M.A. (2017).  
1104 Chloride conducting light activated channel GtACR2 can produce both cessation of firing and generation of action  
1105 potentials in cortical neurons in response to light. *Neurosci Lett* 640, 76-80.
- 1106 Mardinly, A.R., Oldenburg, I.A., Pegard, N.C., Sridharan, S., Lyall, E.H., Chesnov, K., Brohawn, S.G., Waller, L.,  
1107 and Adesnik, H. (2018). Precise multimodal optical control of neural ensemble activity. *Nat Neurosci* 21, 881-893.
- 1108 Margrie, T.W., Brecht, M., and Sakmann, B. (2002). In vivo, low-resistance, whole-cell recordings from neurons in the  
1109 anaesthetized and awake mammalian brain. *Pflugers Arch* 444, 491-498.
- 1110 Mattis, J., Tye, K.M., Ferenczi, E.A., Ramakrishnan, C., O'Shea, D.J., Prakash, R., Gunaydin, L.A., Hyun, M., Fenno,  
1111 L.E., Gradinaru, V., *et al.* (2011). Principles for applying optogenetic tools derived from direct comparative analysis of  
1112 microbial opsins. *Nat Methods* 9, 159-172.
- 1113 Menelaou, E., and McLean, D.L. (2012). A gradient in endogenous rhythmicity and oscillatory drive matches  
1114 recruitment order in an axial motor pool. *J Neurosci* 32, 10925-10939.
- 1115 Miesenbock, G. (2009). The optogenetic catechism. *Science* 326, 395-399.
- 1116 Miesenbock, G. (2011). Optogenetic control of cells and circuits. *Annu Rev Cell Dev Biol* 27, 731-758.
- 1117 Mohamed, G.A., Cheng, R.K., Ho, J., Krishnan, S., Mohammad, F., Claridge-Chang, A., and Jesuthasan, S. (2017).  
1118 Optical inhibition of larval zebrafish behaviour with anion channelrhodopsins. *BMC Biol* 15, 103.
- 1119 Portugues, R., Severi, K.E., Wyart, C., and Ahrens, M.B. (2013). Optogenetics in a transparent animal: circuit function  
1120 in the larval zebrafish. *Curr Opin Neurobiol* 23, 119-126.
- 1121 Prigge, M., Schneider, F., Tsunoda, S.P., Shilyansky, C., Wietek, J., Deisseroth, K., and Hegemann, P. (2012). Color-  
1122 tuned channelrhodopsins for multiwavelength optogenetics. *J Biol Chem* 287, 31804-31812.
- 1123 Reynolds, A., Brustein, E., Liao, M., Mercado, A., Babilonia, E., Mount, D.B., and Drapeau, P. (2008). Neurogenic  
1124 role of the depolarizing chloride gradient revealed by global overexpression of KCC2 from the onset of development. *J*  
1125 *Neurosci* 28, 1588-1597.
- 1126 Sagasti, A., Guido, M.R., Raible, D.W., and Schier, A.F. (2005). Repulsive interactions shape the morphologies and  
1127 functional arrangement of zebrafish peripheral sensory arbors. *Curr Biol* 15, 804-814.

- 1128 Saint-Amant, L., and Drapeau, P. (1998). Time course of the development of motor behaviors in the zebrafish embryo. *J*  
1129 *Neurobiol* *37*, 622-632.
- 1130 Saint-Amant, L., and Drapeau, P. (2000). Motoneuron activity patterns related to the earliest behavior of the zebrafish  
1131 embryo. *J Neurosci* *20*, 3964-3972.
- 1132 Saint-Amant, L., and Drapeau, P. (2003). Whole-cell patch-clamp recordings from identified spinal neurons in the  
1133 zebrafish embryo. *Methods Cell Sci* *25*, 59-64.
- 1134 Scheer, N., and Campos-Ortega, J.A. (1999). Use of the Gal4-UAS technique for targeted gene expression in the  
1135 zebrafish. *Mech Dev* *80*, 153-158.
- 1136 Schneider, F., Grimm, C., and Hegemann, P. (2015). Biophysics of Channelrhodopsin. *Annu Rev Biophys* *44*, 167-186.
- 1137 Scott, E.K., Mason, L., Arrenberg, A.B., Ziv, L., Gosse, N.J., Xiao, T., Chi, N.C., Asakawa, K., Kawakami, K., and  
1138 Baier, H. (2007). Targeting neural circuitry in zebrafish using GAL4 enhancer trapping. *Nat Methods* *4*, 323-326.
- 1139 Sjulson, L., Cassataro, D., DasGupta, S., and Miesenbock, G. (2016). Cell-Specific Targeting of Genetically Encoded  
1140 Tools for Neuroscience. *Annu Rev Genet* *50*, 571-594.
- 1141 Song, J., Ampatzis, K., Bjornfors, E.R., and El Manira, A. (2016). Motor neurons control locomotor circuit function  
1142 retrogradely via gap junctions. *Nature* *529*, 399-402.
- 1143 Suster, M.L., Abe, G., Schouw, A., and Kawakami, K. (2011). Transposon-mediated BAC transgenesis in zebrafish.  
1144 *Nat Protoc* *6*, 1998-2021.
- 1145 Warp, E., Agarwal, G., Wyart, C., Friedmann, D., Oldfield, C.S., Conner, A., Del Bene, F., Arrenberg, A.B., Baier,  
1146 H., and Isacoff, E.Y. (2012). Emergence of patterned activity in the developing zebrafish spinal cord. *Curr Biol* *22*, 93-  
1147 102.
- 1148 Williams, R.H., Tsunematsu, T., Thomas, A.M., Bogyo, K., Yamanaka, A., and Kilduff, T.S. (2019). Transgenic  
1149 Archaelhodopsin-3 Expression in Hypocretin/Orexin Neurons Engenders Cellular Dysfunction and Features of Type 2  
1150 Narcolepsy. *J Neurosci*.
- 1151 Wyart, C., Del Bene, F., Warp, E., Scott, E.K., Trauner, D., Baier, H., and Isacoff, E.Y. (2009). Optogenetic dissection  
1152 of a behavioural module in the vertebrate spinal cord. *Nature* *461*, 407-410.
- 1153 Yizhar, O., Fenno, L.E., Davidson, T.J., Mogri, M., and Deisseroth, K. (2011). Optogenetics in neural systems. *Neuron*  
1154 *71*, 9-34.
- 1155 Zhang, F., Wang, L.P., Brauner, M., Liewald, J.F., Kay, K., Watzke, N., Wood, P.G., Bamberg, E., Nagel, G.,  
1156 Gottschalk, A., *et al.* (2007). Multimodal fast optical interrogation of neural circuitry. *Nature* *446*, 633-639.
- 1157 Zhang, R.W., Wei, H.P., Xia, Y.M., and Du, J.L. (2010). Development of light response and GABAergic excitation-to-  
1158 inhibition switch in zebrafish retinal ganglion cells. *J Physiol* *588*, 2557-2569.
- 1159

# Figure 1

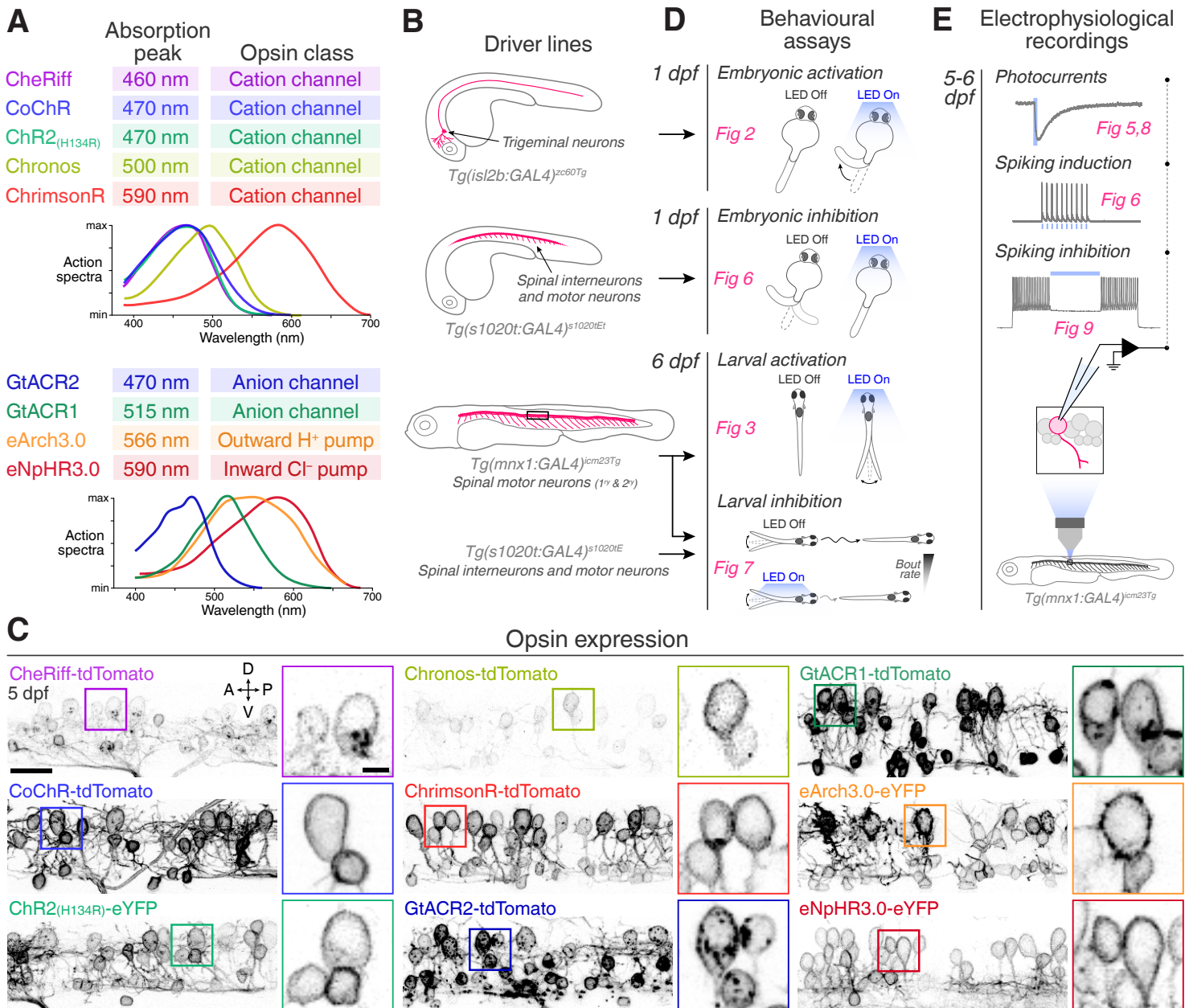


**Figure 1. Toolkit for targeted opsin expression**

**A** List of selected opsins, with spectral absorption and opsin class.

**B** Schematics of expression patterns in the GAL4 transgenic driver lines used in this study.

**C** Opsin expression in spinal neurons in *Tg(mnx1:GAL4;UAS:opsin-FP)* larvae at 5 dpf (for eNpHR3.0, the *s1020t:GAL4* transgene was used). Insets show magnified cell bodies to illustrate opsin membrane expression (for insets, brightness and contrast were adjusted independently for each opsin to aid visualisation). A, anterior; D, dorsal; P, posterior; V, ventral. Scale bar 20 μm in large images, 5 μm in insets.

**D** Behavioural assays and corresponding figure numbers.

**E** *In vivo* electrophysiological recordings and figure numbers.

# Figure 2

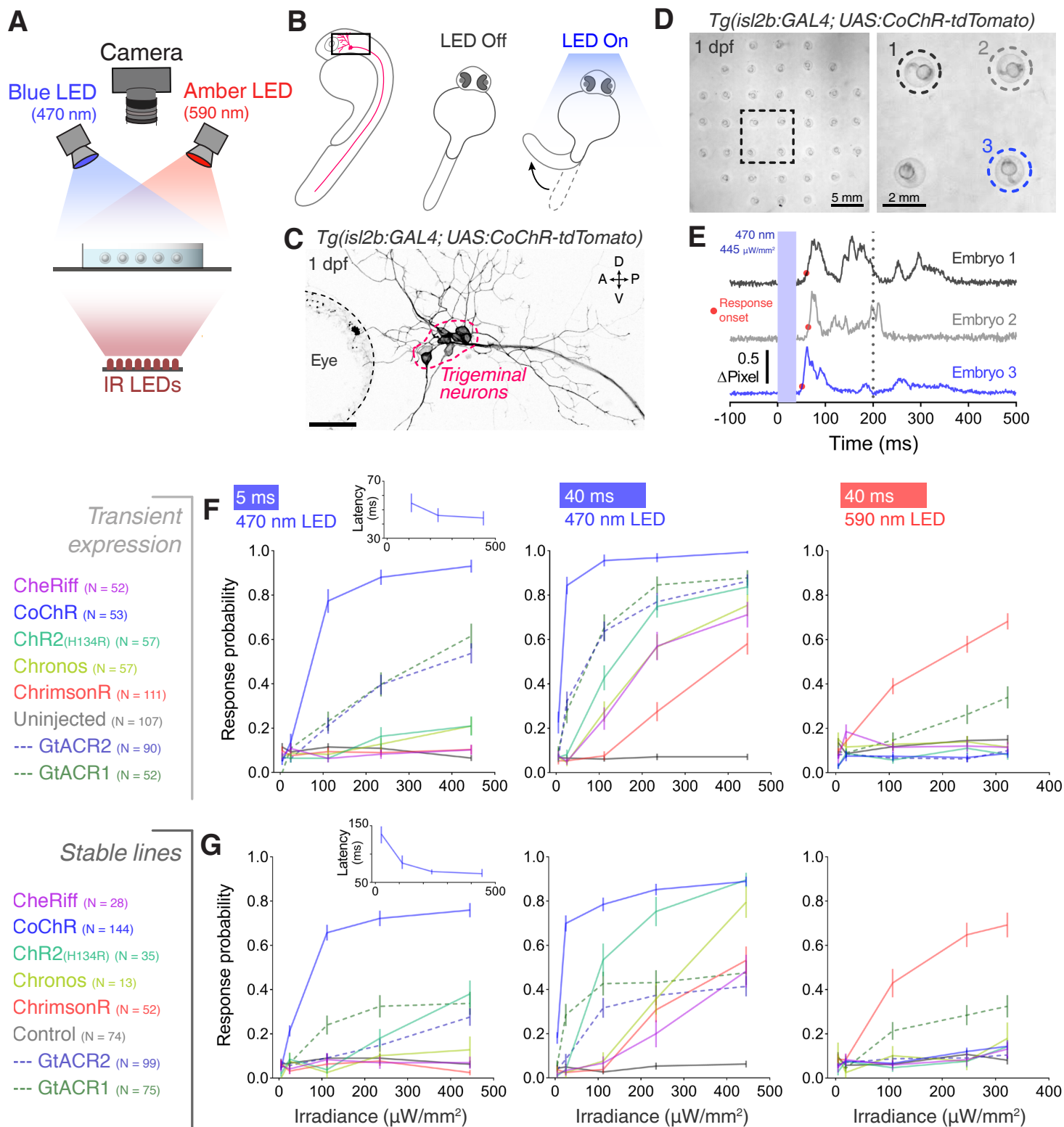


**Figure 2. Optogenetic activation of embryonic trigeminal neurons triggers escape responses**

**A** Experimental setup for optogenetic stimulation and behavioural monitoring. IR, infrared.

**B** Schematic of behavioural assay.

**C** Opsin expression in trigeminal neurons in a *Tg(isl2b:GAL4;UAS:CoChR-tdTomato)* embryo at 1 dpf. Imaging field of view corresponds to black box in (B). A, anterior; D, dorsal; P, posterior; V, ventral. Scale bar 50  $\mu\text{m}$ .

**D** *Tg(isl2b:GAL4;UAS:CoChR-tdTomato)* embryos positioned in individual agarose wells. Behaviour was monitored at 1,000 frames per second across multiple embryos (28–30 hpf;  $N = 69 \pm 26$  fish per opsin group, mean  $\pm$  SD) subjected to 5 or 40 ms pulses of full-field illumination (470 or 590 nm, 4.5–445  $\mu\text{W}/\text{mm}^2$ ) with a 15 s inter-stimulus interval.

**E** Optogenetically-triggered escape responses detected from  $\Delta\text{Pixel}$  traces in the 3 embryos indicated in (D). Dotted line indicates maximum latency (200 ms) for a response to be considered optogenetically-triggered.

**F,G** Response probability for transient (E) or stable (F) transgenic embryos expressing different opsins (mean  $\pm$  SEM, across fish). Insets show response latency for 5 ms blue light pulses in CoChR-expressing embryos (median  $\pm$  95% CI, across fish).

# Figure 2–figure supplement 1

## Transient expression

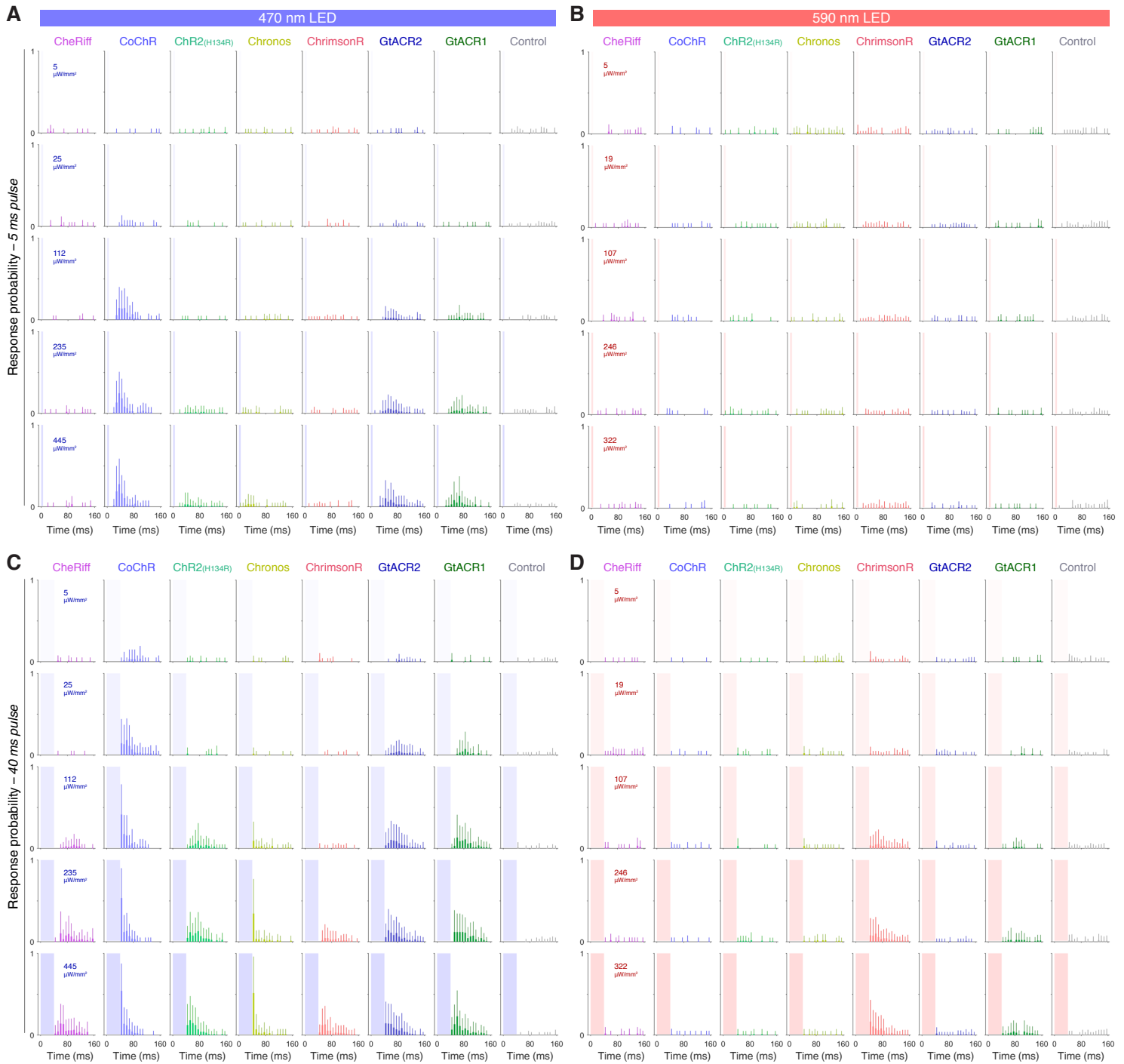


**Figure 2–figure supplement 1. Response probability vs. time in transient transgenic embryos expressing opsins in trigeminal neurons**

**A–D** Distribution of response probability vs. time for *Tg(isl2b:GAL4)* embryos (28–30 hpf) expressing different opsins through transient transgenesis (mean + SD, across fish). Embryos were stimulated with 5 ms (A,B) or 40 ms (C,D) pulses of blue (470 nm; A,C) or amber (590 nm; B,D) light. Each time bin corresponds to 8 ms.

# Figure 2–figure supplement 2

## Stable lines

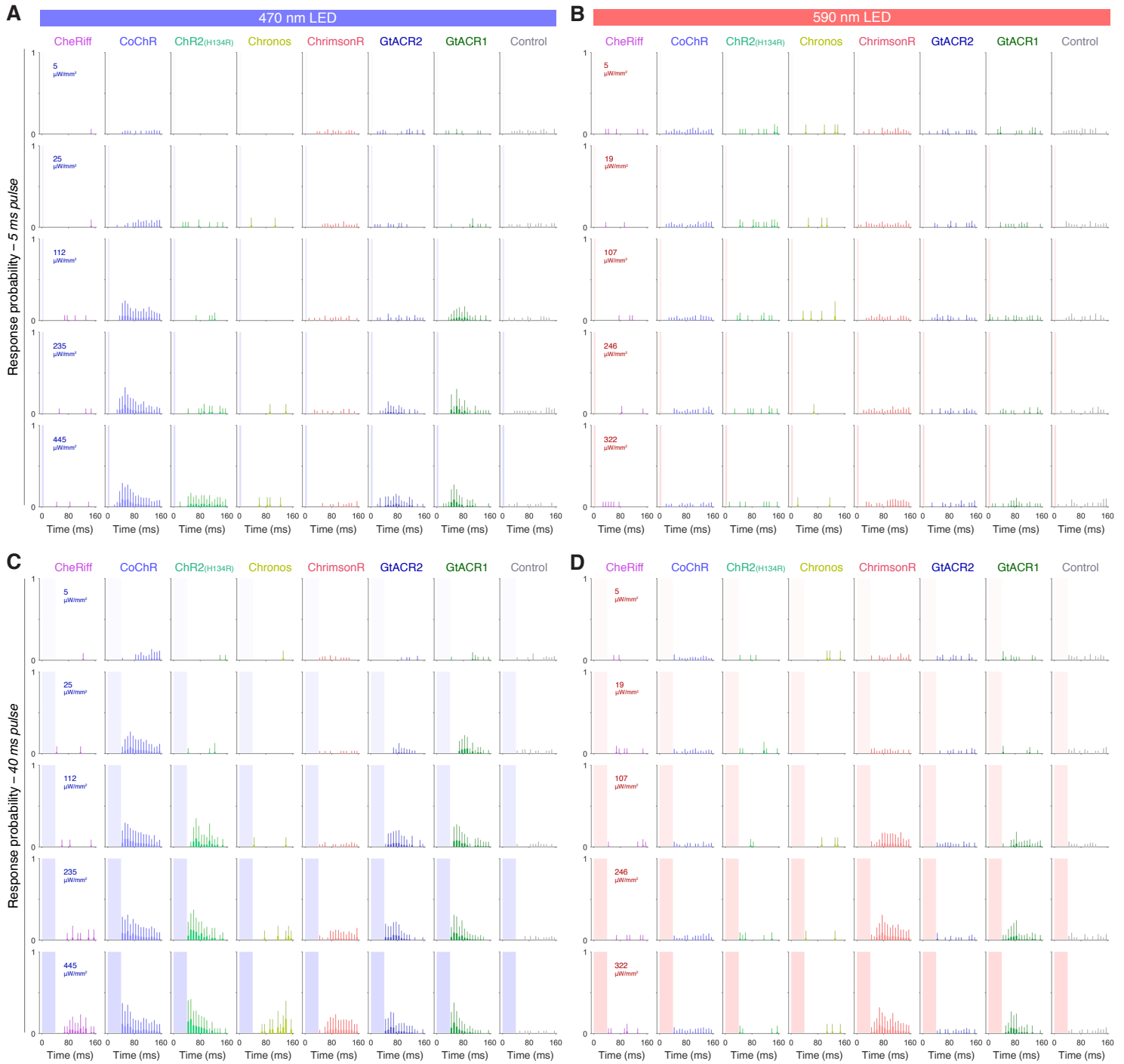


**Figure 2–figure supplement 2. Response probability vs. time in stable transgenic embryos expressing opsins in trigeminal neurons**

**A–D** Distribution of response probability vs. time for *Tg(isl2b:GAL4)* embryos (28–30 hpf) expressing different opsins through stable transgenesis (mean + SD, across fish). Embryos were stimulated with 5 ms (A,B) or 40 ms (C,D) pulses of blue (470 nm; A,C) or amber (590 nm; B,D) light. Each time bin corresponds to 8 ms.

# Figure 3

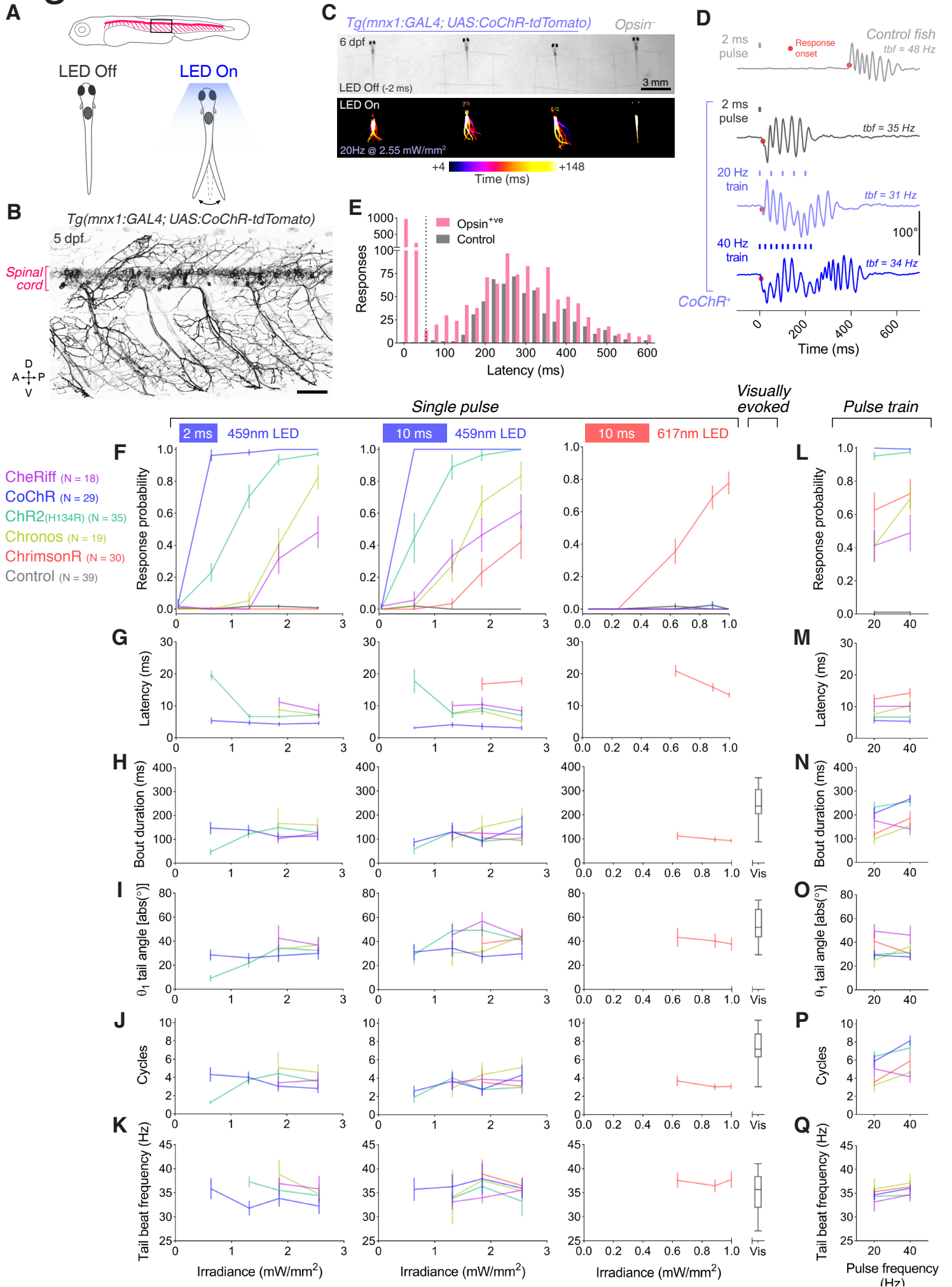




**Figure 3. Optogenetic activation of larval spinal motor neurons triggers tail movements**

- A** Schematics of behavioural assay. Head-restrained, tail-free larvae (6 dpf;  $N = 28 \pm 8$  fish per opsin group, mean  $\pm$  SD) were exposed to 2 or 10 ms pulses of light (459 or 617 nm, 0.04–2.55 mW/mm<sup>2</sup>) with a 20 s inter-stimulus interval while their behaviour was monitored at 500 fps. We also provided 250 ms trains of light pulses at 20 or 40 Hz.
- B** Opsin expression in spinal motor neurons in a *Tg(mnx1:GAL4;UAS:CoChR-tdTomato)* larva at 5 dpf. Imaging field of view corresponds to black box in (A). A, anterior; D, dorsal; P, posterior; V, ventral. Scale bar 50  $\mu$ m.
- C** Swim bouts elicited by a pulse train in *Tg(mnx1:GAL4;UAS:CoChR-tdTomato)* larvae (left). The control, opsin-negative larva (right), does not respond within 148 ms after stimulus onset.
- D** Tail tracking, showing optogenetically-evoked swim bouts in a CoChR-expressing larva (bottom three rows) and a visually-evoked swim in a control opsin-negative larva (top). tbf, tail beat frequency.
- E** Distribution of response latencies for all tail movements in opsin-expressing (red) and control opsin-negative larvae (grey). Dotted line indicates maximum latency (50 ms) for a response to be considered optogenetically-triggered. Control larvae exclusively show long latency responses. Each time bin corresponds to 25 ms.
- F,L** Response probability of larvae expressing different opsins for single-pulse (F) or pulse-train (L) stimulation (mean  $\pm$  SEM, across fish).
- G–Q** Latency (G,M), bout duration (H,N), tail angle of the first half beat (I,O), number of cycles (J,P) and tail beat frequency (K,Q) for single-pulse (G–K) or pulse-train (M–Q) stimulation (mean  $\pm$  SEM, across fish).

# Figure 3–figure supplement 1

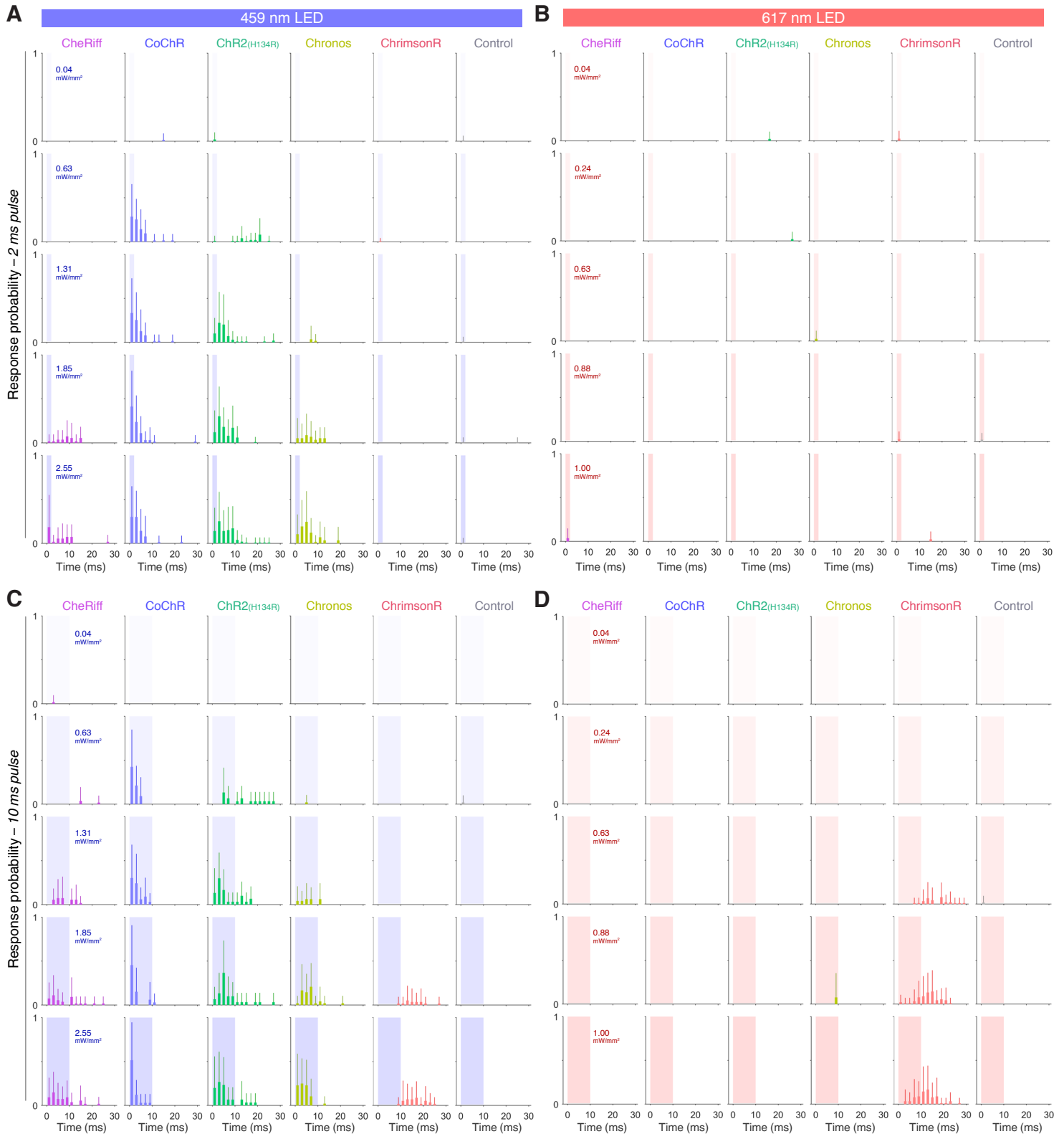


**Figure 3–figure supplement 1. Response probability vs. time in larvae expressing opsins in spinal motor neurons**  
**A–D** Distribution of response probability vs. time for *Tg(mnx1:GAL4)* larvae (6 dpf) expressing different opsins (mean + SD, across fish). Larvae were stimulated with single 2 ms (A,B) or 10 ms (C,D) pulses of blue (459 nm; A,C) or red (617 nm; B,D) light. Each time bin corresponds to 2 ms.

# Figure 4

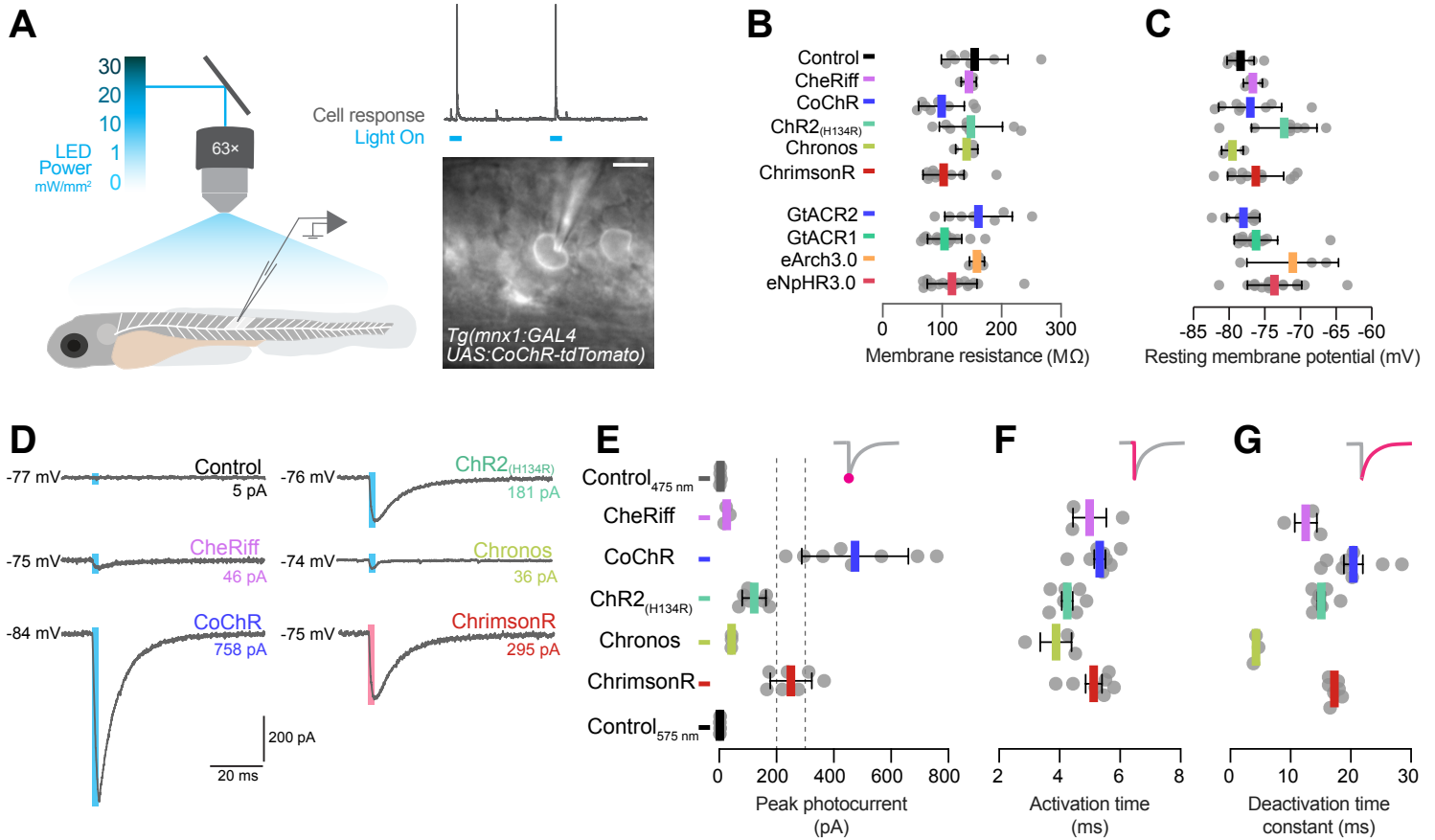


## Figure 4. Electrophysiological recording of photocurrents in primary motor neurons

**A** Schematics of experimental setup for optogenetic stimulation with in vivo whole-cell patch clamp recordings. Image shows a patched primary motor neuron (pMN) expressing CoChR in a 6 dpf *Tg(mnx1:GAL4;UAS:CoChR-tdTomato)* larva. Scale bar 5  $\mu\text{m}$ .

**B** Membrane resistance was not affected by opsin expression (mean  $\pm$  SD, across cells).

**C** Resting membrane potential was similar between opsin-expressing and control neurons (mean  $\pm$  SD).

**D** Examples of inward photocurrents in response to 5 ms light pulses (20  $\text{mW}/\text{mm}^2$ ).

**E** Peak photocurrent amplitude. CoChR and ChrimsonR induced the largest photocurrents (mean  $\pm$  SEM, across cells). Dotted lines show range of pMN rheobase. Data is pooled across stimulus intensity (1–30  $\text{mW}/\text{mm}^2$ ) but see Figure 4–figure supplement 1 for data at varying irradiance.

**F** Photocurrent activation time was similar across opsins (mean  $\pm$  SEM).

**G** Chronos photocurrents had the fastest deactivation time constant, while CoChR and ChrimsonR showed similar deactivation kinetics (mean  $\pm$  SEM).

# Figure 4–figure supplement 1

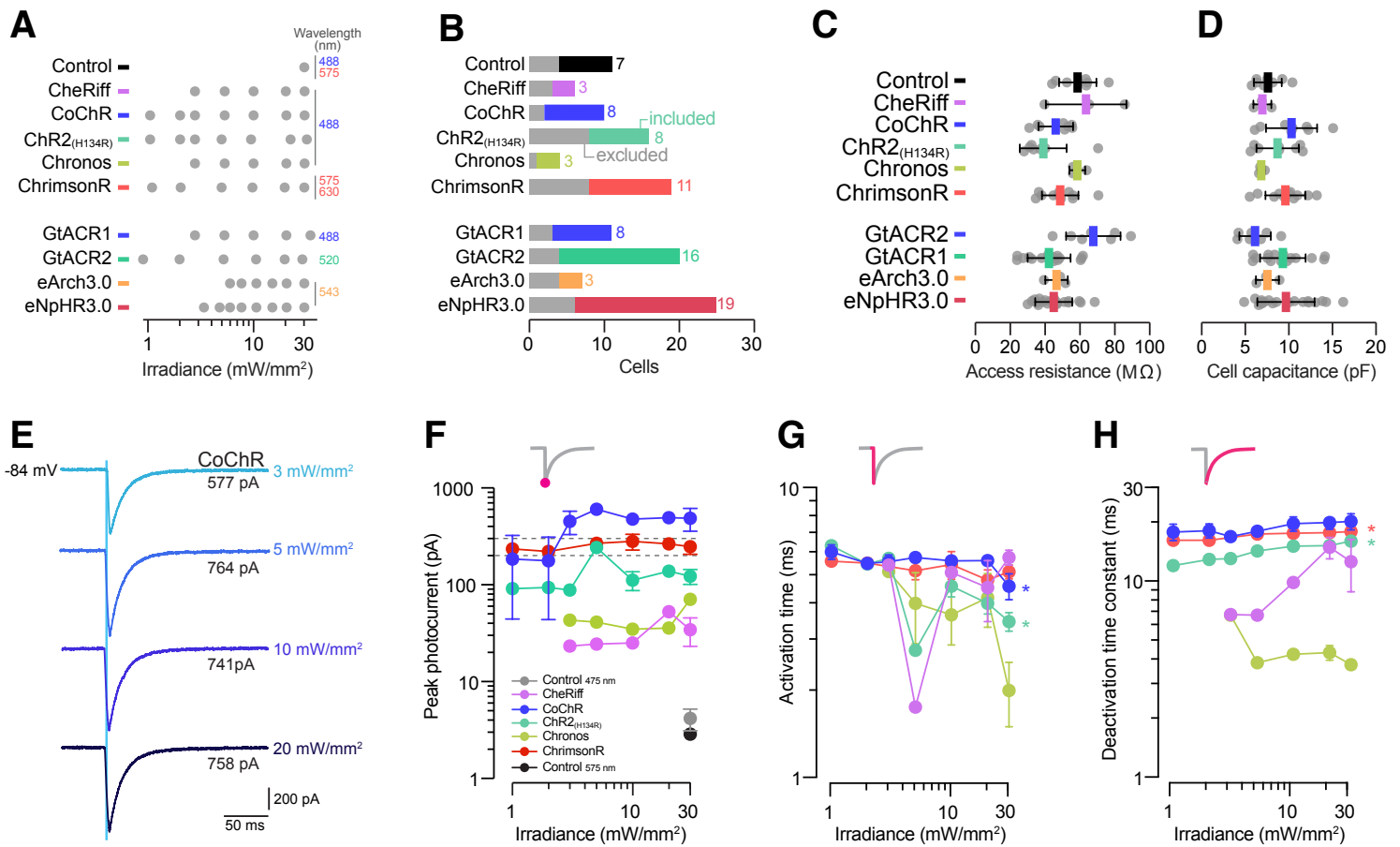


**Figure 4–figure supplement 1. Wavelengths used in electrophysiological recordings and photocurrent properties vs. irradiance**

**A** Wavelengths and irradiance levels used for each opsin line and control cells.

**B** Number of cells patched in each group. Numbers and coloured bars indicate included cells while grey bars indicate excluded cells (see Materials and methods for inclusion criteria).

**C, D** Access resistance (C) and cell capacitance (D) were comparable between groups (mean ± SD, across cells).

**E** Example photocurrents from a CoChR-expressing cell at different irradiance levels (3–20 mW/mm<sup>2</sup>).

**F–H** Peak photocurrent amplitude (F), activation time (G) and deactivation time constant (H) vs. irradiance (mean ± SEM, across cells). Dotted lines in (F) show range of pMN rheobase. Asterisks indicate a significant non-zero slope.

# Figure 5

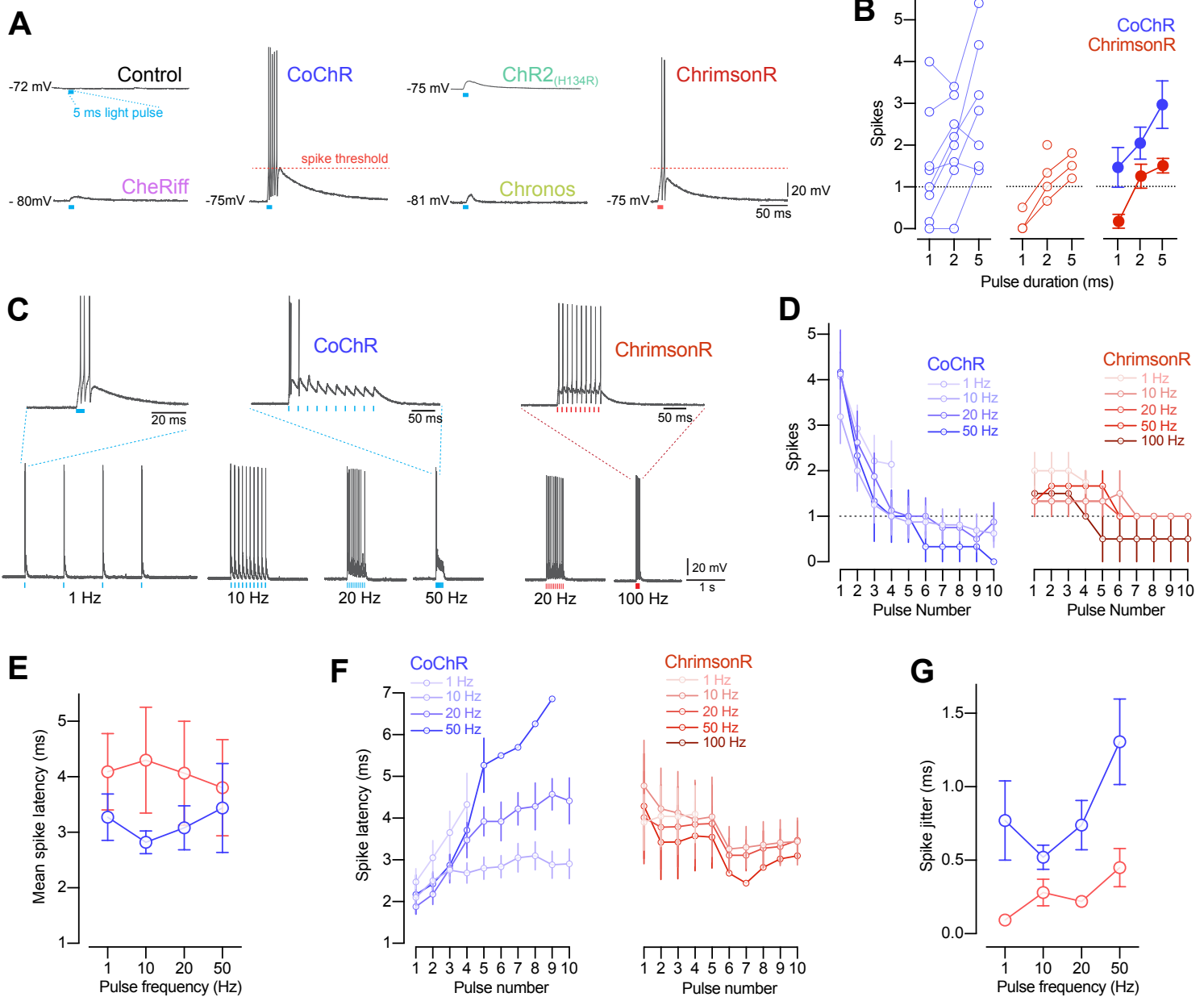


**Figure 5. CoChR and ChrimsonR elicited spiking in primary motor neurons**

**A** Example membrane depolarisations induced by 5 ms light pulses (20 mW/mm<sup>2</sup>).

**B** Number of optogenetically-evoked spikes vs. pulse duration (across irradiance levels 1–30 mW/mm<sup>2</sup>). Longer pulse duration induced more spikes in both CoChR- and ChrimsonR-expressing cells. Left plots show single neurons and right plot shows mean ± SEM across cells.

**C** Example voltage responses from CoChR- and ChrimsonR-expressing cells upon pulse train stimulation (1–100 Hz, 2–5 ms pulse duration).

**D** Number of spikes vs. pulse number within a train (mean ± SEM, across cells). In CoChR-expressing cells, the initial 3–4 pulses of the train induced bursts of 2–4 spikes.

**E** Mean spike latency vs. pulse frequency (mean ± SEM).

**F** Spike latency vs. pulse number (mean ± SEM). With increasing pulse frequency, CoChR-expressing cells showed progressively longer spike latency throughout the pulse train.

**G** Spike jitter vs. pulse frequency (mean ± SEM). ChrimsonR-expressing cells showed lower spike jitter than CoChR-expressing cells.

# Figure 5–figure supplement 1

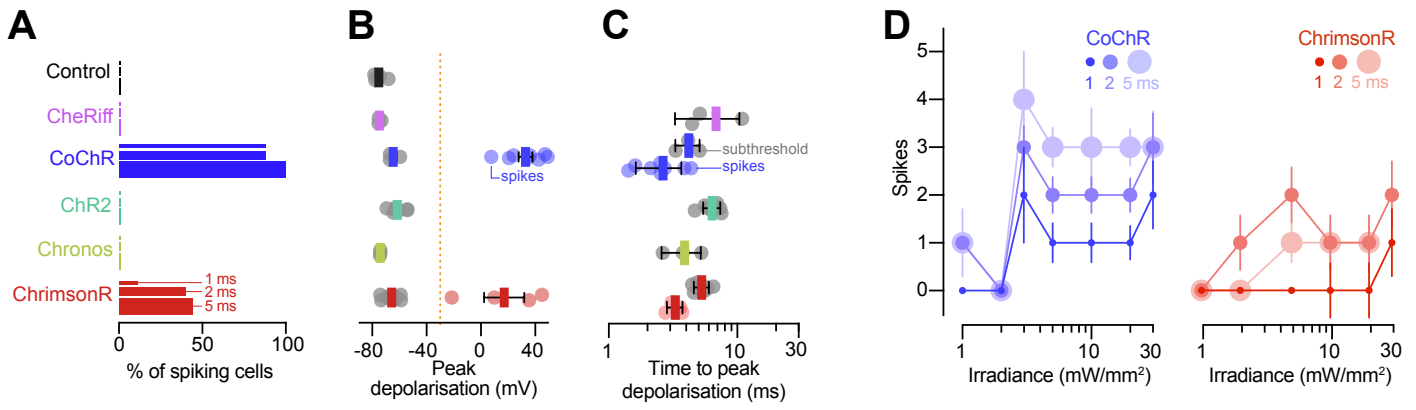


## Figure 5–figure supplement 1. Optogenetically-evoked voltage responses

**A** Fraction of cells that generated spikes in response to single light pulses (1–5 ms).

**B** Peak depolarisation across irradiance levels (1–30 mW/mm<sup>2</sup>; mean ± SEM, across cells). Orange line indicates threshold for spike detection (–30 mV).

**C** Time to peak depolarisation (mean ± SEM).

**D** Number of evoked spikes vs. irradiance (1–5 ms pulse duration). In CoChR-expressing cells, 2–5 ms light pulses induced spike bursts (mean ± SEM).

# Figure 6

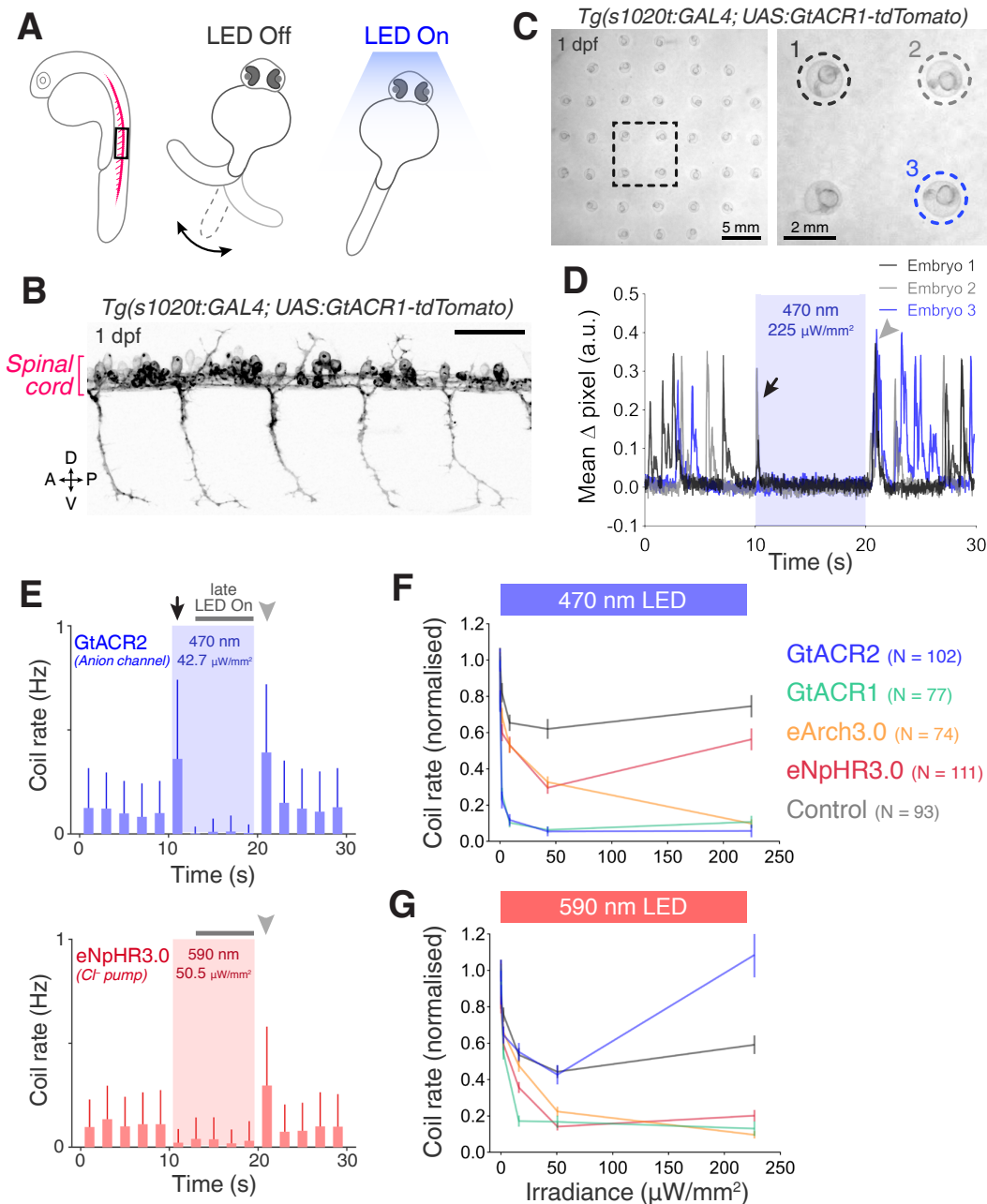


**Figure 6. Optogenetic suppression of coiling behaviour in embryos**

**A** Schematic of the behavioural assay.

**B** Opsin expression in spinal motor neurons and interneurons in a *Tg(s1020t:GAL4;UAS:GtACR1-tdTomato)* embryo at 1 dpf. Imaging field of view corresponds to black box in (A). A, anterior; D, dorsal; P, posterior; V, ventral. Scale bar 50  $\mu\text{m}$ .

**C** Camera field of view showing *Tg(s1020t:GAL4;UAS:GtACR1-tdTomato)* embryos positioned in individual agarose wells. Behaviour was monitored at 50 frames per second across multiple embryos (24–27 hpf; N = 91  $\pm$  16 fish per group, mean  $\pm$  SD) subjected to 10 s light periods (470 or 590 nm, 0–227  $\mu\text{W}/\text{mm}^2$ ) with a 50 s inter-stimulus interval.

**D** Tracking of coiling behaviour (mean  $\Delta\text{Pixel}$  from 3 trials) for the 3 embryos shown in (C). Black arrow indicates movements at light onset, whereas grey arrowhead indicates synchronised restart of coiling behaviour following light offset.

**E** Optogenetically-induced changes in coil rate (mean  $\pm$  SD, across fish) in embryos expressing the anion channelrhodopsin GtACR1 (N = 77 embryos, top) or the Cl<sup>-</sup> pump eNpHR3.0 (N = 111 embryos, bottom). Horizontal dark grey bars indicate the 'late LED On' period. Each time bin corresponds to 2 s.

**F,G** Normalised coil rate during the 'late LED On' period in embryos expressing different opsins (mean  $\pm$  SEM, across fish). Control opsin-negative siblings were subjected to the same light stimuli.

# Figure 6–figure supplement 1

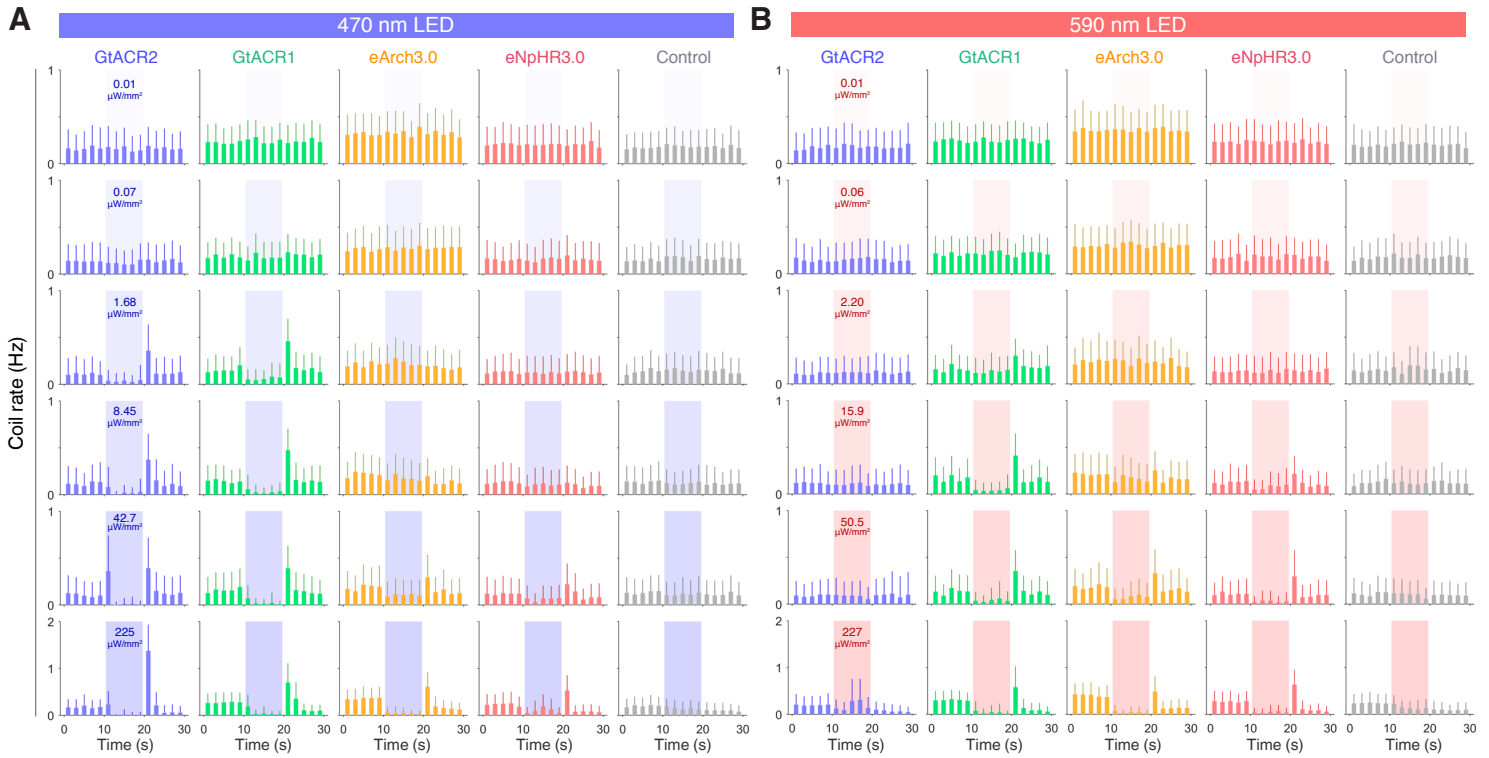


**Figure 6–figure supplement 1. Coil rate vs. time in embryos expressing different opsins in spinal neurons**  
**A,B** Distribution of coil rate vs. time for *Tg(s1020t:GAL4)* embryos (24–27 hpf) expressing different opsins (mean + SD, across fish). Embryos were subjected to 10 s pulses of blue (470 nm; A) or amber (590 nm; B) light. Each time bin corresponds to 2 s.



# Figure 6–figure supplement 2

LED On – initial 2 seconds

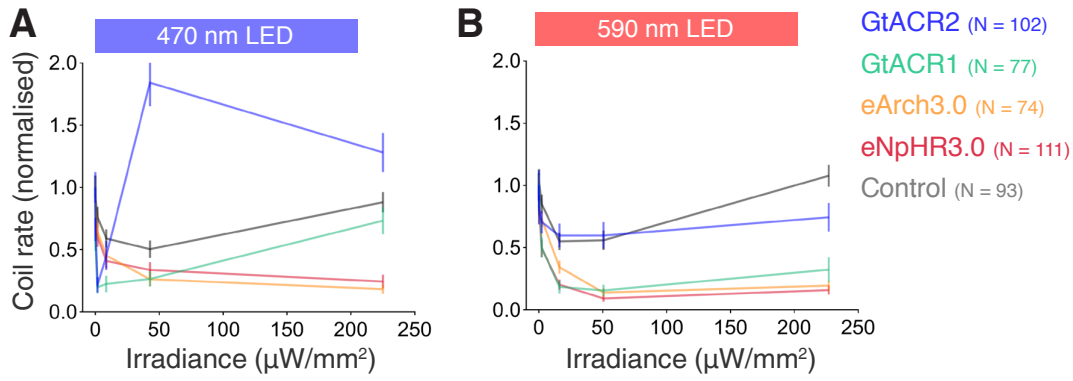


**Figure 6–figure supplement 2. Coil rate vs. irradiance for the initial 2 seconds of light exposure**  
**A,B** Normalised coil rate during the initial 2 s of the LED On period in embryos (24–27 hpf) expressing different opsins (mean  $\pm$  SEM, across fish). Control opsin-negative siblings were subjected to the same light stimuli.

# Figure 7

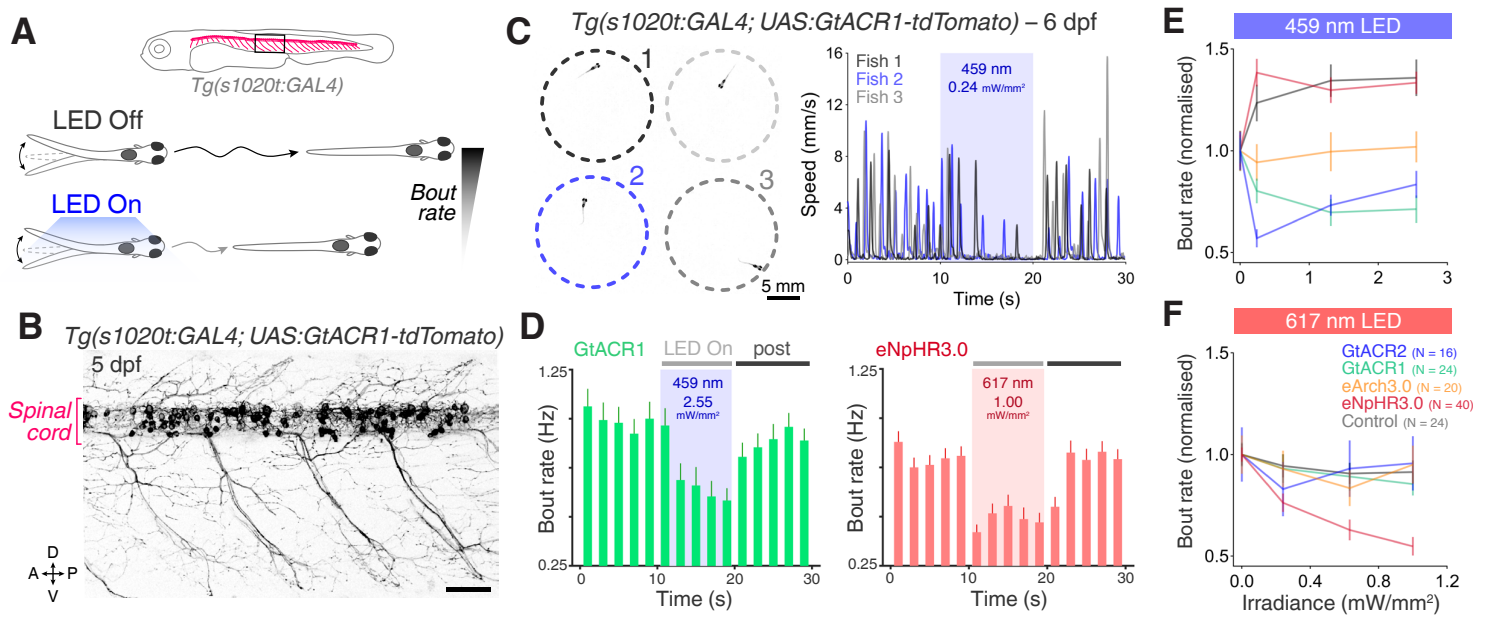


## Figure 7. Optogenetic suppression of swimming in larvae

**A** Schematic of behavioural assay.

**B** Opsin expression in spinal motor neurons and interneurons in a *Tg(s1020t:GAL4;UAS:GtACR1-tdTomato)* larva at 5 dpf. Imaging field of view corresponds to black box in (A). A, anterior; D, dorsal; P, posterior; V, ventral. Scale bar 50  $\mu$ m.

**C** *Tg(s1020t:GAL4;UAS:GtACR1-tdTomato)* larvae were positioned in individual agarose wells (left) and instantaneous swim speed was monitored by centroid tracking (right) at 50 fps (6 dpf;  $N = 25 \pm 9$  fish per group, mean  $\pm$  SD). 10 s light periods were delivered (459 or 617 nm, 0–2.55  $mW/mm^2$ ) with a 50 s inter-stimulus interval.

**D** Optogenetically-induced changes in bout rate (mean  $\pm$  SEM, across fish) in *Tg(s1020t:GAL4)* larvae expressing GtACR1 ( $N = 24$  larvae, left) or eNpHR3.0 ( $N = 40$  larvae, right). Horizontal grey bars indicate the time windows used to quantify behavioural changes. Each time bin corresponds to 2 s.

**E,F** Normalised bout rate during the ‘LED On’ period in larvae expressing different opsins (mean  $\pm$  SEM, across fish) and in control, opsin-negative, siblings.

# Figure 7–figure supplement 1

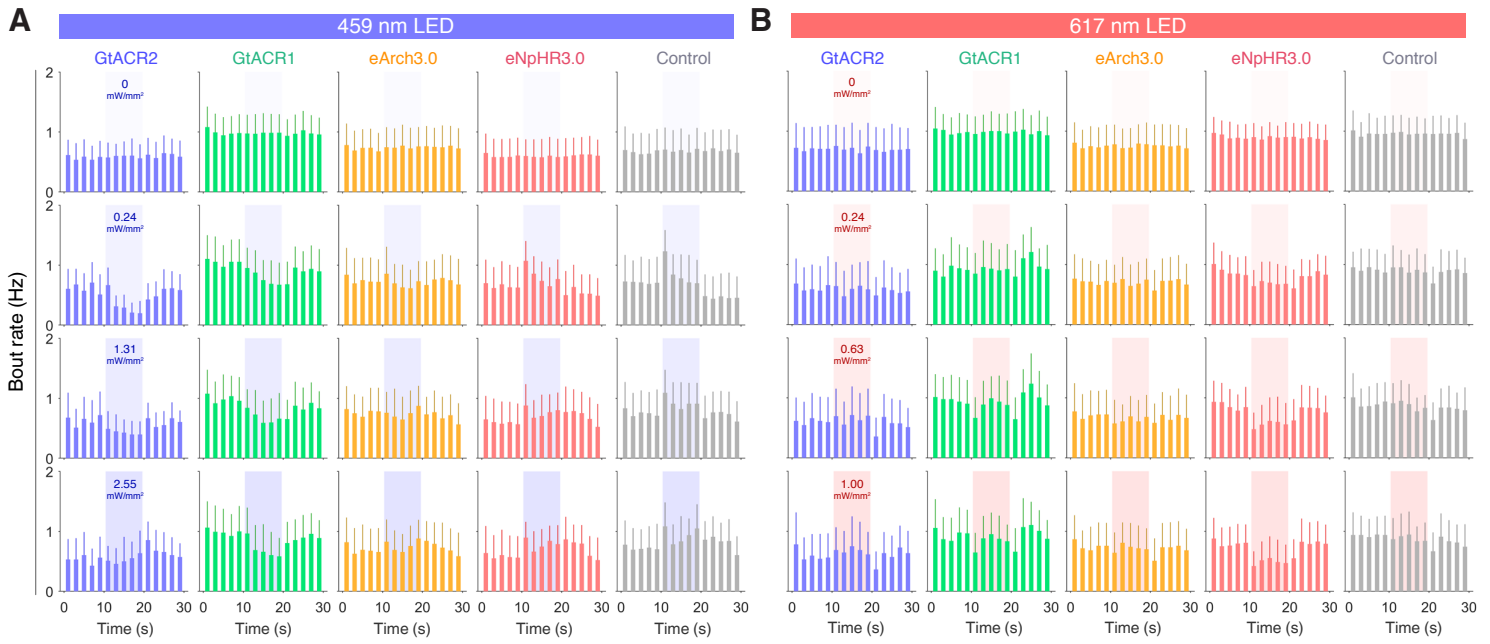


**Figure 7–figure supplement 1. Bout rate vs. time in larvae expressing different opsins in spinal neurons**

**A,B** Distribution of bout rate vs. time for *Tg(s1020t:GAL4)* larvae (6 dpf) expressing different opsins (mean + SD, across fish). Larvae were subjected to 10 s pulses of blue (459 nm; A) or red (617 nm; B) light. Each time bin corresponds to 2 s.

# Figure 7–figure supplement 2

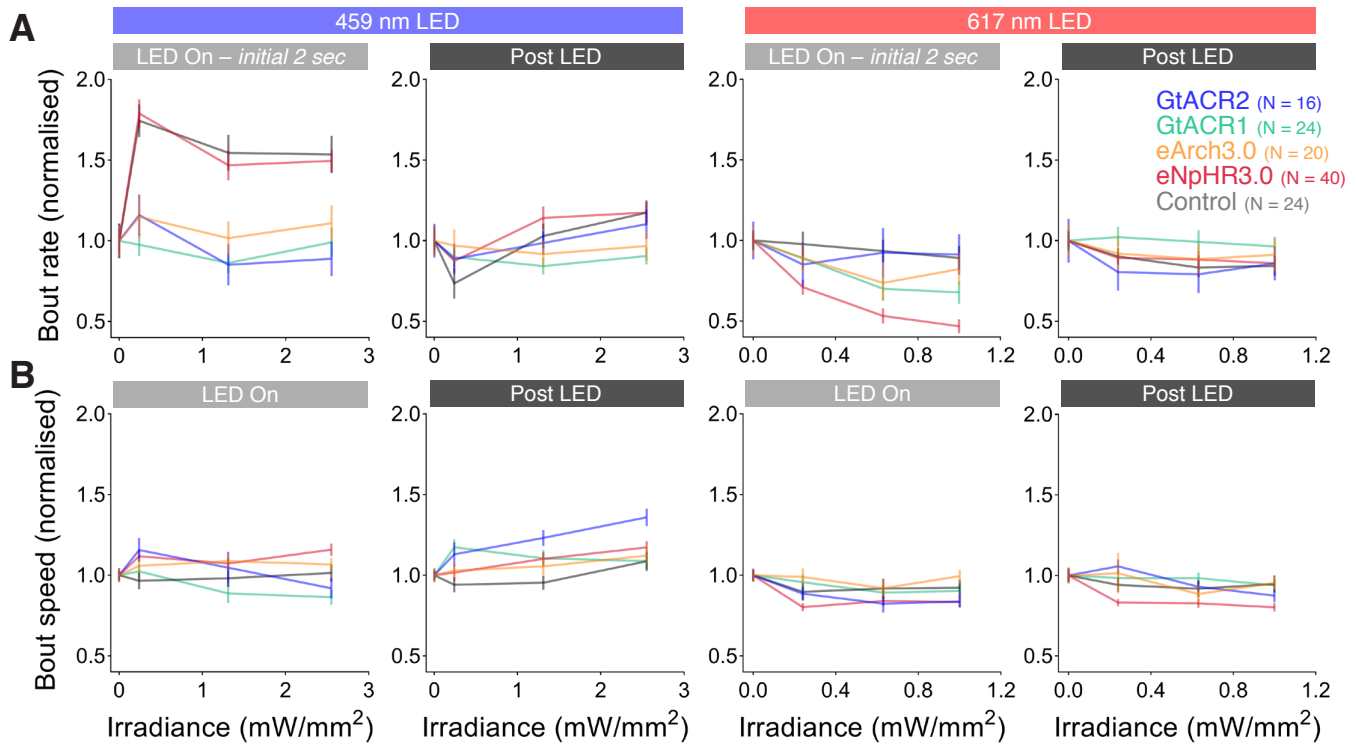


**Figure 7–figure supplement 2. Bout rate and speed vs. irradiance during different time periods in *Tg(s1020t:GAL4)* larvae**  
**A,B** Normalised bout rate (A) or bout speed (B) during the whole LED On period, the initial 2 s of light exposure and the 'post LED' 8 s period in *Tg(s1020t:GAL4)* larvae (6 dpf) expressing different opsins (mean  $\pm$  SEM, across fish). Control opsin-negative siblings were subjected to the same light stimuli.

# Figure 7–figure supplement 3

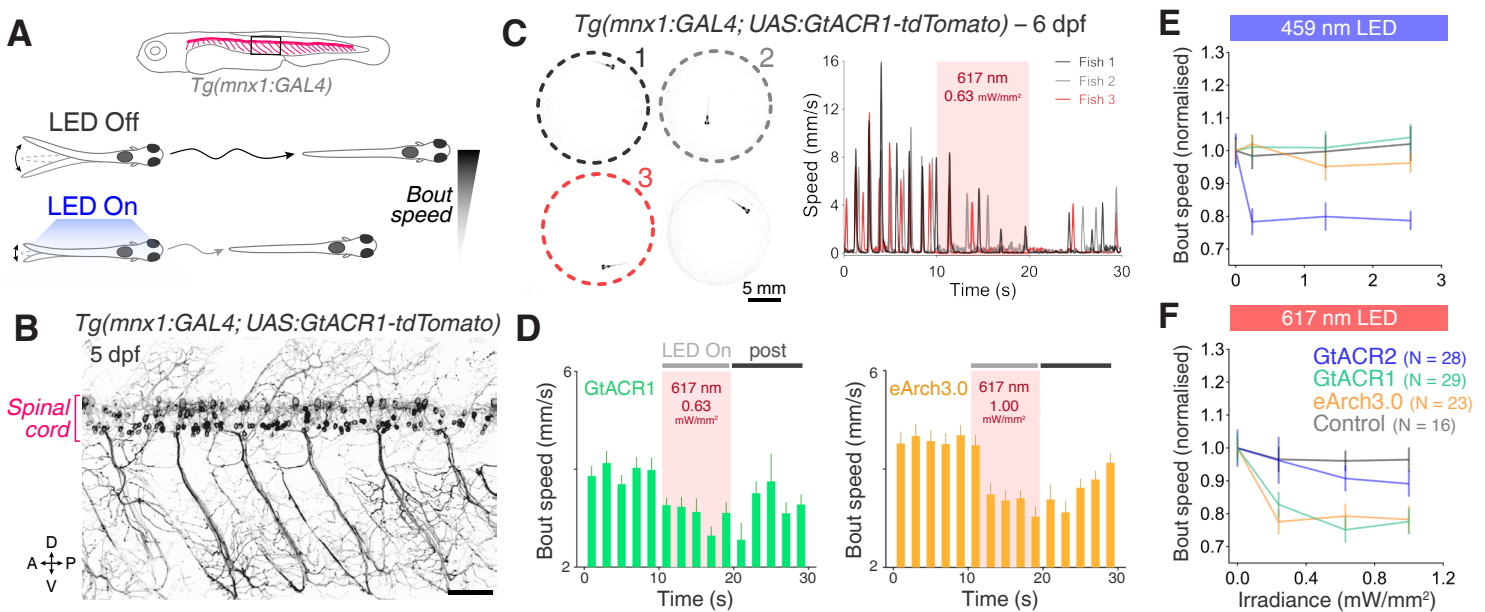


## Figure 7–figure supplement 3. Optogenetic suppression of swimming in *Tg(mnx1:GAL4)* larvae

**A** Schematics of opsin expression pattern and behavioural assay.

**B** Opsin expression in spinal motor neurons and interneurons in a *Tg(mnx1:GAL4; UAS:GtACR1-tdTomato)* larva at 5 dpf. Imaging field of view corresponds to black box in (A). A, anterior; D, dorsal; P, posterior; V, ventral. Scale bar 50  $\mu\text{m}$ .

**C** Background-subtracted camera field of view showing *Tg(mnx1:GAL4; UAS:GtACR1-tdTomato)* larvae positioned in individual agarose wells (left) and tracking of swimming speed for selected larvae (right). Behaviour was monitored at 50 fps across multiple freely-swimming larvae (6 dpf;  $N = 24 \pm 6$  fish per group, mean  $\pm$  SD) while they were subjected to 10 s light periods (459 or 617 nm, 0–2.55  $\text{mW}/\text{mm}^2$ ) with a 50 s inter-stimulus interval.

**D** Optogenetically-induced changes in bout rate (mean + SEM, across fish) in *Tg(mnx1:GAL4)* larvae expressing GtACR1 ( $N = 29$  larvae, left) or eArch3.0 ( $N = 23$  larvae, right). Horizontal grey bars indicate the time windows used for comparative quantification of behavioural changes. Each time bin corresponds to 2 s.

**E, F** Normalised bout speed during the 'LED On' period in larvae expressing different opsins (mean  $\pm$  SEM, across fish). Control opsin-negative siblings were subjected to the same light stimuli.

# Figure 7–figure supplement 4

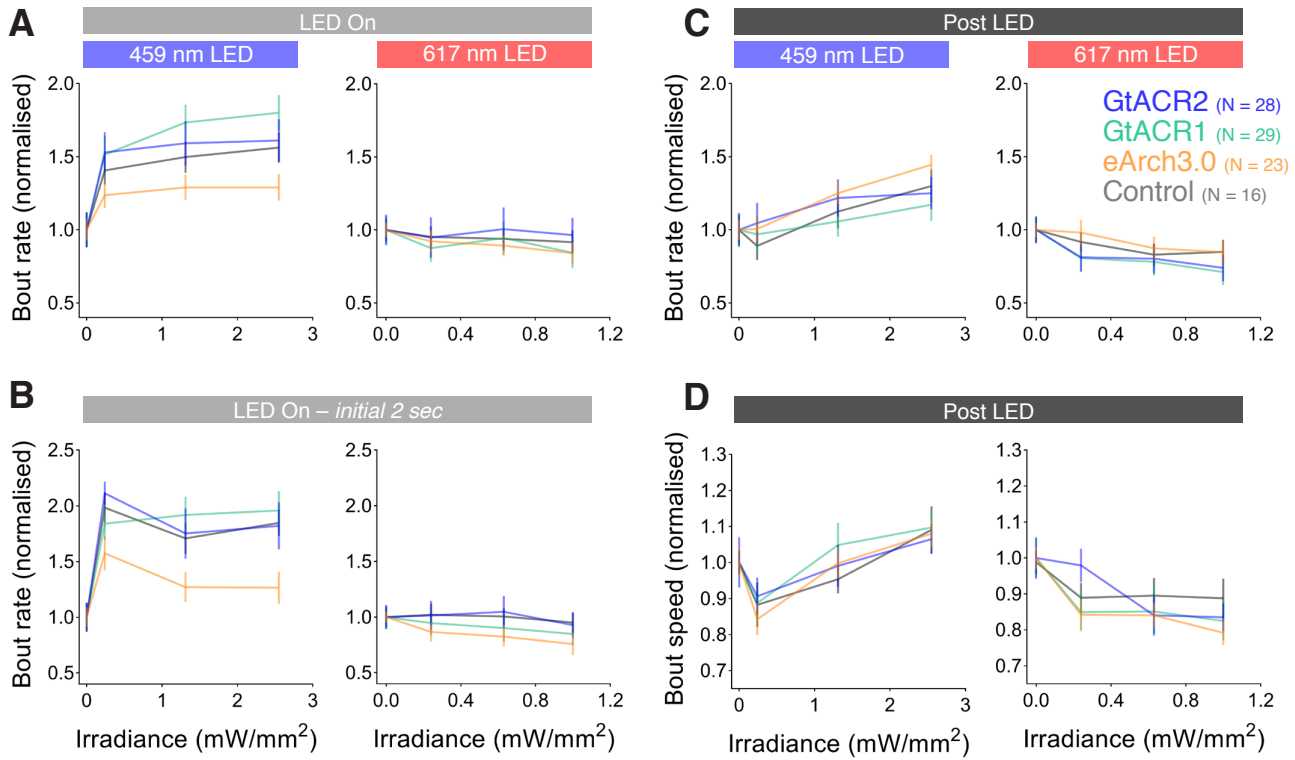


**Figure 7–figure supplement 4. Bout rate and speed vs. irradiance during different time periods in *Tg(mnx1:GAL4)* larvae**  
**A–D** Normalised bout rate (A–C) or bout speed (D) during the whole ‘LED On’ period (A), the initial 2 s of the light period (B), or the ‘post LED’ 8 s period (C,D) in *Tg(mnx1:GAL4)* larvae (6 dpf) expressing different opsins (mean  $\pm$  SEM, across fish). Control opsin-negative siblings were subjected to the same light stimuli.

# Figure 8

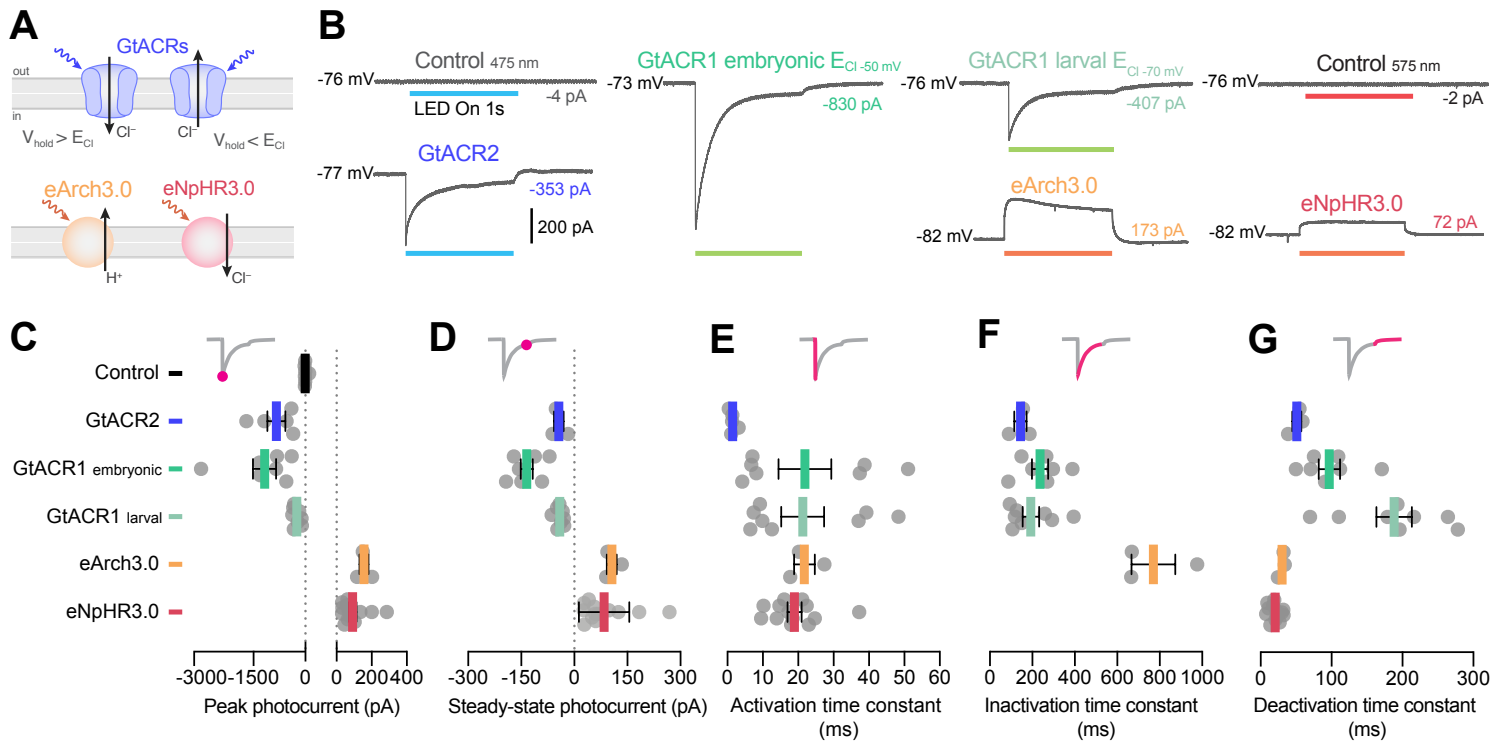


**Figure 8. Photocurrents induced by anion channelrhodopsins and chloride/proton pumps**

**A** Action of anion channelrhodopsins (top) and Cl<sup>-</sup>/H<sup>+</sup> pumps (bottom). For anion channelrhodopsins, photocurrent magnitude and direction depend on chloride reversal potential (E<sub>Cl</sub>) and holding potential (V<sub>hold</sub>), while Cl<sup>-</sup>/H<sup>+</sup> pumps always induce outward currents.

**B** Example photocurrents in response to a 1 s light exposure (20 mW/mm<sup>2</sup>).

**C, D** Photocurrent peak (C) and steady-state (D) amplitude (mean ± SEM, across cells). GtACRs induced larger photocurrents than Cl<sup>-</sup>/H<sup>+</sup> pumps.

**E–G** Photocurrent activation (E), inactivation (F) and deactivation (G) time constants (mean ± SEM). Photocurrents induced by Cl<sup>-</sup>/H<sup>+</sup> pumps showed minimal inactivation and faster deactivation kinetics than GtACRs. eNpHR3.0 photocurrents did not inactivate hence no inactivation time constant was computed.

# Figure 8–figure supplement 1

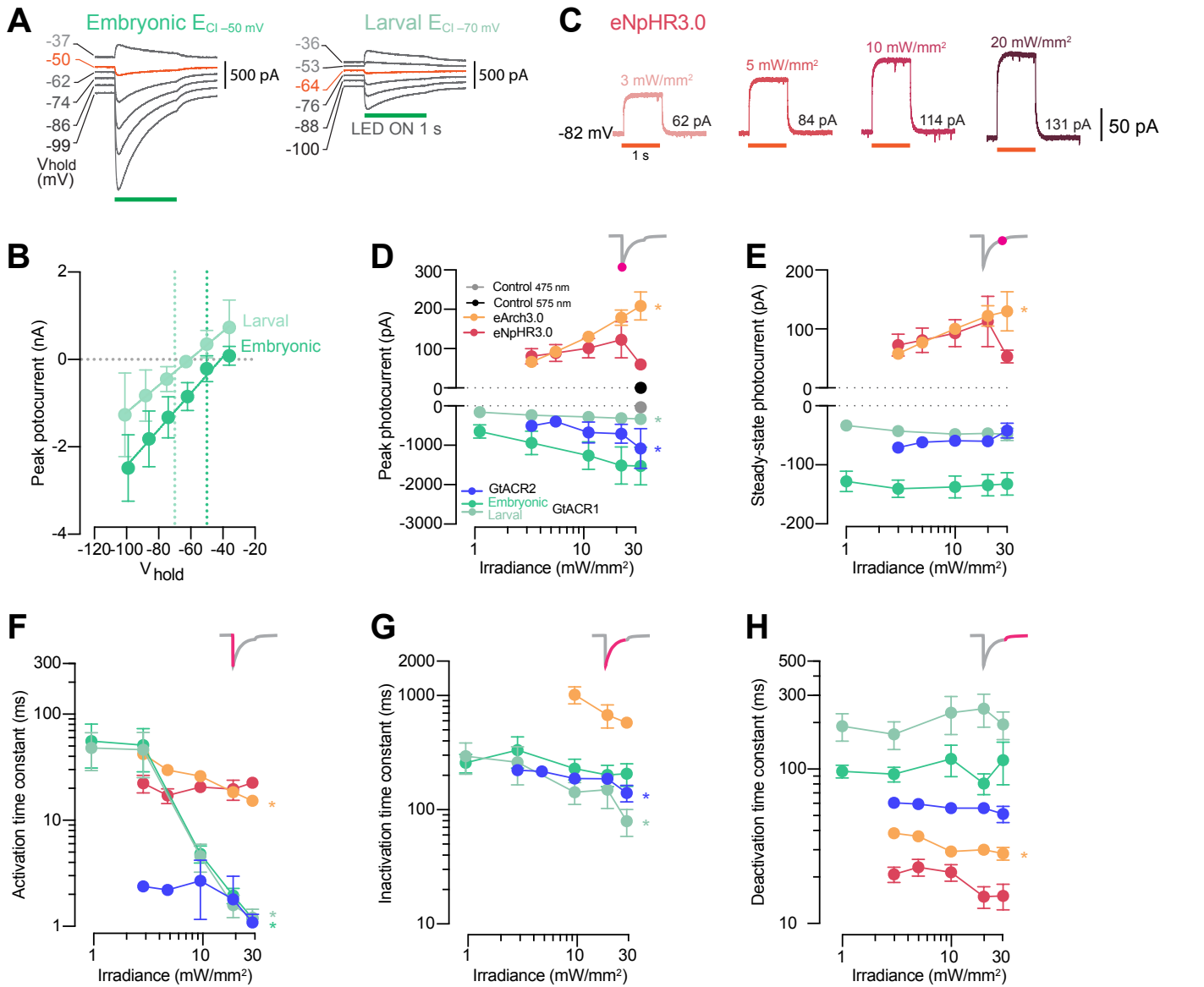


## Figure 8–figure supplement 1. Photocurrent properties vs. irradiance

**A** Example GtACR1 photocurrents obtained by providing a 1 s light periods at different holding potentials ( $V_{hold}$ ) using intracellular solutions approximating either embryonic or larval  $E_{Cl}$ . Orange traces denote holding potentials closest to  $E_{Cl}$ . **B** GtACR1 photocurrent I-V curves (mean  $\pm$  SD). Photocurrents reverse with a positive 5–10 mV shift relative to  $E_{Cl}$  (dotted lines) in both solutions.

**C** Example photocurrents from an eNpHR3.0-expressing cell at different irradiance levels (3–20 mW/mm<sup>2</sup>).

**D,E** Photocurrent peak (D) and steady-state (E) amplitude vs. irradiance (mean  $\pm$  SEM, across cells). Asterisks indicate a significant non-zero slope.

**F–H** Photocurrent activation (F), inactivation (G) and deactivation (H) time constants vs. irradiance (mean  $\pm$  SEM). eNpHR3.0 photocurrents did not inactivate hence no inactivation time constant was computed.



# Figure 9

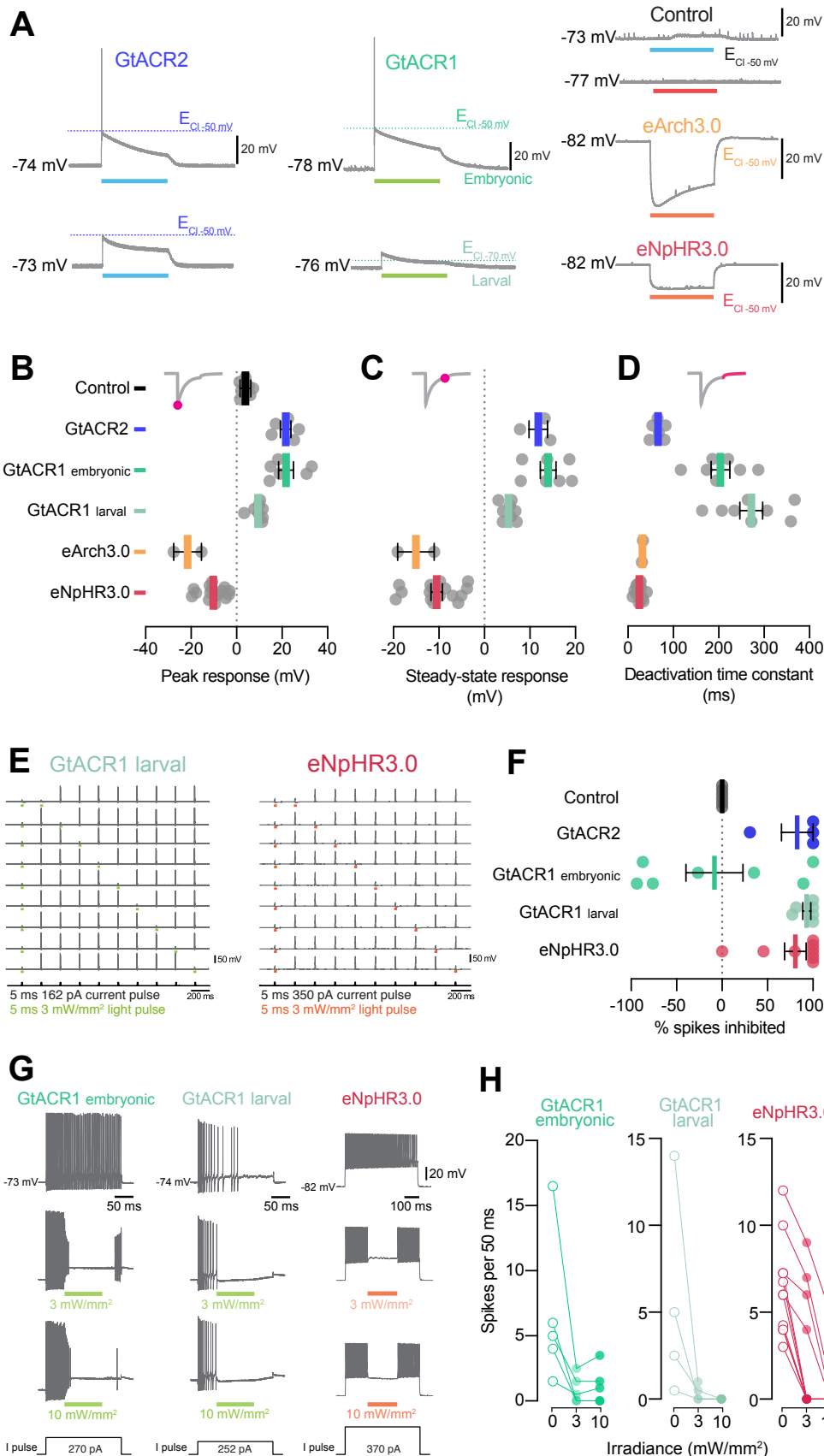


# Figure 9—figure supplement 1

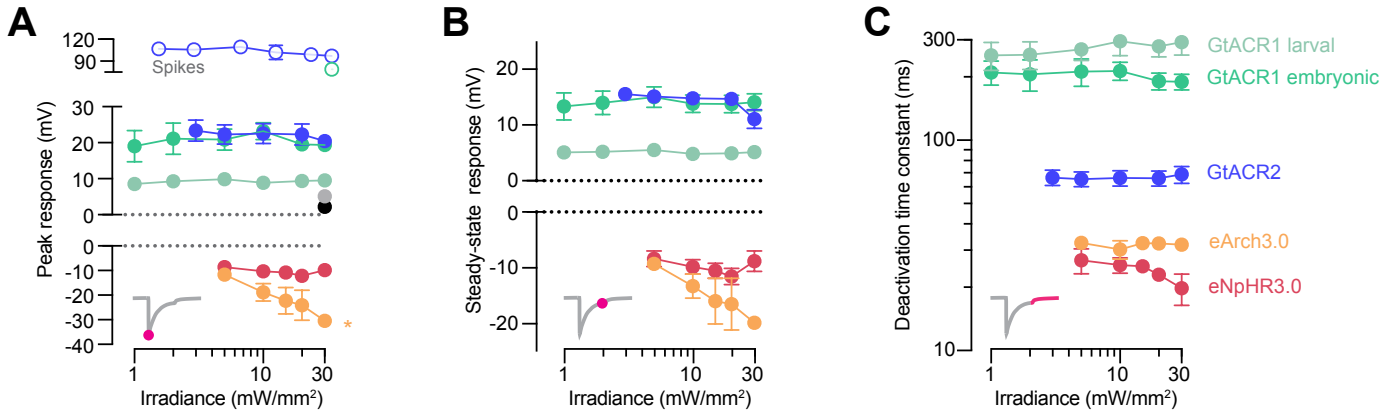


**Figure 9-figure supplement 1. Optogenetically-evoked voltage responses vs. irradiance**

**A–C** Peak (A) and steady-state (B) responses and deactivation time constant (C) of voltage deflections vs. irradiance (mean  $\pm$  SEM, across cells). eArch3.0 was the only opsin showing irradiance-dependent modulation of peak voltage response.